E-20-F05
#1

Full Scale tests of Steel Connections with SMA Components

Justin Ocel

Professor Roberto Leon

Professor Reginald Desroches

Gregory W. Hess

Submitted August 27, 2001

TABLE OF CONTENTS

LIST OF FIGURES III
LIST OF TABLES VI

CHAPTER I - Description of Test Set-up 1

1.1 Facility Features 1
1.2 Load Frame 3
1.3 Supporting Substructure 3
1.4 Lateral Bracing System 6
1.5 Actuator 7

CHAPTER II - Specimen Details 8

2.1 SMA Connection I 8
2.1.1 Constructability 12
2.2 SMA Connection II 15

CHAPTER III - Experimental Procedure 20

3.1 Loading Procedure 20
3.2 Actuator Control System 22
3.3 Instrumentation and Data Collection 23
3.3.1 SMA Connection I Tendons 23
3.3.2 SMA Connection II Tendons 26
3.3.3 Beam Instrumentation 27
3.3.4 Column Instrumentation 28
3.3.5 Load Pins 31

CHAPTER IV - SMA Connection I Experimental Results 32

4.1 Testing Events 32
4.2 Experimental Results of Initial Test for SMA Connection I 38
4.3 Tendon Heat Straightening 44
4.4 Retesting of SMA Connection I 46
4.5 Experimental Results of Retest for SMA Connection I 49

CHAPTER V - SMA Connection II Experimental Results 50

5.1 SMA Connection II Initial Testing Events 50

5.2 Experimental Results of Initial Test for SMA Connection II 52

5.3 First Tendon Heat Straightening 56

5.4 Second Tendon Heating 58

5.5 SMA Connection II Retest 61

5.6 Experimental Results of Retest for SMA Connection II 62

5.7 Dynamic Testing of SMA Connection II 65

CHAPTER VI - Connection Comparsions 73

6.1 SMA Connection I Comparisons 73

6.2 SMA Connection II Comparisons 75

6.3 Comparisons of the Two Connections 77

6.3.1 Energy Dissipation 77

6.3.2 Fractures 79

CHAPTER VII - SMA Connection I Experimental Data 80

A.1 Initial Testing 80

A.2 Retest 86

CHAPTER VIII - SMA Connection II Experimental Data 89

B.1 Initial Test 89

B.2 Retest 93

B.3 Dynamic Testing 97

LIST OF FIGURES

Figure		Page
1-1	View of Backend of Structures Lab	3
1-2	Load Frame	5
1-3	MTS 243 Series Actuator	7
2-1	Idealized Stress/Strain Characteristic for Martensitic SMA	9
2-2	View of SMA Connection I	11
2-3	15" SMA Tendon	11
2-4	Shimming of Top Anchorage Block	13
2-5	Welding of Bottom Anchorage Block	14
2-6	Shimming of Bottom Anchorage Block	14
2-7	View of SMA Connection II	17
2-8	Stress/Strain Behavior of 18" Nitinol SMA Tendon	18
2-9	18" SMA Tendon	18
3-1	SAC Loading Protocol	21
3-2	Modified SAC Loading Protocol	22
3-3	SMA I Tendon Instrumentation	25
3-4	Non-Contact Pyrometer	25
3-5	SMA II Tendon Instrumentation	26
3-6	Beam Instrumentation	27
3-7	Panel Zone LVDT's	29
3-8	Column Rotation and Axial Strain Gauge Instrumentation	30
3-9	Panel Zone Strain Rosettes	30
3-10	Load Pin Assembly	31
4-1	SMA I Tendon Yielding	33
4-2	Unrestrained Top Anchorage Block Movement	34
4-3	Tendon Buckling Under Compressive Load	36
4-4	Yielding due to Beam Flange Warping	36
4-5	One inch Fracture in Shear Tab Weld	37
4-6	Load/Displacement History of SMA Connection I	38
4-7	Moment/Total Rotation History of SMA I	39
4-8	Moment/Concentrated History of SMA I	41
4-9	Tendon Stress/Strain History from SMA I	43
4-10	Tendons Before and After Heating	45
4-11	Connection Modifications to SMA I	47
4-12	Fracture Surface of a SMA I Tendon	48
4-13	Moment/Total Rotation History of SMA I Retest	49
5-1	Load/Displacement History of SMA II Initial Test	52
5-2	Moment/Total Rotation History of SMA II Initial Test	53
5-3	Moment/Concentrated Rotation History of SMA II Initial Test	54

5-4 Stress/Strain History of SMA II Tendon 2 55
5-5 Tendon Heating with Propane/MAPP Gas Torches 57
5-6 Load/Displacement History Through First Tendon Heating 58
5-7 Oxy-Acetylene Torching 60
5-8 Tendon Temperature Gradient After Acetylene Torching 60
5-9 Evidence of Tendon Rubbing 61
5-10 Load/Displacement History of SMA II Retest 62
5-11 Moment/Total Rotation History of SMA II Retest 63
5-12 Stress/Strain History of Tendons for SMA II 64
5-13 Fracture Surface of SMA II Tendon #4 66
5-14 Load/Displacement History from Dynamic Test of SMA II 67
5-15 Moment/Total Rotation History from Dynamic Testing of SMA II . . . 68
5-16 Stress/Strain History of Tendon 3 from Dynamic Testing of SMA II 69
5-17 Tendon #3 in Tension at 5% Drift 70
5-18 Beam Flange Yielding at 5% Drift 71
5-19 Moment/Total Rotation for 5% Drift Cycle for SMA II 72
5-20 Moment/Concentrated Rotation at 5% Drift for SMA II 72
6-1 Moment/Total Rotation Comparison for SMA Connection I 74
6-2 First 4% Drift cycles for SMA Connection II 75
6-3 Moment/Total Rotation Comparisons for SMA Connection I 76
6-4 Connection I and II Moment/Total Rotation Comparison 77
6-5 SMA Tendon Fracture Surfaces 79
A-1 Load/Displacement History from Initial Test 80
A-2 Moment/Total Rotation History from Initial Test 81
A-3 Moment/Concentrated Rotation from Initial Test 81
A-4 Moment/Column Rotation History from Initial Test 82
A-5 Moment/Panel Zone Shear History from Initial Test 82
A-6 Stress/Strain History of Tendons from Extensometers 83
A-7 Stress/Strain History of Tendon 1 using Strain Gauges 83
A-8 Stress/Strain History of Tendon 2 using Strain Gauges 84
A-9 Stress/Strain History of Tendon 3 using Strain Gauges 84
A-10 Stress/Strain History of Tendon 4 using Strain Gauges 85
A-11 Load/Stroke History for Retest 86
A-12 Moment/Total Rotation for Retest 86
A-13 Moment/Concentrated Rotation for Retest 87
A-14 Moment/Column Rotation History for Retest 87
A-15 Moment/Panel Zone Shear History for Retest 88
A-16 Stress.Strain History of SMA Tendons for Retest 88
B-1 Load/Displacement History for Initial Test 89
B-2 Moment/Total Rotation History for Initial Test 90
B-3 Moment/Concentrated Rotation History for Initial Test 90
B-4 Moment/Column Rotation History for Initial Test 91
B-5 Moment/Panel Zone Shear History for Initial Test 91

B-6 Stress/Strain History for Tendons using Extensometers 92
B-7 Stress/Strain History for Tendons using Strain Gauges 92
B-8 Load/Displacement History for Retest 93
B-9 Moment/Total Rotation History for Retest. 93
B-10 Moment/Concentrated Rotation History for Retest 94
B-11 Moment/Column Rotation History for Retest 94
B-12 Moment/Panel Zone Shear History for Retest 95
B-13 Stress/Strain History of Tendon 3 for Retest 95
B-14 Stress/Strain History of Tendons for Retest 96
B-15 Load/Displacement History for Dynamic Testing 97
B-16 Moment/Total Rotation History for Dynamic Testing 97
B-17 Moment/Concentrated Rotation History for Dynamic Testing. 98
B-18 Moment/Column Rotation History for Dynamic Testing 98
B-19 Moment/Panel Zone Shear History for Dynamic Testing 99
B-20 Stress/Strain History for Tendon 3 using Strain Gauge 99

LIST OF TABLES

Table		Page
2-1	SMA Connection Configuration Comparison	19
3-1	Initial SAC Loading Protocol	21
6-1	Connection Energy Dissipation Comparisons	78

CHAPTER I

DESCRIPTION OF TEST SET-UP

Both tests were carried out in the Georgia Institute of Technology Structures Lab. This facility contains a pair of reaction walls and a thick concrete strong floor. A space-saving, post-tensioned frame, originally constructed for previous connection tests was modified to support the test specimen. This chapter describes facility features, test frame, and actuator specifications.

1.1 Facility Features

The Georgia Institute of Technology Structures Lab building contains a 6 ft. (1.8 m) thick, concrete strong floor, and a pair of reaction walls in an L-shape. The walls are 2 ft. (0.61 m) thick with buttresses that extend back 11 ft. (3.4 m), providing essentially a rigid support. The walls are 24 ft. (7.3 m) high in the low bays and 36 ft. (11 m) high in the high bay areas. Figure 1-1 shows a photo of the strongwall area of the GA Tech Structural Engineering Lab.

Contained within the walls and floor are a series of anchor points at 4 ft. (1.2 m) centers. This four foot pattern extends the length and height of the wall and across the area of the strong floor. Each anchor point on the wall contains four 3" (76 mm) diameter, horizontal tubes in an 8 in. (203 mm) square pattern. These tubes accommodate high strength threaded DWYDAG bars which are inserted through and extend beyond either

face of the wall. Each bar has a service capacity of 50 kips (222 kN), for a total service capacity of 200 kips (888 kN). Important to note is that the service load safety factor per bar is greater than 2.5, to prevent long term fatigue problems. To provide an anchorage to the wall, a bar is inserted in the tube, a nut is threaded onto the backside to prevent pullout, and post-tensioning is applied from the front side (or vice versa) of the wall.

Anchorage to the strong floor is accomplished in a slightly different manner. The threaded bars are cast-in-place, and have an anchor on the bottom end (bottom of slab) and a threaded coupler on the top. The top face of the couplers sits nearly flush with the floor surface and the four anchors are in the same 8"x8" (203x203 mm) pattern as the wall. This allows for bars to be coupled to the floor extending upward for post-tensioning.

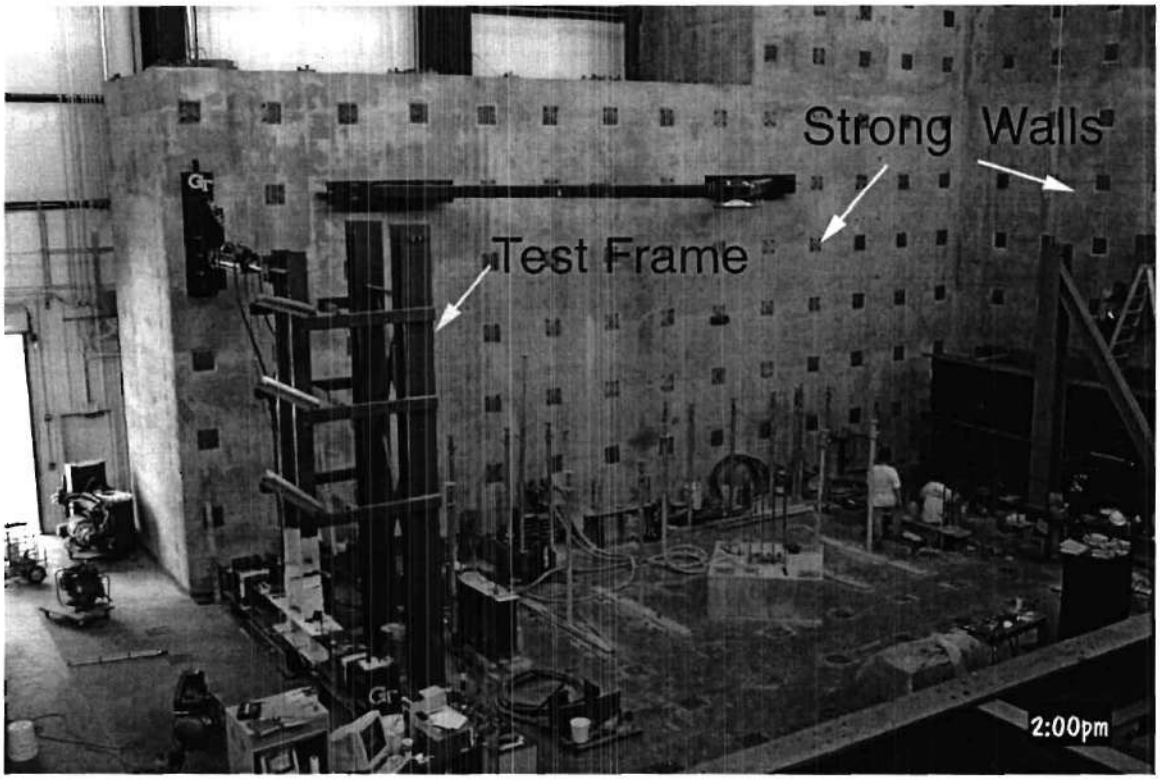

Figure 1-1 View of Backend of Structures Lab

1.2 Load Frame

1.2.1 Supporting Substructure

The pins and actuator were mounted to steel sections positioned over the post-tensioning pattern. These steel sections transferred the load to the wall and floor. Several series of bolt holes were drilled into the sections on the floor (W14x120) so the load pins could be placed anywhere along the section to accommodate different column and beam geometries (see Figure 1-2). The actuator was attached to two sections

(W14x120 and W24x104), this brought the actuator away from the strong wall so the actuator would be near mid-stroke once affixed to the beam.

The floor sections were post-tensioned to the floor using a DWYDAG bar once stiffener plates were welded in-between the flanges of the W14x120 sections, this prevented any local deformations during post-tensioning. Then an 11 in. (280 mm) DWYDAG bar was coupled to floor pattern and a nut was placed on the bar in between the flanges of the section. A DWYDAG coupler joined the 11 in. bar to a longer bar (approx. 4 ft.), that ran through the top flange to the coupler, allowing it to be jacked from above the top flange. After the nut on the 11 in. bar was tightened, the long bar was removed, leaving the top flange clear for the load pins.

Once these floor sections were post-tensioned, bolt holes were drilled in the top flange of the sections to accommodate pin placement. The pins were not connected directly to the floor sections, but rather to two short, stiffened W14x257 sections with welded base plates as shown in Figure 1-2. Due to slip between the W14x257 and W14x120 sections during previous steel connection tests, these W14x257 sections were post-tensioned to the W14x120 sections, in additon to just bolting. This author found that fully tensioning 8 - 1" A490 bolts by the "turn-of-the-nut" method to each stub column was sufficent, and post-tensioning was not needed.

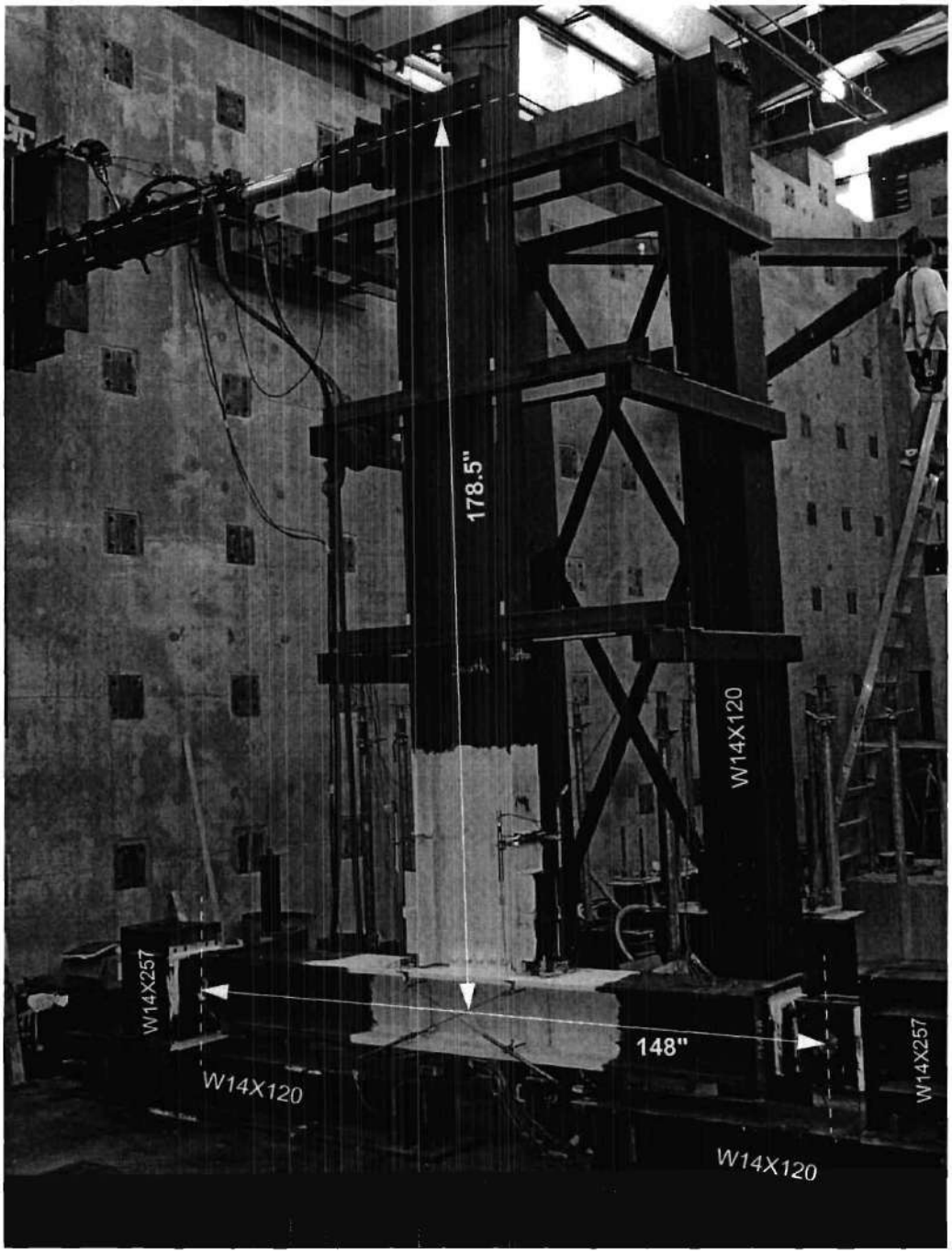

Figure 1-2 Load Frame

1.2.2 Lateral Bracing System

Also shown above in Figure 1-2 is the lateral bracing frame used to prevent lateral distortions of the beam during loading. The columns were fabricated from W14x120 sections with a 1-1/4 in. (32 mm) thick, 18 in. (460 mm) square base plate. They stood 18 ft. (5.5 m) tall and were spaced 4' 8" (1.4 m) apart. Attached to the outer flanges were 6x4x1/4 thick structural rectangular tubing acting as cantilever arms to support the L5x5x3/8 sections that act as the three brace points. To reduce friction, high-pitched steel noises, and prevent sudden slips between the beam and the angles, teflon sheets were glued to the angles and coated with a light oil.

The spacing of the tubes (braces) were 5', 9.5', and 13.5'. (1.5, 2.9, and 4.1 m) from the column face. These tubes were bolted through the flanges and fillet welded for extra rigidity. They extended outward approximately 6 ft. (1.8 m) and several holes in the top side of the tubes were used to connect the bracing angles and accommodate different beam sizes.

To limit sway of the columns and help stabilize the bracing system, two sets of diagonal braces were installed between the columns. These were made with L4x4x3/8 sections and bolted to tabs that were welded onto the column flanges.

After the column is in place, the angle braces can be opened up to allow a beam specimen to be inserted. The angles are then snugged against the beam and bolted to the tubes.

1.2.3 Actuator

A hydraulic, servo-valved actuator (MTS 243.45) was connected to the top of the beam. The actuator has a total stroke of 30 in. (.762 m) and a maximum capacity of 146 kips (649 kN) in compression and 100 kips (445 kN) in tension. At mid-stroke (15 in. / .381 m), the actuator is 102.5 in. (2.6 m) long. Since the actuator's bolt pattern was too wide for the beam, an "adaptor" was used to connect the two.

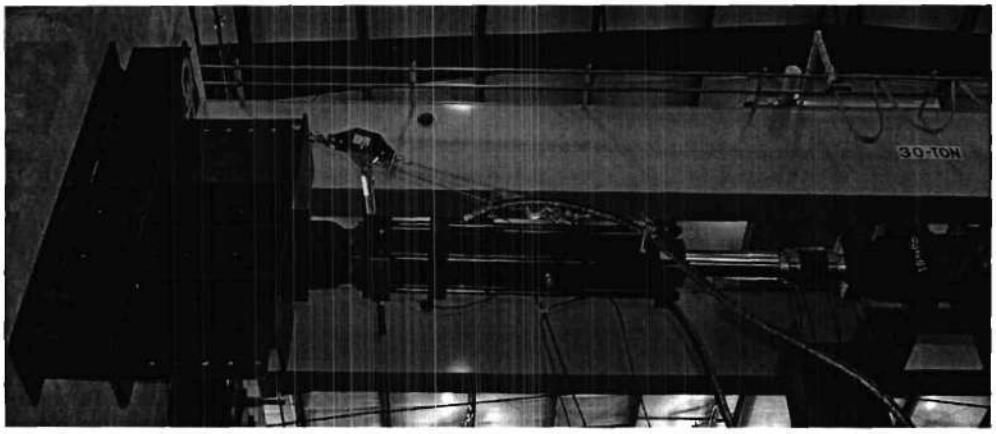

Figure 1-3 MTS 243 Series Actuator

CHAPTER II

SPECIMEN DETAILS

This chapter is intended to provide insight into the specimen design, specifically its materials, geometry, and construction. The SMA connections tested were designed by the E*Sorb Corporation.

2.1 SMA Connection I

This connection was used to join a W14x159 column section to a W24x94 beam. Figure 2-2 shows a photo of the actual connection to aid in further descriptions.

The shear tab was a 15"x 5"x 3/8" steel plate with one 1" (25 mm) oversized hole in the center and two more 1" x 1.0625" (25 mm x 27 mm) slotted holes on each of the two sides. The outside holes were slotted to allow the beam to freely rotate about the center hole without transferring moment. The shear tab was welded with a SMAW process by a certified welder using a 3/8" (10 mm) fillet weld and E7018 electrodes. The tab was positioned such that the beam web lied directly over the column web after it was bolted to the tab. The beam was drilled with 1" (25 mm) oversized holes and 1" A490 twist-off bolts were used to clamp the two surfaces together. The twist-off feature of the bolts ensured the bolts were fully pretensioned. With the bolts pretensioned, the shear tab could transfer some moment but it was assumed only to transfer shear. All the moment transfer was then assumed to be handled solely by the SMA tendons.

The SMA material used in this experiment was a fully annealed, binary NiTi alloy with an austenite finish, A_f, (the temperature above which the alloy is 100% austenite) of ~200 F (95 C). Details of the composition and manufacturing process can not be divulged as the entire technology is proprietary. The material's stress-strain relationship was not known at the time of this report's submission, but tests were scheduled to be carried out at the University of Illinois on an extra tendon made with the original batch. Figure 2-1 below shows a typical stress-strain diagram of an idealized Nitinol specimen in the martensitic phase.

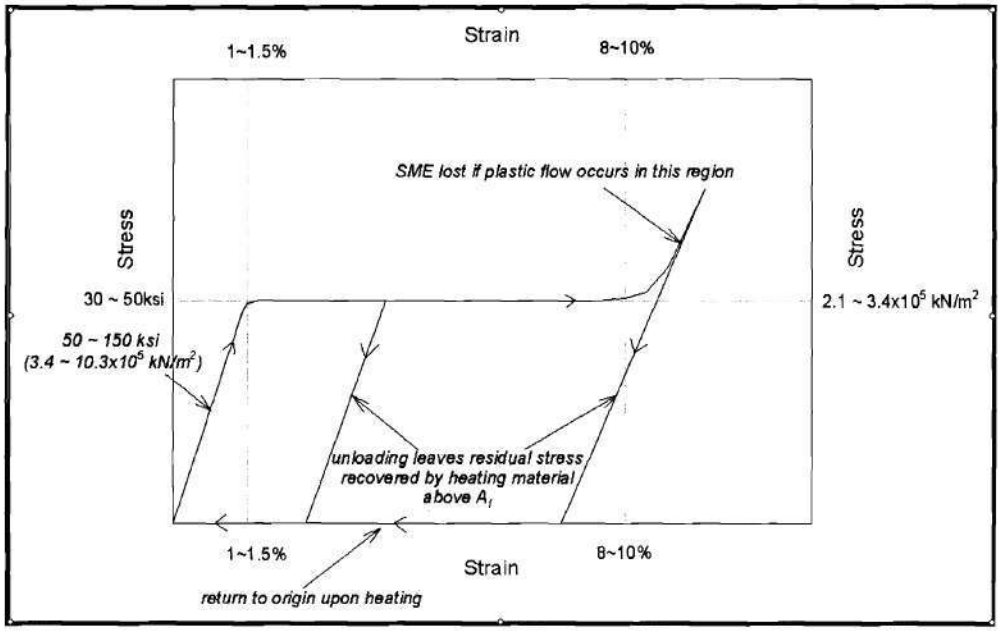

Figure 2-1 Idealized Stress/Strain Characteristic for Martensitic SMA

The tendons themselves were 15" (381 mm) long with a central gage length of 9" (229 mm) at a diameter of 1.375" (35 mm) as seen in Figure 2-3. The ends of the tendons were 1.75" (44 mm) in diameter and were machined with a 12-pitch thread pattern. The threading was needed to firmly secure the SMA tendons into the test fixture. Two 4"x8"x0.5" (102 mm x 204 mm x 13 mm) rectangular tubes were welded to the beam with 0.5" (13 mm) fillet welds and a solid 2"x4"x8" (51 mm x 102 mm x 204 mm) block (Top Anchorage Block in Figure 2-2) was inserted between the two rectangular tubes. The solid block had two 1.75" (44 mm) diameter holes on 4.75" (121 mm) centers drilled and tapped such that one end of the SMA tendon could be screwed into it. The other end of the SMA tendon screwed into a 3"x3"x12" (76 mm x 76 mm x 305 mm) solid block (Bottom Anchorage Block in Figure 2-2) that was wedged in between the column flanges. This block also had a hole drilled and tapped such that the SMA tendon could be screwed down into it. A 2" (51 mm) diameter hole was drilled in the column flange to allow the tendon to be passed through the column flange. This set-up allowed the SMA tendon to be placed in both tension and compression to allow for cyclic testing.

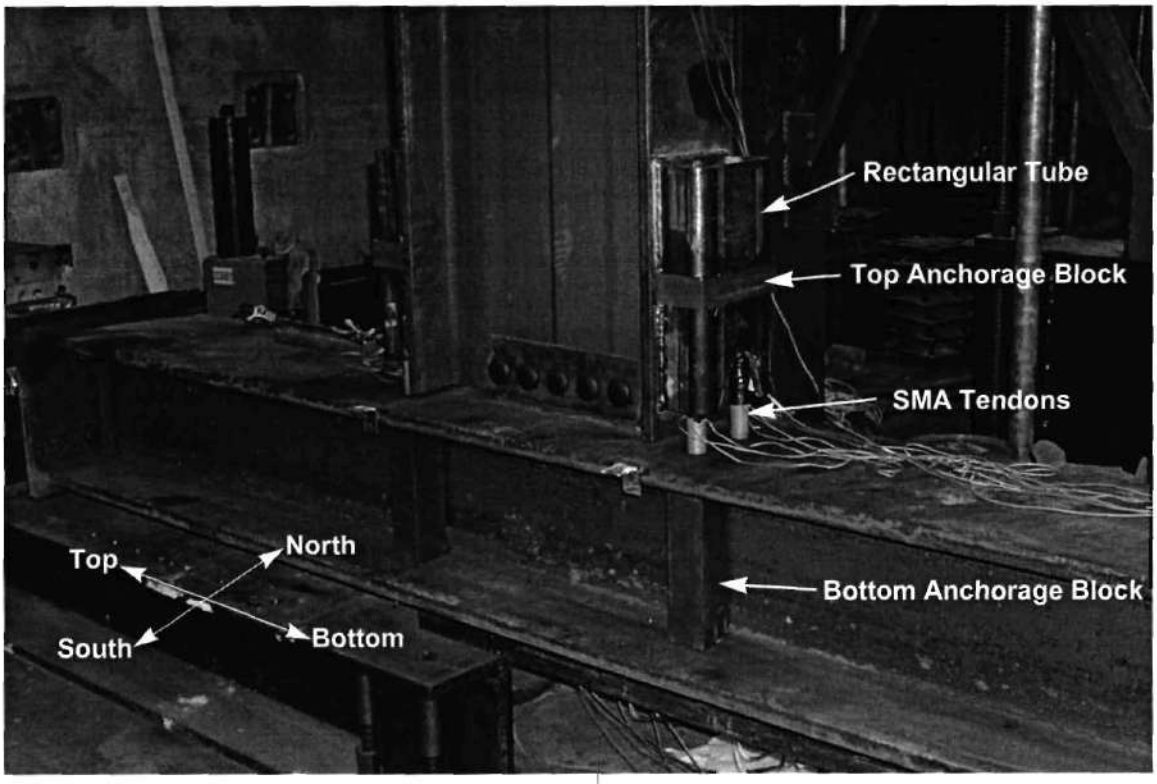

Figure 2-2 View of SMA Connection I

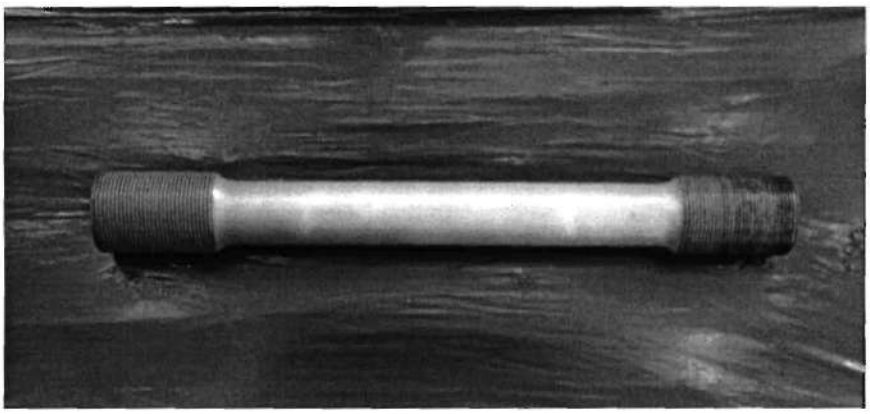

Figure 2-3 15" SMA Tendon

2.1.1 Constructability

The method for placing the SMA tendons into the system of this particular connection was not found to be practical. The SMA tendons were required to be screwed all the way through the Top Anchorage Block, down into the Bottom Anchorage Block between the column flanges. This process proved to be difficult since three different components needed to be lined up exactly to allow the SMA tendon threads to properly engage. The main reason for this difficulty was the block between the column flanges was required to almost rest directly against the web of the column. However, in the machining of the block, not enough tolerance was left so the block could fit over the fillet in the k-region of the column section. In future test, the SMA tendons should be spaced farther apart or the machining of the block should take into account the large radius fillet of the column.

The second problem dealt with issues of tolerances. The two rectangular tubes welded to the beam section were designed to snugly hold the Top Anchorage Block. This was not the case in the experimental procedure. During the welding process, the tubes slipped slightly and a gap ranging from 1/32"-1/8" (0.8 mm - 3 mm) was left between the block and the tubes. The tubes were also cut to length with a band saw and that is all the machining they received. The band saw cut left a bearing face that was not straight nor true to the surface of the block. The same problem occurred with the block that was to be wedged inside the column flanges. Due to the inexact process of rolling steel shapes, the block did no fit exactly between the flanges and it to left a gap ranging from 1/8" -1/4" (3 mm - 6 mm). The ideal solution to this problem would be to weld the all the boundaries of

the two blocks. However, this was not possible for the top block because a surface sufficient to welding was not possible, so the gaps with filled with shim stock until all surfaces were bearing. The bottom block was welded to the bottom flange of the column, but the top had to remain unwelded for fear the SMA would lose its heat treatment from the heat input from the welding process. The top of it was shimmed in the same manner as the Top Anchorage Block.

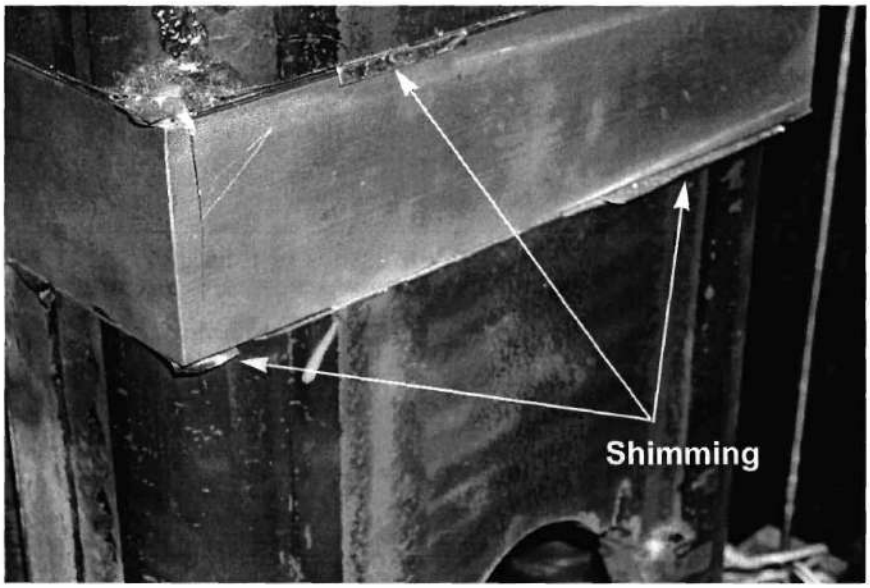

Figure 2-4 Shimming of Top Anchorage Block

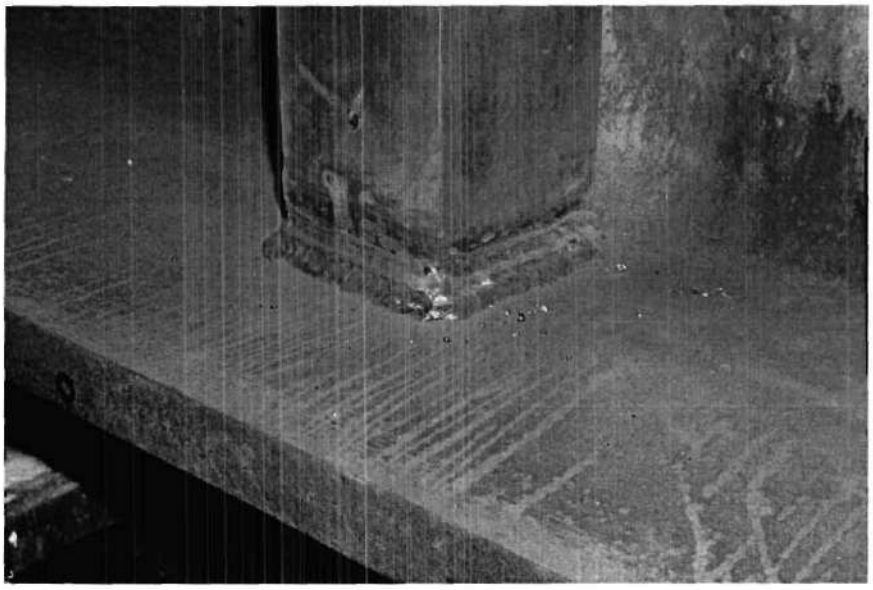

Figure 2-5 Welding of Bottom Anchorage Block

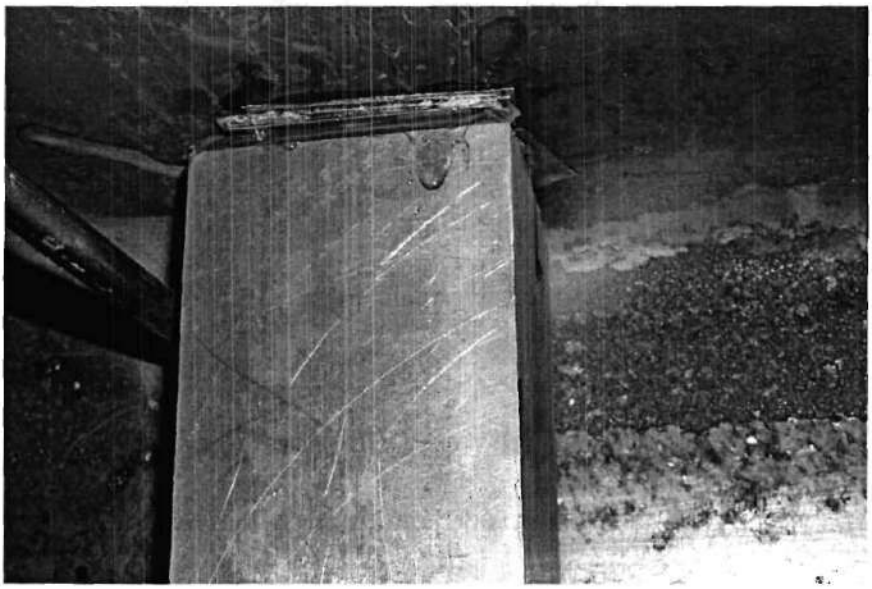

Figure 2-6 Shimming of Bottom Anchorage Block

2.2 SMA Connection II

The second connection was designed by the author and was mostly modeled after the first connection. This design adopted modifications that were intended to address the construction problems with the first connection. This connection was between a W14x159 column and a W24x55 beam. The smaller beam was used to increase the $M_{connection}/M_{p\ beam}$ ratio from the first test.

The same column section was reused for this connection since no damage was sustained from the SMA Connection I test. Before the column could be reutilized, it needed to be prepped. First, the Bottom Anchorage Blocks needed to be removed since they were not left in a vertical condition, and therefore were misaligned for installation of the new tendons. The 3/8" (10 mm) fillet weld at the bottom of the blocks was arc gouged and the blocks were removed. Second, the shear tab weld was inspected with red dye penetrant to reassure there were no cracks in the weld. No cracks were found so the shear tab was also reused. Finally, the Top Anchorage Block could not be reused since its removal from the first connection was too difficult, and a new one was fabricated. Since the hole which the tendons passed through in the column were already drilled, the new Top Anchorage Blocks had to have their holes offset from center since the W24x55 had 3/4" (19 mm) less depth than the W24x94 used in SMA Connection I. This also meant the force couple distance between the two connections was equal.

Tendon installation was difficult in SMA Connection I because a person's hands could not get inside the rectangular tubes. To address this problem, the rectangular tubes from SMA Connection I were replaced by stiffened angles (see Figure 2-7). The stiffened

angles were constructed from 8"x5"x1" (203mm x 127mm x 25mm) angles with three 1/2" (13 mm) triangular steel plates welded in-between the legs of the angle. The angles were then welded to the beam flanges using 1/2" (13 mm) E71T-1 G-FCAW welds, leaving enough space for the Top Anchorage Block to fit in-between them. The angles allowed full visual and physical inspection of the SMA tendons along their length.

The SMA tendons utilized the same Nitinol material used in SMA Connection I. The stress/strain characteristics (see Figure 2-8) of this bar were found by testing of a fifth bar at the University of Illinois. The SMA tendon design was altered for this test too. It was believed the small radius transition of the SMA Connection I tendons was the cause of the tendon fracture in the first test. The new design increased that transition radius from 0.5" (13 mm) to 5" (127 mm), which forced the overall tendon length to increase by 3" (76 mm) to a total length of 18" (457 mm) as seen in Figure 2-9. The gauge length also increased to a length of 11" (279 mm) with a diameter of 1.4375" (36.5 mm). The tendons also included a 1/8" (3 mm) slot machined into the top that along with an adapter and a socket handle, aided with the installation of the tendons. The tendons installed on the Bottom Side of the connection screwed into place with only hand force[1]. However, the two tendons on the Top Side needed help from a wrench to screw the two tendons in place. The Top-North tendon was particularly difficult to turn into place and was left about 1/8" (3 mm) higher than the other three tendons.

Once the tendons were installed, the Bottom Anchorage Blocks were fillet welded into place at both the top and bottom with 1/2" E7018 SMAW fillet welds. It was

---

1.See Figure 2-2 for convention of Top, Bottom, North, and South Sides

concluded that welding at the top was more beneficial to the connection design than the possibility of altering the metallurgy of the tendon due to heat input from the welding process. The Top Anchorage block was also welded to both of the stiffened angles.

Four smaller stiffened angles were welded to the column flange, to restrict the out-of-plane movement of the beam flanges. This was done because SMA Connection I showed that tendon buckling caused the beam flanges to warp to a point where the shear tab weld fractured.

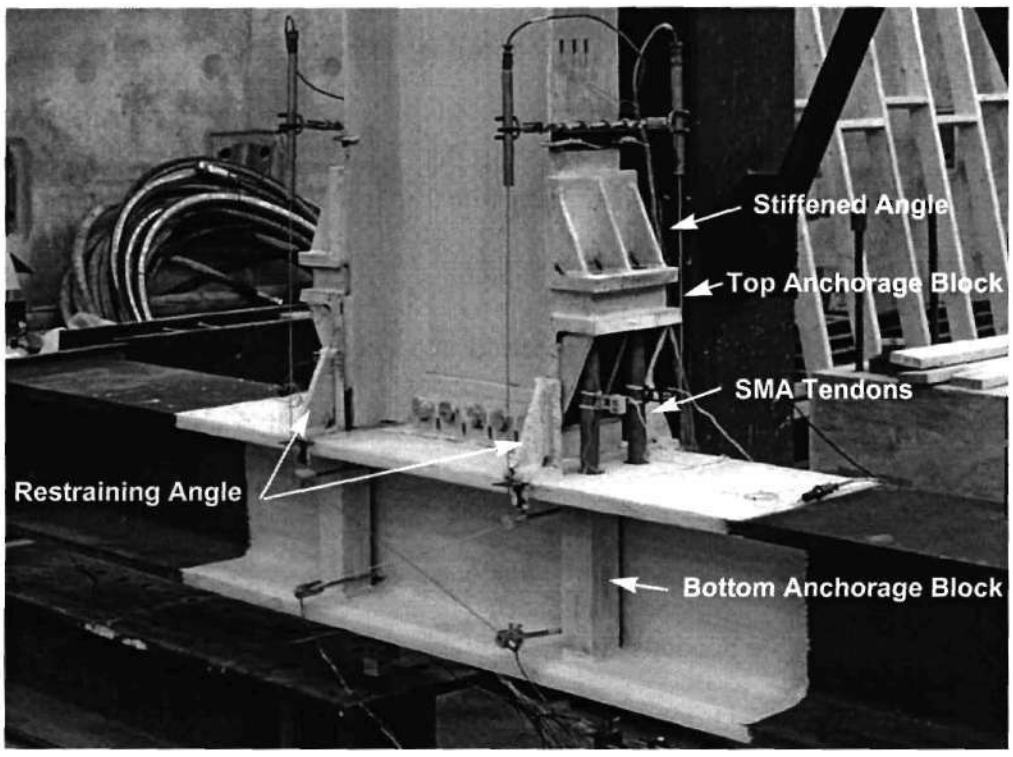

Figure 2-7 View of SMA Connection II

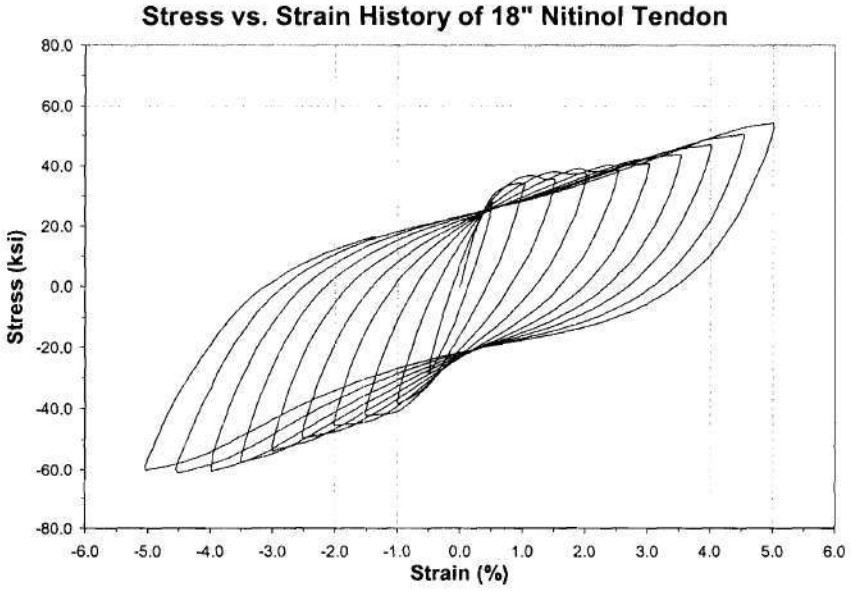

Figure 2-8 Stress/Strain Behavior of 18" Nitinol SMA Tendon

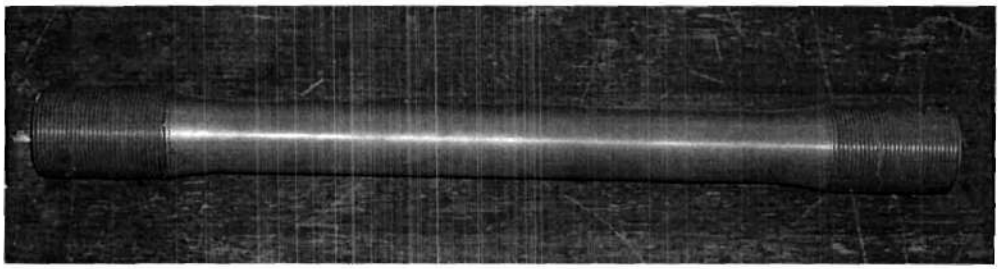

Figure 2-9 18" SMA Tendon

Table 2-1 SMA Connection Configuration Comparison

	SMA Connection I	**SMA Connection II**
Beam	W24x94	W24x55
Column	W14x159	W14x159
Shear Tab	15" x 5" x 3/8" plate	15" x 5" x 3/8" plate
SMA Tendon Material	Martensitic Nitinol	Martensitic Nitinol
Tendon Gauge Length	9"	11"
Tendon Gauge Diameter	1.375"	1.4375"
Connecting Element for Top Anchorage Block	4" x 8" x 0.5" Steel Tubes	8" x 5" x 1" Stiffened Angles

CHAPTER III

EXPERIMENTAL PROCEDURE

The tests were run in accordance to SAC test protocols as much as possible. The SAC guidelines were used to guide sensor selection, sensor placement, and loading protocol. Hand notes were taken throughout the testing, recording all significant observations, and any abrupt changes in the experimental procedure.

3.1 Loading Procedure

The initial loading tests were run in displacement control in accordance with SAC Protocol load history [13]. This load history is based on the interstory drift angle which is the beam tip displacement divided by the beam length (from actuator centerline to column centerline). Table 3-1 shows the stepwise loading used in the test. The fixed displacements were applied to the tip of the beam using a MTS hydraulic actuator at a rate of 2"/min. (51 mm/min.). This loading rate was increased to 4"/min. (102 mm/min.) during the retesting of the two connections. The retesting of the connections utilized a modified version of the SAC Protocol in order to subject the connection to more intense drift cycles quicker.

Table 3-1 Initial SAC Loading Protocol

Load Step Number	Interstory Drift (%)	Number of Cycles	Beam Tip Deflection
1	0.375	6	0.669"
2	0.5	6	0.893"
3	0.75	6	1.339"
4	1	4	1.785"
5	1.5	2	2.678"
6	2	2	3.570"
7	3	2	5.355"
8	4	2	7.140"
9	5	2	8.925"

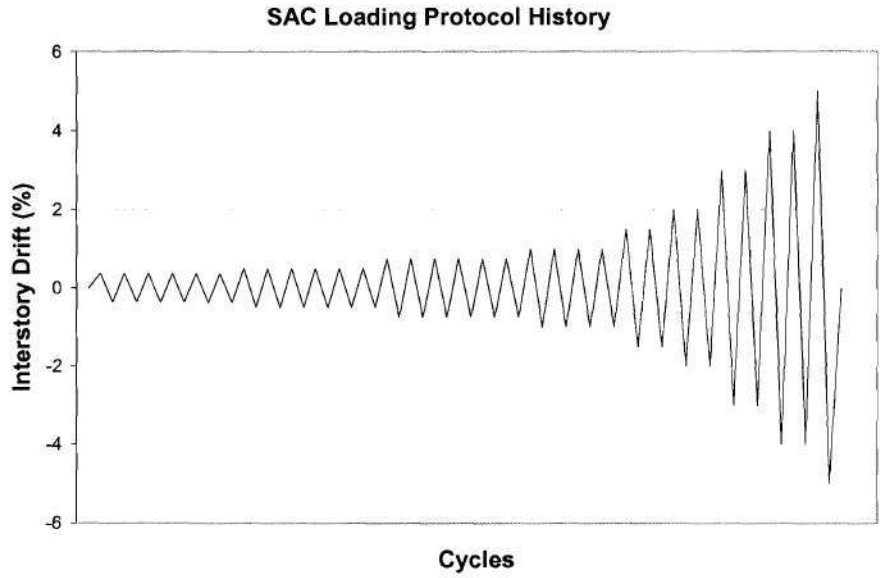

Figure 3-1 SAC Loading Protocol

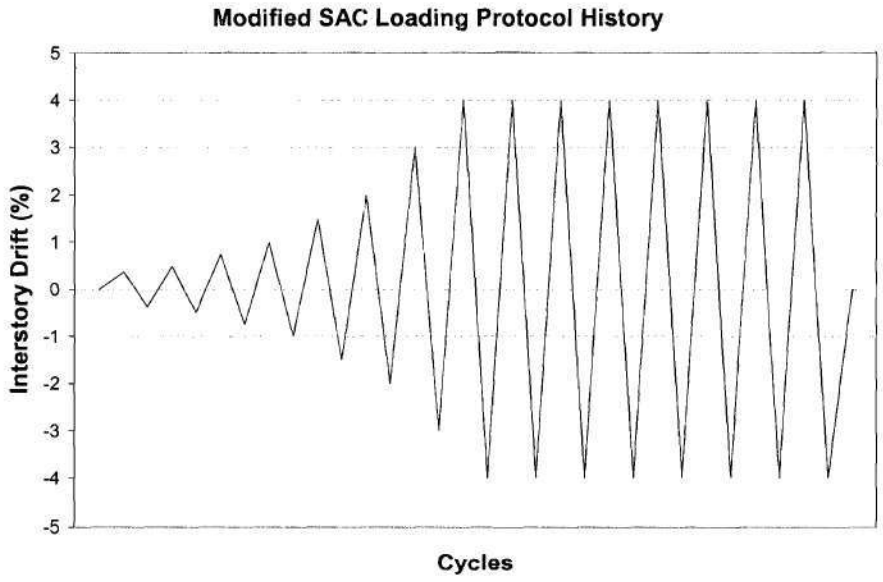

Figure 3-2 Modified SAC Loading Protocol

3.2 Actuator Control System

For SMA Connection I, the actuator was controlled using a MTS Test Star Controller, and Test Control software running on a stand-alone computer. The Testware software allows the user to control the actuator during testing by specifying loading rate, desired displacement or force limits, and number of cycles. The Test-Control software is used for two functions: 1) to specify through what channels the actuator and control box communicate and 2) to define actuator parameters such as stroke and force limits.

For SMA Connection II, a MTS 407 controller was used. The advantage of this controller is that its function generators, valve and feedback drivers are self-contained and do not require a separate computer.

3.3 Instrumentation and Data Collection

The specimen was instrumented with a variety of sensors including 18 axial strain gauges, 3 three-element rosettes, up to 11 linear variable differential transducers (LVDT's), four temperature gauges, three load cells, and two string potentiometers. The data was collected from all the sensors using an OPTIM Electronics MEGADAC model 3415AC. It is capable of sampling data up to 25,000 times per second and has a maximum capacity of 300 channels of input. It also can provide a constant current and voltage excitation for most instruments.

Although the MEGADAC 3415AC is capable of storing 64 megabytes of data, it has no keypad or display; therefore, an external computer is used to control it remotely. OPTIM's TCS (Test Control Software) software running on the external computer, communicates with the MEGADAC and is used to export the data files from the MEGADAC to its hard drive.

The 43 channels of data were collected at a rate of 2 Hz, throughout the entire load history. Data was converted to ASCII format and downloaded to a remote computer after each load step. Data sets were converted to ASCII format and exported to a remote computer after every load step. Additionally, TCS can transform raw data into meaningful data such as moment-rotation curves for real-time monitoring.

3.3.1 SMA Connection I Tendons

Each tendon was fitted with two high elongation strain gauges (Tokyo Sokki Kenkujo Co. YFLA-5-1L, 120 ohm). These gauges were affixed in the center of the tendon and placed 180 degrees apart around the axis of the tendon (only one gauge was

used for SMA II). This gauge line was aligned with the plane of bending for the beam. Doing this allowed both axial and bending strains to be known within the tendon. Since the SMA tendons were going see very high cyclic strains (~ 8%), it was assumed the high elongation strain gauges may debond in the first few cycles. Since the strain would still need to be known, extensometers, with a range of 10% strain, were also placed on three tendons. Due to clearance problems with the welded tubes to the beam, the extensometers were not to be placed in the center of the tendon, but instead they were placed about 2" (51 mm) from the center of the tendon.

In addition to the two strain gauges, each tendon was also fitted with a temperature gauge (Tokyo Sokki Kenkujo Co. TFL-6). The temperature gauge looks just like a strain gauge however it varies its resistance based on temperature changes, not strain. This gauge was also placed in the center of the tendon, in between the two high elongation strain gauges. However, it was aligned perpendicular to the tendon axis as if it where measuring transverse strain. This was done to minimize any resistance changes in the gauge due to the axial strain in the tendon. The temperature gauges change resistance by as much as 60 Ohms through a temperature range of 200 C. This meant the MEGADAC data system could not be used to collect the data, and the temperature gauges were monitored by hand using a digital multimeter and results were recorded in a spreadsheet during the test.

During the heat straightening process, a non-contact pyrometer (OMEGA OS55O Series) was used to monitor the temperature of one tendon. The pyrometer is a device which measures temperature from a distance (~8" or 203 mm) through optical refraction.

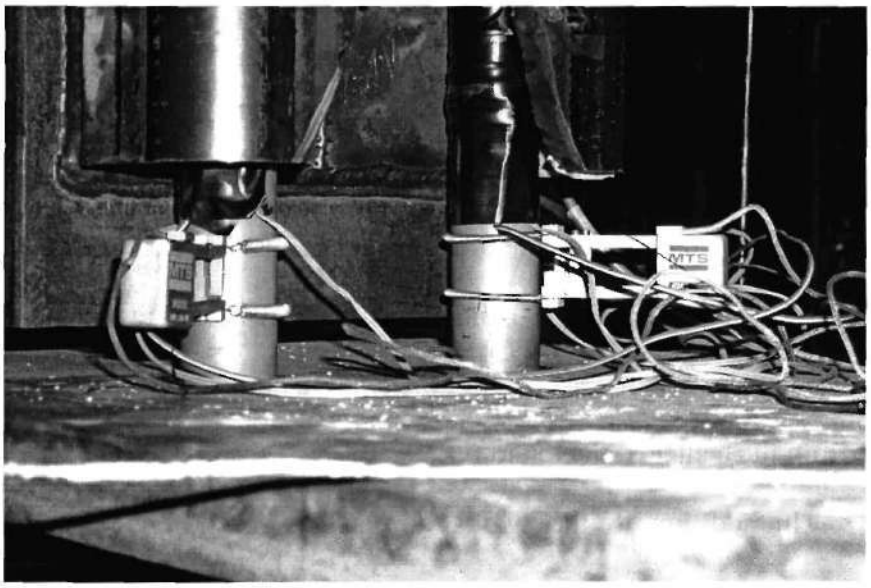

Figure 3-3 SMA I Tendon Instrumentation

Figure 3-4 Non-Contact Pyrometer

3.3.2 SMA Connection II Tendons

After the testing of SMA I, it was realized that the tendons in SMA Connection I were over instrumented. The data from SMA I showed that bending effects were negligible during the elastic cycles, and only one high-elongation gauge was placed in the center of the tendon for SMA II. The temperature gauges also showed a negligible temperature increase in the tendons during the cycling, therefore, they were not used in SMA Connection II. The same extensometers were still used during the testing of SMA Connection II.

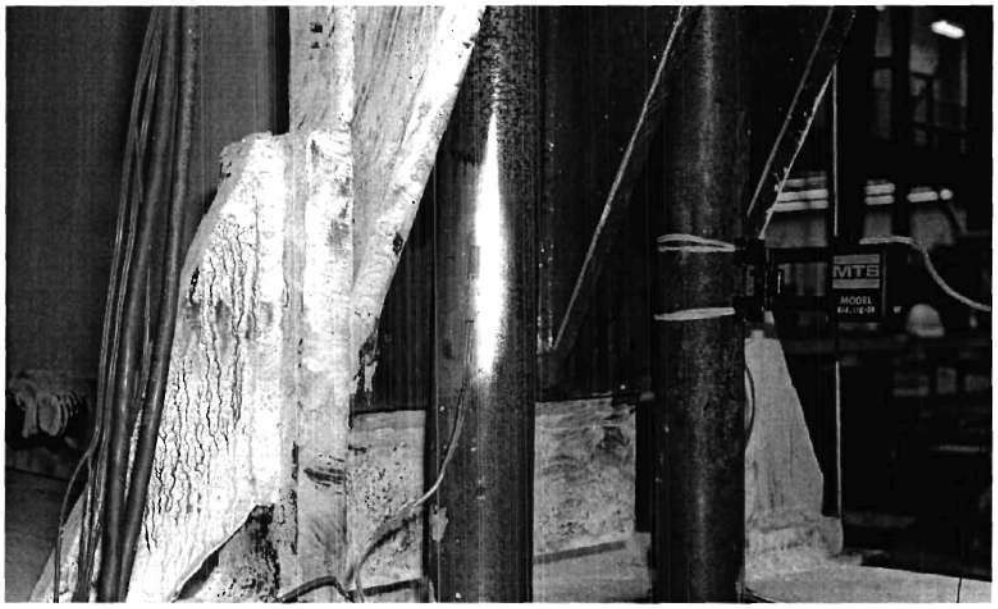

Figure 3-5 SMA II Tendon Instrumentation

3.3.3 Beam Instrumentation

Four linear variable differential transducers (LVDT's) were used to measure the rotation of the connection. Each 2" LVDT was placed on each flange tip of the beam to measure the concentrated rotation of the connection. The transducers were clamped to the flange at an approximate distance of one beam depth from the column face. Specifically, this distance was 25" for SMA I and 28" for SMA II. The cores were connected to small pieces of angle that were welded to the column flange directly below the transducers.

The beam was also fitted with six strain gauges. The gauges were placed on the extreme fibers of each flange. Each flange was fitted with three gauges, one directly over the web, one 1.0" from the flange tip, and one at the third point of the flange ($b_f/3$ from the flange tip). These six gauges were used to monitor the onset of flexural yielding that may occur in the beam section. They also served as a check to monitor how much moment was being transmitting by the beam.

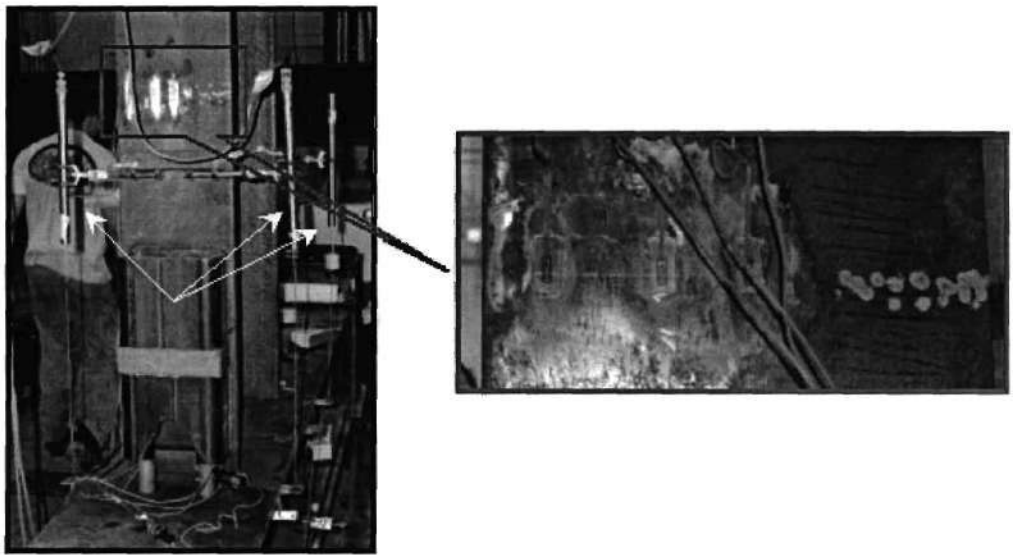

Figure 3-6 Beam Instrumentation

3.3.4 Column Instrumentation

Two LVDT's were placed in the panel zone to measure the shear deformations that occur due to rotation. To do this, four 0.5" (13 mm) steel rods were welded to the column web in the corners of the panel zone. To maintain the ability to weld, the center of each rod was placed 1" (25 mm) down from the column flange, to avoid the brittle k-region, and 1" (25 mm) away from the anchorage block. The rods allowed the LVDT's to be placed outside the column otherwise the column flanges would interfere with the placement of the transducers. The LVDT's attached to the rods such that each end of the LVDT was anchored on opposing corners of the panel zone. For SMA Connection I, 3" (76 mm) LVDT's were used, and were switched to 1/10" (2.5 mm) for SMA II to increase the measurement accuracy.

Displacement transducers were also attached to the bottom flange (that opposing the beam) to measure the rotation of the column. For SMA Connection I, two string potentiometers were attached to the center of the column flange, directly below the beam rotation LVDT's. The accuracy of these devices was found to be too coarse during testing, and these potentiometers were replaced with 1/10" (2.5 mm) LVDT's for SMA Connection II.

Four more axial strain gauges (Tokyo Sokki Kenkujo Co. WFLA-6-11-1L, 120 Ohm) were placed on the extreme fiber of the column, opposite of the beam. These four gauges were used to monitor the moment gradients that would occur due to rotation of the connection and to capture any hinging action that may occur.

Three strain rosettes (Tokyo Sokki Kenkujo Co. WFRA-6-11-3LT, 120 ohm) were also placed in the panel zone to measure the local axial and shearing strains, beyond the average given by the panel zone LVDT's. One rosette was placed in the center of the panel zone. The remaining two were placed near the top and bottom of one Bottom Anchorage Block, 2" (51 mm) away from the column flanges in a line directly below the beam flanges.

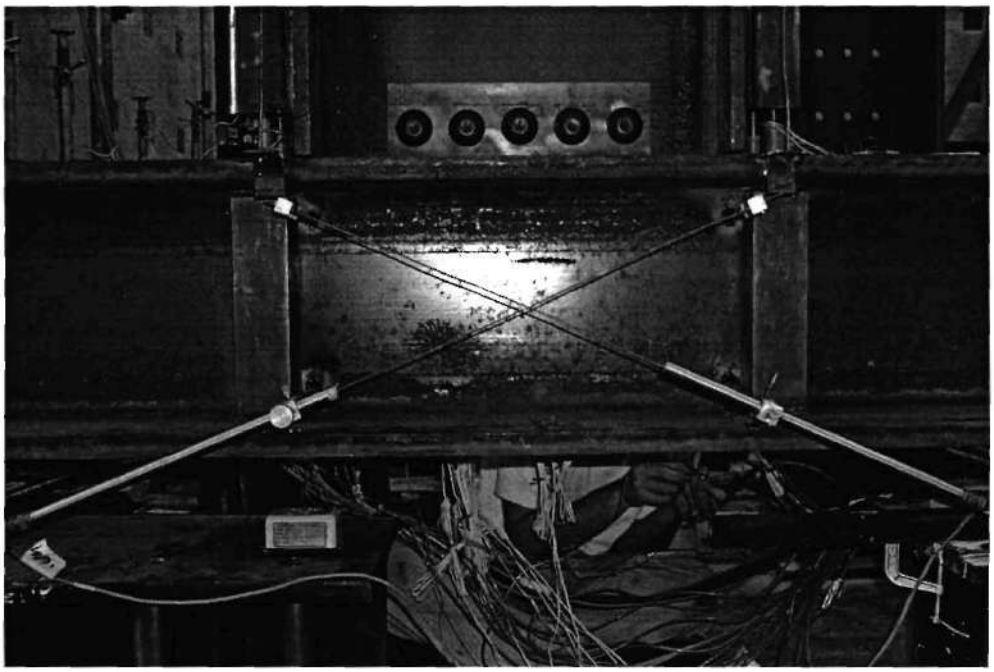

Figure 3-7 Panel Zone LVDT's

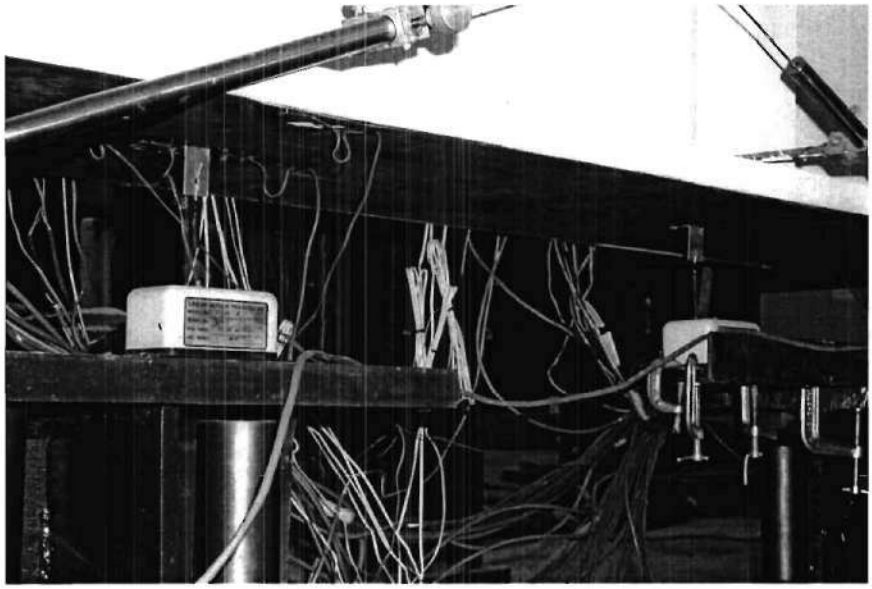

Figure 3-8 Column Rotation and Axial Strain Gauge Instrumentation

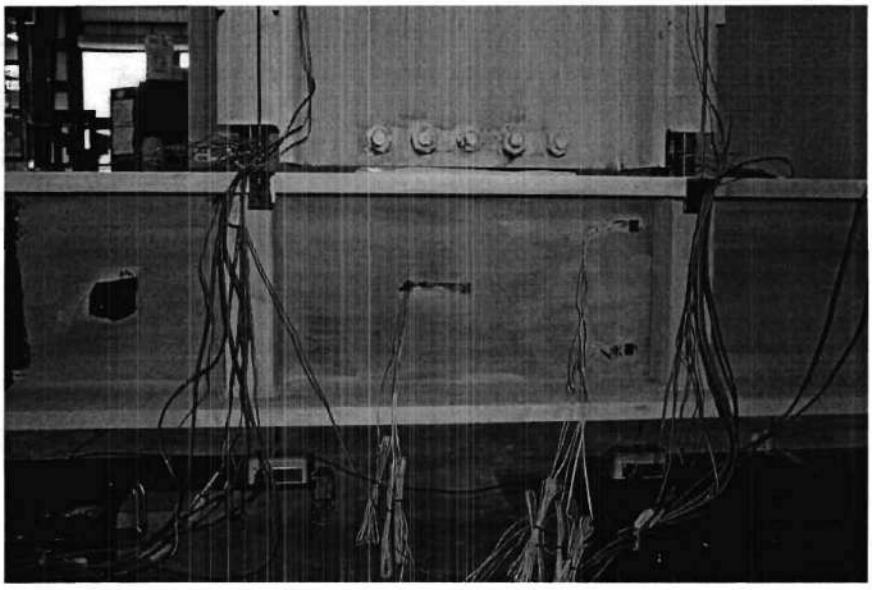

Figure 3-9 Panel Zone Strain Rosettes

3.3.5 Load Pins

The actuator (MTS 243.45) was fitted with a load cell to measure the force applied to the beam and a LVDT to measure the displacement of the piston, which corresponds to the beam tip displacement. The remaining two load cells were used in the pin connections between the column and the load frame. These load cells were a combined structure that offered a rotating pin and load cell all in one device. These load pins were set up to measure the force in the pin normal to the floor.

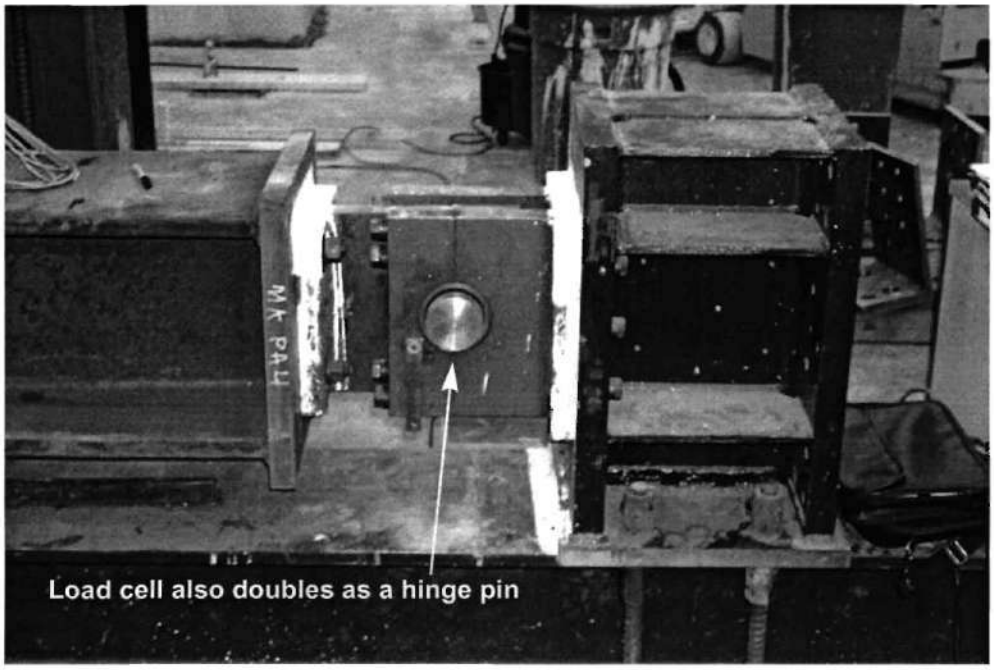

Figure 3-10 Load Pin Assembly

CHAPTER IV

SMA CONNECTION I EXPERIMENTAL RESULTS

This chapter provides a summary of the data collected during the full-scale SMA I connection test. All major events are also documented as they occurred throughout the test.

4.1 Testing Events

The initial loading tests were run in displacement control in accordance with SAC Protocol load history. This load history is outlined in more detail in Section 3.1 and Table 3-1 shows the stepwise loading increments used in the initial test. The fixed displacements were applied to the tip of the beam using the MTS hydraulic actuator at a rate of 2"/min. (51 mm/min.).

First, a sequence of six elastic cycles at 0.2% drift were applied to ensure the data and actuator systems were running properly. These were followed by the first two load steps of the SAC protocol. No surprising events occurred through the first two load steps. After insuring the integrity of the data being collected, the rest of the testing began on July 27, 2000.

In the fourth cycle of the 0.75% drift level, the first worthwhile event was loud pops emanating from the connection, indicating the bolts were slipping on the shear tab. This popping noise continued for the remainder of the test. In the middle of the 1% drift load step, the hard oxide coating on the SMA tendons was found to be flaking off as shown in Figure 4-1. The maximum strain in the tendons up to this point was 0.5%, however, the live data plotting had not yet shown that the SMA tendons had reached their plateau stress.

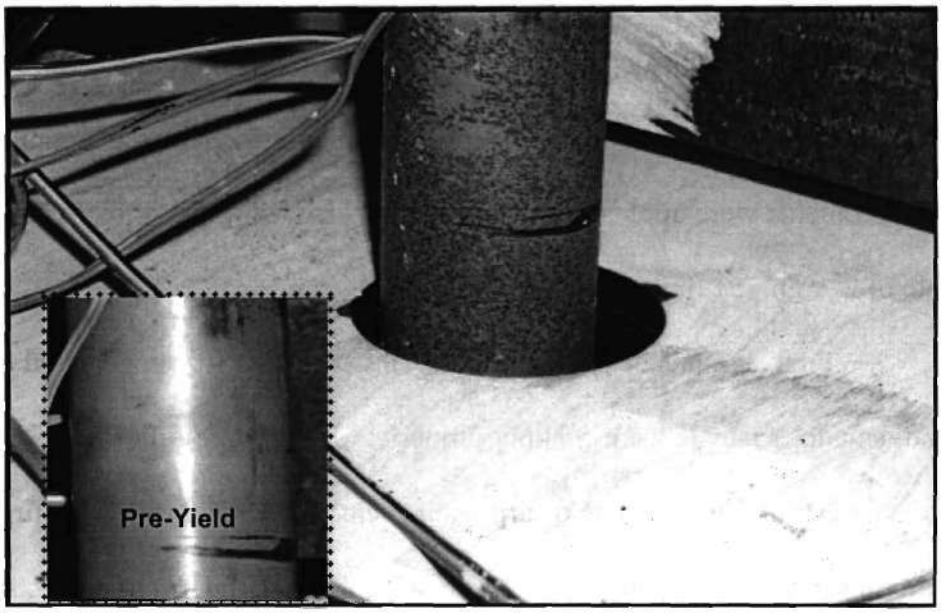

Figure 4-1 SMA I Tendon Yielding

During the 1.5% drift load step, the Top Anchorage Block, on the Top Side of the beam was noticed to have slipped about ~3/16" (5 mm) to the South[1] and ~1/8" (3 mm) away from the beam flange (see Figure 4-2). There were no sudden indicators (popping noise, or load drop) of this, meaning it must have been a slow, gradual process. This was originally thought to have been caused by the tendons straightening themselves out under load from any misalignments that may have been locked in during construction. The later load steps proved this to be the wrong conclusion.

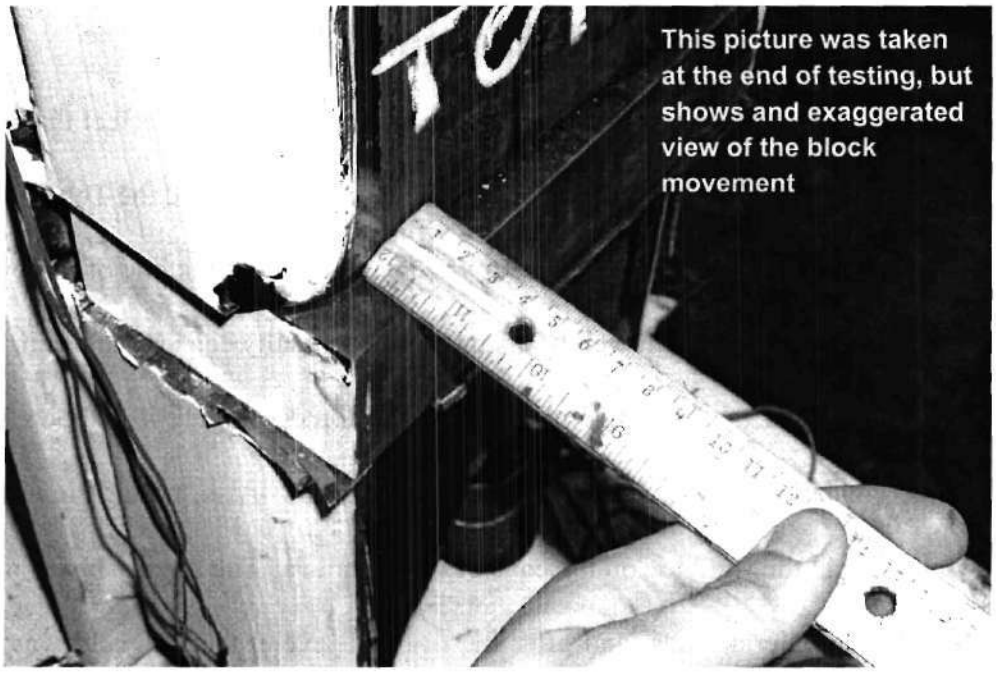

Figure 4-2 Unrestrained Top Anchorage Block Movement

1.See Figure 2-2 for convention of Top, Bottom, North, and South sides

In the first cycle of the 2% drift load step, the Top Anchorage Block on the bottom side of the beam was noticed to have slipped. The amplitudes were not measured but they were approximately the same as the other block. Again, there were no sudden, significant indications of this happening, indicating it was a gradual slipping of the block.

The 3% drift cycles started to show more activity. During the initial displacement of the load step, a few shims holding the Top Anchorage Block in place were observed to fall out. Then, later in this load step, the SMA tendons in compression were observed to be severely buckled. Figure 4-3 shows a picture of the large lateral displacement of the buckled tendons. After this was noticed, it was clear that the anchorage blocks offered little restraint against translation, and the only reason the blocks moved was to accommodate the buckling of the tendons.

The buckling of the SMA tendons caused a secondary effect that was the reason for stopping the first test. Once the buckled tendons had shifted the Top Anchorage Block enough, a small, out-of-plane moment was created because the line of force was no longer symmetric about the beam web. This moment eventually caused the beam flange to warp around the shear tab in an attempt to align the forces. Figure 4-4 shows how the beam flange yielded as it was warped around the shear tab. Also, notice the disappearance of whitewash at the weld toe on the ends of the shear tab. The shear tab was not designed to handle such lateral loads, and after the 4% drift cycle, the tab weld was noticed to be fractured, about 2" (51 mm) on each end (see Figure 4-5). For fear of a sudden brittle fracture in the shear tab weld, the test was stopped before a second 4% drift cycle could be completed.

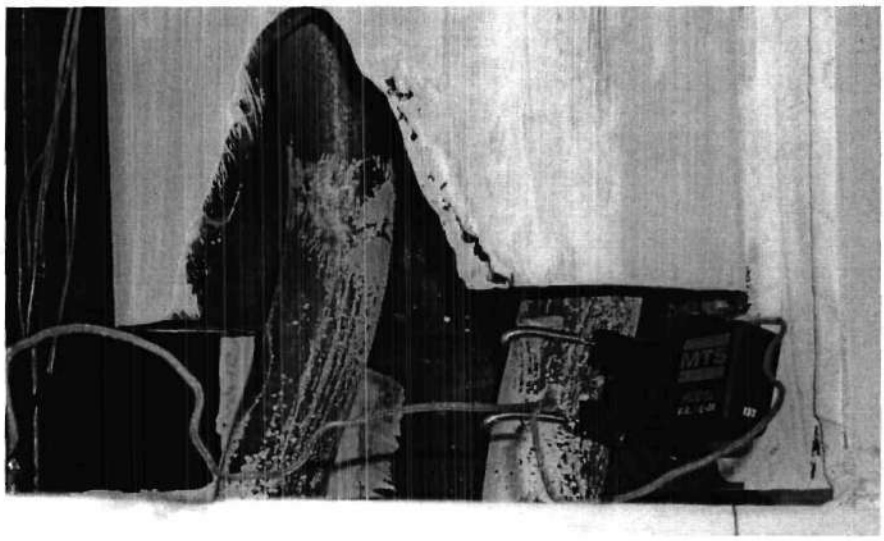

Figure 4-3 Tendon Buckling Under Compressive Load

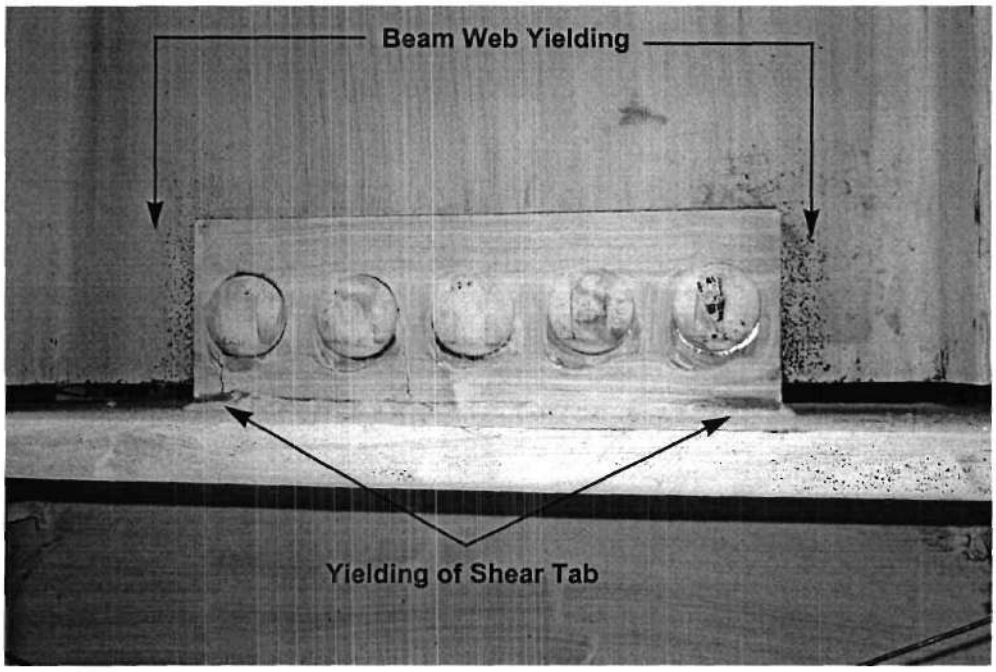

Figure 4-4 Yielding due to Beam Flange Warping

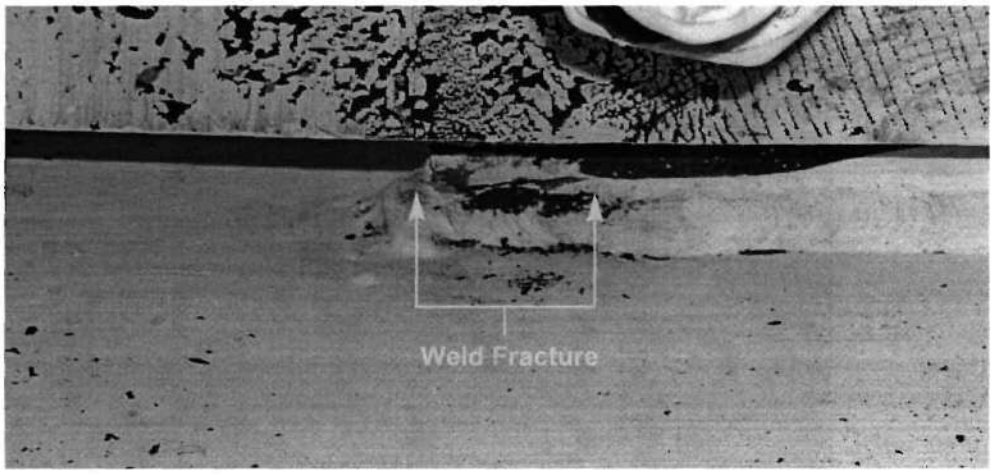

Figure 4-5 One inch Fracture in Shear Tab Weld

4.2 Experimental Results of Initial Test for SMA Connection I

Figure 4-6 shows a plot of the actuator load versus beam tip displacement throughout the entire load history. The maximum displacement corresponded to the 4% drift cycle with a magnitude of 7.14" (181.4 mm), which corresponds to a load of 31.8 kips (141.5kN) at the beam tip.

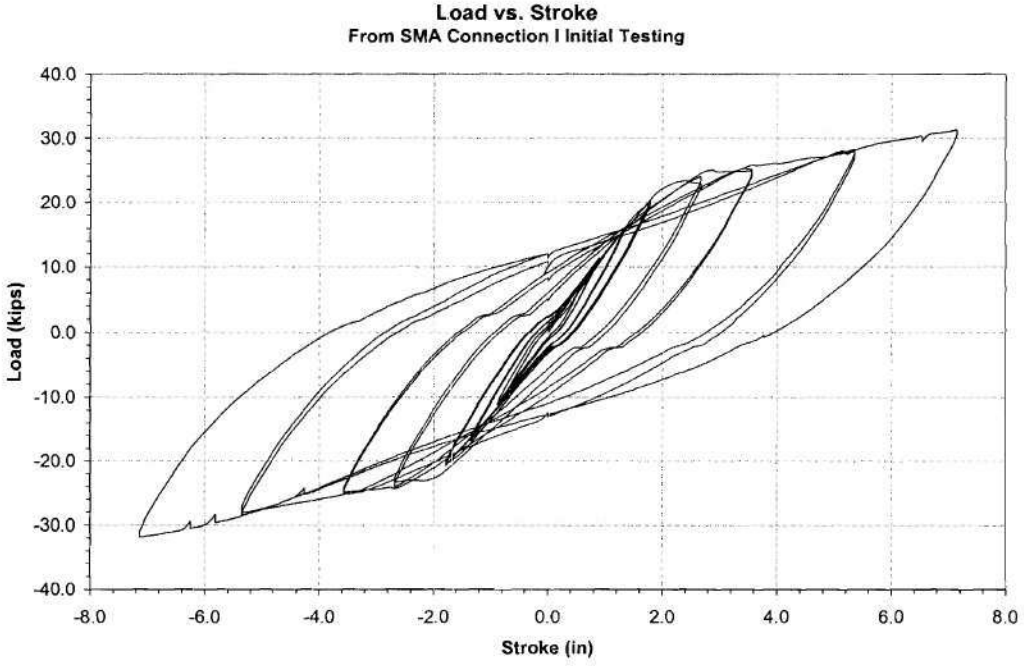

Figure 4-6 Load/Displacement History of SMA Connection I

Figure 4-7 displays the plot of moment in the connection (actuator load * beam length) versus the total rotation (actuator displacement / beam length) of the connection, and thus has exactly the same shape as Figure 4-6. The maximum moment attained was 5,677 kip-in (641 kN-m). Since the nominal plastic moment capacity of the beam is 12,700 kip-in (1435 kN-m), $M_{connection}/M_p = 0.45$. As this ratio is much less than unity, this prototype can be classified as a partial strength (PS) connection.

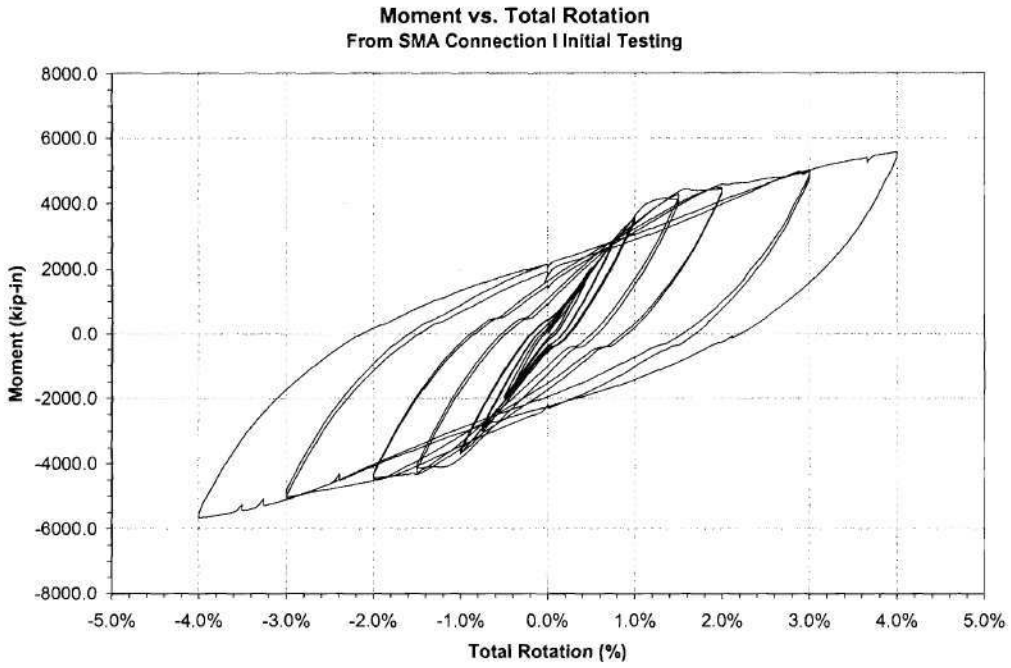

Figure 4-7 Moment/Total Rotation History of SMA I

Several characteristics of the Moment/Total Rotation curve should be noted. First, the 3% and 4% drift cycles are much flatter (less slope) than the early cycles, indicating that significant yielding in the tendons was occurring during the larger cycles. Second, there are no pronounced stiffness increases at large rotations in the higher cycles. This is due to the relatively small degradation of the behavior in the SMA connection, whose behavior was almost elasto-plastic. This attribute can also be used to infer that the hardening region of the SMA material (see Figure 2-1) was not encountered. Finally, the deformation capacity of the connection is excellent - evidenced by the large area and steady size increase of the hysteresis loops. The total area of the hysteresis loops is 1141 kip-in. (130 kN-m). However, this energy dissipation only included the cycles from the initial testing. The test was stopped for extraneous reasons with only one 4% drift cycle completed. However, if the beam were restrained from warping, many more 4% drift cycles should be possible given the nature of the SMA.

Figure 4-8 shows a plot of the moment versus the concentrated rotation measured by the LVDT's on the beam. This plot is similar to the Moment/Total Rotation plot, but one important item can be deduced from it. The beam had a maximum rotation of 4% drift: however, Figure 4-8 shows the maximum concentrated rotation was 3.8% drift. The remaining 0.2% drift can be accounted for in the rotation of the column and panel zone deformation, which can be found in Appendix A. However, since there was no inelastic behavior in the beam or column, the 3.8% concentrated rotation must have been due solely to the SMA tendons. This means the tendons can be accounted for 95% of the connection's deformation.

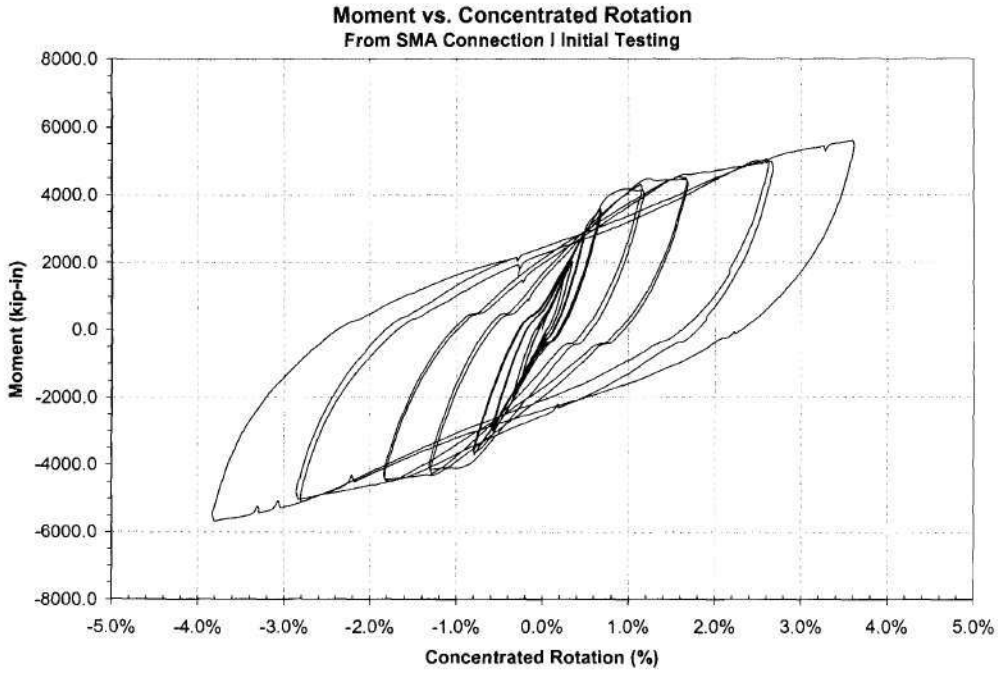

Figure 4-8 Moment/Concentrated History of SMA I

The reliability of the data collected from the SMA tendon instrumentation is uncertain. Even though the tendons were fitted with several devices to record axial and bending strains, buckling of the bars and debonding of the post-yield gauges makes deciphering much of the recorded data very difficult[1]. Figure 4-9 shows a plot of the stress versus strain relationship of SMA tendon #3 (Top-South tendon) using an extensometer. The remaining plots for the other tendons with extensometers can be found in Appendix A. The other two extensometers were in the area of the tendon that buckled. This rotated the extensometer and caused them to slip. The data from these sensors was thought to be skewed because of this slip, and were thus their data needs to be interpreted carefully.

The tendons remained linear elastic up through the 1% drift cycles. Since service load levels in a structure correspond to approximately 0.3% drift, the SMA connection would certainly be elastic at service load levels. The SMA appears to also have more deformation capability in compression than tension. This is probably due to the buckling that occurred with the compression tendons, otherwise the behavior would be less symmetric. One point should be made, the tendon saw a maximum strain of 5.2%, but the SMA should be capable of at least 8% strain before plastic flow initiates. This only reinforces the fact that the connection should be capable of more intense drift cycles than the experimental connection was subjected to.

1.No load cell was attached to the SMA tendons, therefore, force in the tendon was calculated through static equilibrium inside the connection (Moment / d_b+4").

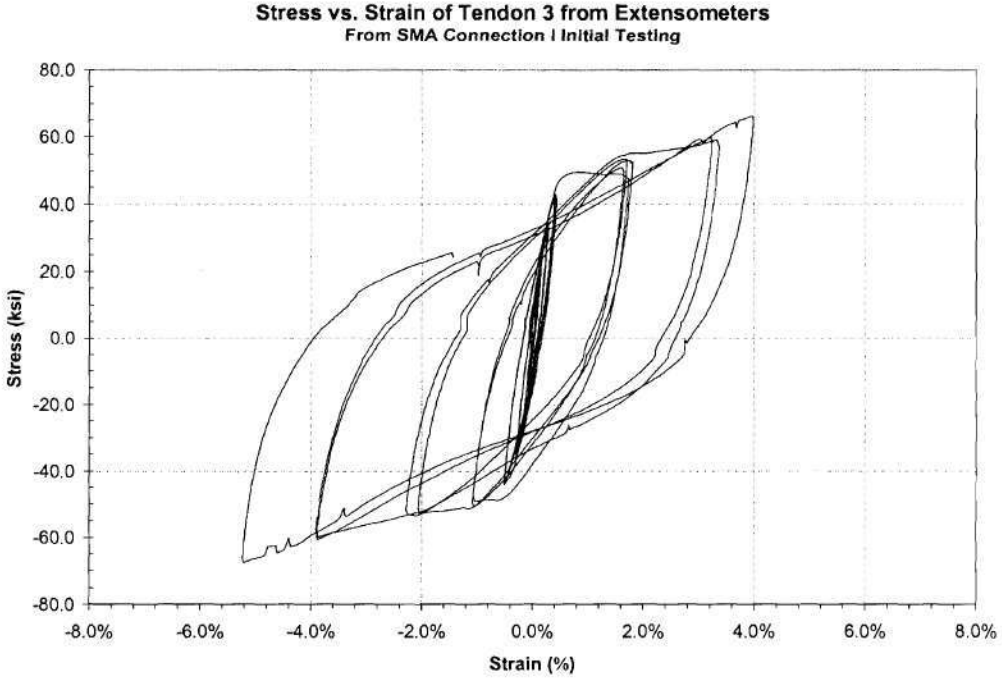

Figure 4-9 Tendon Stress/Strain History from SMA I

4.3 Tendon Heat Straightening

Theoretically, heating the SMA tendons past their A_f temperature would trigger the "memory effect" - returning the SMA tendons to their original shape and recover the -0.92" (-23.4 mm) of residual tip deflection. Prior to heating, how much restoring force the tendons could impart on the connection when heated was unknown. Therefore, whether the tendons could straighten themselves and overcome the beam warping and shear bolt friction was questionable. Two different devices were used to heat the tendons, first a heat tape (BriskHeat Corporation) and then propane gas torches (Benzomatic SureFire). A thermal pyrometer (OMEGA OS55O Series) was used to measure the surface temperature of one tendons. Tendons were heated in pairs; not all four at the same time. All tendon instrumentation was removed before heating the tendons.

Heat tape was used as the first heating device because the tape's ability to "wrap" around the specimen and heat it from all sides was appealing. The Bottom Side tendons (tension side) were wrapped and heated for a total of 135 min. with a maximum temperature of 284 F (140 C). The rate and time to reach the A_f (205 F / 96.1 C) were 0.06 F/sec. (0.033 C/sec.) and 35 min., respectively. With the actuator in displacement-control mode, the force in the actuator was monitored for sudden increases due to tendon rebound. However, no significant actuator load jumps, were noticed and tip displacement recovery was less than 0.1" (2.5 mm).

Since slow heating is undesired for triggering the SME and can even "erase" it, a faster way of heating the material was necessary. Two propane/MAPP gas torches were used to heat the Bottom tendons again. This time, the tendons were heated for 30 minutes.

The initial temperature rate was 1 F/sec. (.56 C/sec.) until the temperature stabilized around 550 F (288 C) in the 8th minute. It took only 4 min. to reach the A_f temperature. However, the tendons showed no signs of any additional rebound.

Finally, the Top tendons (compression side), which had not been heated with the tape, were heated using the torches. Instead of waiting for the tendons to pull on the actuator, 5 kips (22.2 kN) of load was put in the direction of rebound to help the tendons "remember". The heating procedure and therefore the temperature in these tendons followed the same trend as during the torching of the Bottom tendons. The results, however, were completely different. During the first 5 min., the actuator force decreased steadily from 5 to 2 kips (22.4 to 8.9 kN), equivalent to ~19 kip (84 kN) total release in the two tendons. After this initial recovery, the results were minimal. When the Bottom tendon torching was finished, ~0.6" (1.5 cm) of the tip displacement had been recovered to give a total of 0.7" (1.8 cm) recovered after all the heating. This is approximately 75% of the residual tip displacement.

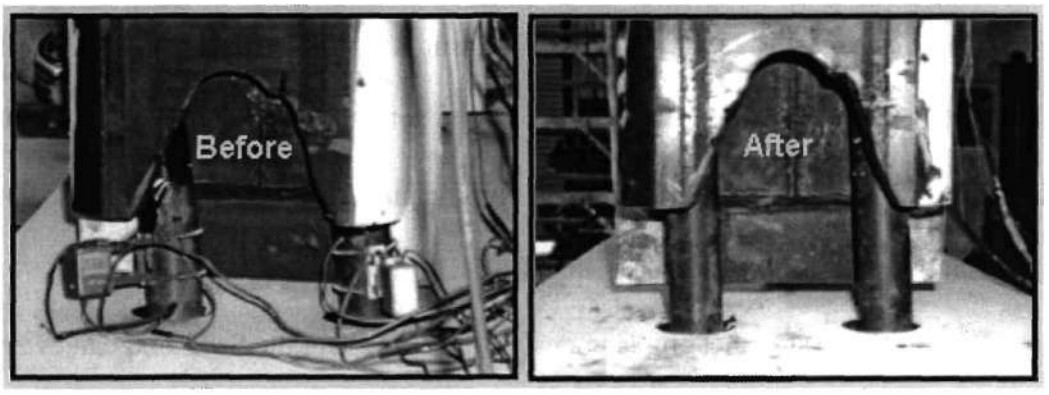

Figure 4-10 Tendons Before and After Heating

4.4 Retesting of SMA Connection I

Once the tendons were straightened, modifications were made to the connection, so testing could continue until failure. First, small sections of angles were welded to the column flange next to the beam flanges. These angles provided lateral support against warping of the beam flanges. Second, the Top Anchorage Block was welded to the rectangular tubes so its movement could also be restrained. Since heating the tendons did not relieve all their residual strain, C-clamps were used to force the Top Anchorage Blocks into place before welding. The last modification was to address the shear tab weld fracture. The solution was to layer on a thicker fillet weld, all the way around the existing weld. Figure 4-11 illustrates these modifications.

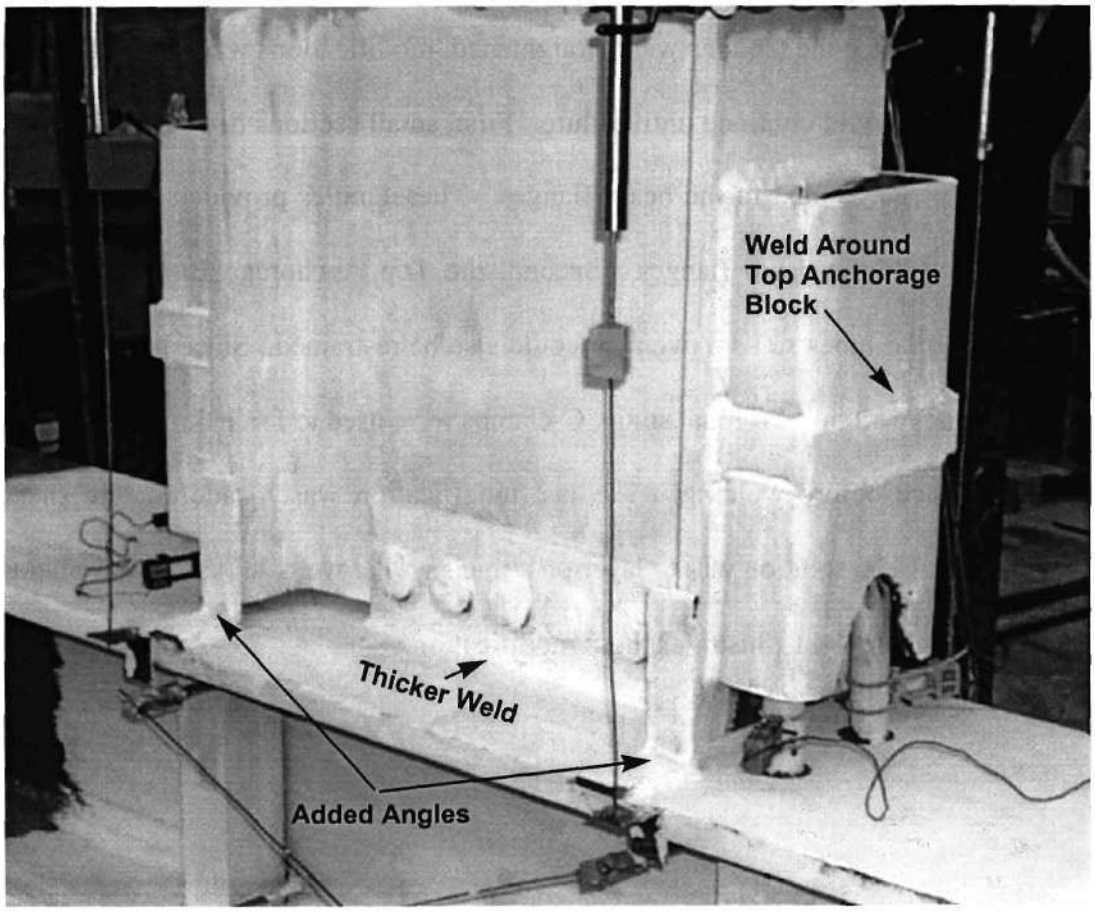

Figure 4-11 Connection Modifications to SMA I

The loading history for the retesting consisted of one 1%, 2%, 3%, and twenty 4% drift cycles at a rate of 4"/min. (102mm/min.). The specimen made it through the eighth, 4% cycle when a very loud noise came from the load frame. There was a slight drop in load, and one of the tension tendons was found to have fractured. The loading was resumed for a few seconds until the other tension tendon fractured. Figure 4-12 shows the fracture surface of one of the broken tendons. Notice how the fracture occurred at the cross-sectional transition fillet. This small fillet gave rise to a high stress concentration in the presence of a combined axial and bending load, which was thought to be the cause of the fracture.

Figure 4-12 Fracture Surface of a SMA I Tendon

4.5 Experimental Results of Retest for SMA Connection I

Until the tendons fractured, the connection exhibited interesting behavior. Figure 4-13 shows the Moment/Total Rotation curve for the load history of the second testing. Observe how the hysteresis loops are one on top of the other for eight consecutive 4% drift cycles. This means the SMA exhibits no strength degradation after many severe stress reversals. Integrating the interior of the hysteresis loops found the second test dissipated 2825 kip-in (319 kN-m) of energy.

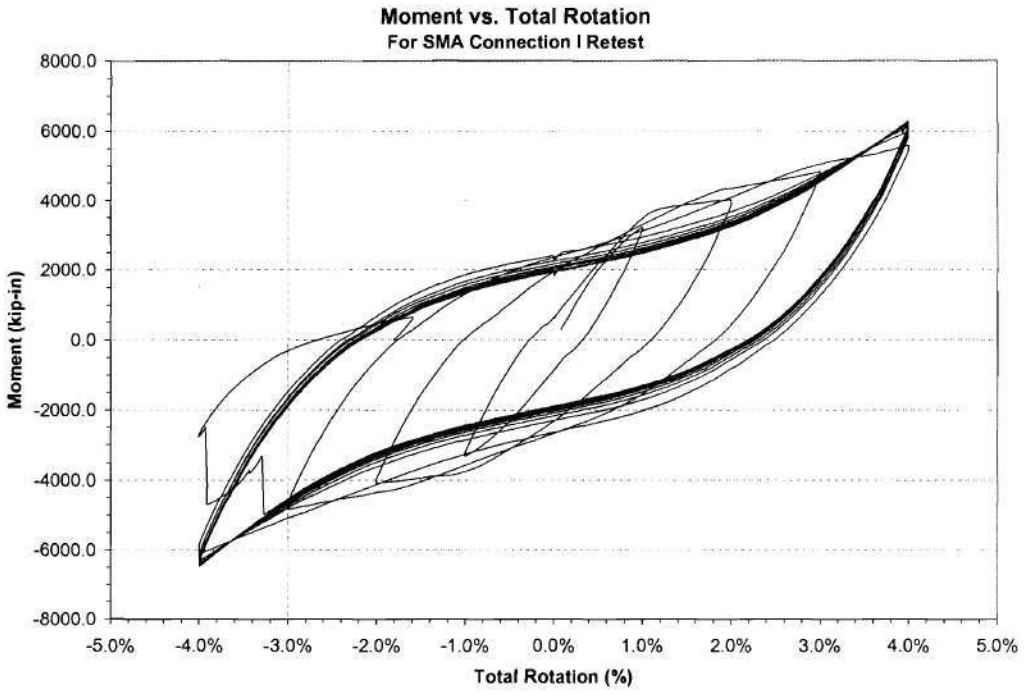

Figure 4-13 Moment/Total Rotation History of SMA I Retest

CHAPTER V

SMA CONNECTION II EXPERIMENTAL RESULTS

This Chapter is intended to provide a summary of the data collected during the full-scale SMA Connection II test. All major events are also documented as they occurred throughout the test.

5.1 SMA Connection II Initial Testing Events

After the first two displacement levels (0.375% and .5% drift) of the SAC Protocol were performed, the data was downloaded and analyzed for inconsistencies. The testing continued the next working day after ascertaining that both the data acquisition and controlling systems were functioning correctly.

The next working day, the rest of the SAC Protocol was continued beginning with the 0.75% drift cycles. Approximately, in the third cycle of this displacement cycle, the tendons were first noticed to begin scaling, a sign that yielding may be occurring. However, it was not until the first 1% drift cycle that the strains in the SMA tendons reached their constant stress plateau, evidenced from the strain gauge data.

Once testing progressed into the 1.5% drift cycles, the beam flanges were noticed to be engaged against the restraining angles, an indication that tendons had begun to buckle. This first occurred at the second peak of the first 1.5% drift cycle when the Bottom South restraining angle became engaged[1]. Once the cycle reversed, the Top South

restraining angle also engaged. For the remainder of the test, these beam flanges came into contact with the same two restraining angles, at appropriate points in the loading cycle. The testing continued until two 4% drift cycles were completed. This is not in accordance with the SAC Protocol, which would require pairs of more intense drift cycles in increments of 1% until connection failure. Only two 4% drift cycles were used since it was the same loading history that SMA Connection I went through before the tendons were heated up for the first time. At the end of testing, the beam was left with -3.4" (88.4 mm) of displacement, which corresponds, to -1.95% drift.

1.See Figure 2-2 for convention of Top, Bottom, North, and South sides

5.2 Experimental Results of Initial Test for SMA Connection II

Figure 5-1 shows a plot of the actuator load versus beam tip displacement throughout the entire load history. The maximum displacement corresponded to the -4% drift cycle with a magnitude of -7.17" (-182.1 mm), which created a load of -32.5 kips (-144.6 kN) at the beam tip.

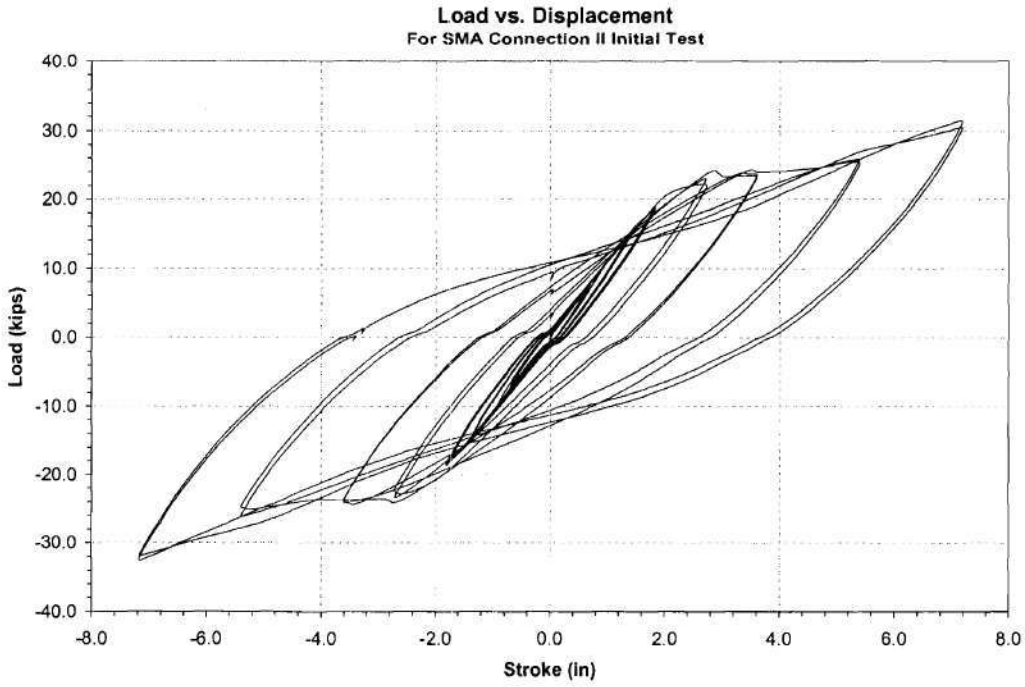

Figure 5-1 Load/Displacement History of SMA II Initial Test

Figure 5-2 displays the plot of moment in the connection versus the total rotation of the connection. The maximum moment attained was -5813 kip-in (656.7 kN-m), which is 86.8% of the beam's plastic moment. Integrating the area under all the hysteresis loops found the connection dissipated 1174 k-in (132 kN-m) of energy.

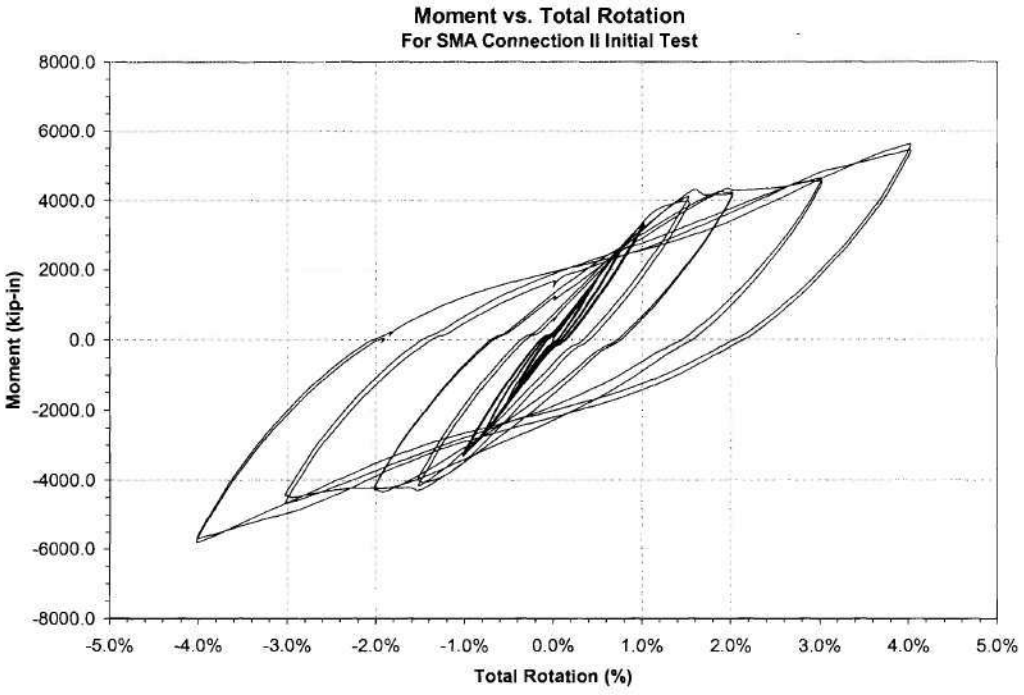

Figure 5-2 Moment/Total Rotation History of SMA II Initial Test

The Moment/Concentrated Rotation plot, as seen in Figure 5-3, shows similar behavior to SMA Connection I. As with the first connection, the concentrated rotation is a large portion of the total rotation. In this case the maximum concentrated rotation at the final displacement level was 90% of the total 4% rotation. As in SMA Connection I, no inelastic behavior in the beam or column meant the SMA tendons accounted for all this deformation.

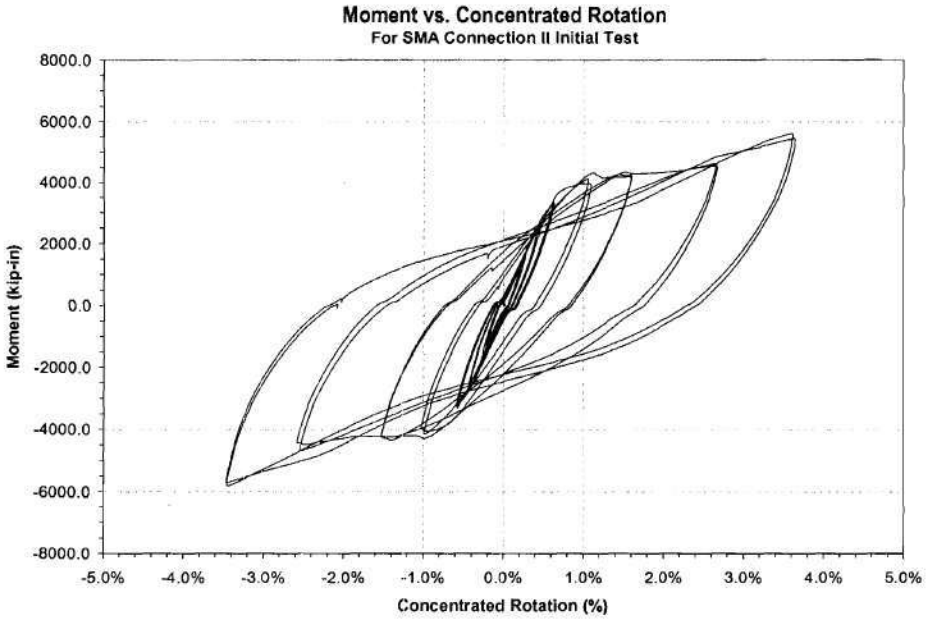

Figure 5-3 Moment/Concentrated Rotation History of SMA II Initial Test

Figure 5-4 shows the stress/strain history of one tendon in the connection. The plot for Tendon #2 was chosen because it was most symmetric and least congested than the other three tendons. As with SMA Connection I, the tendon remained primarily elastic through the 1% drift cycles, and the stress plateaued in the first 1.5% drift cycle.

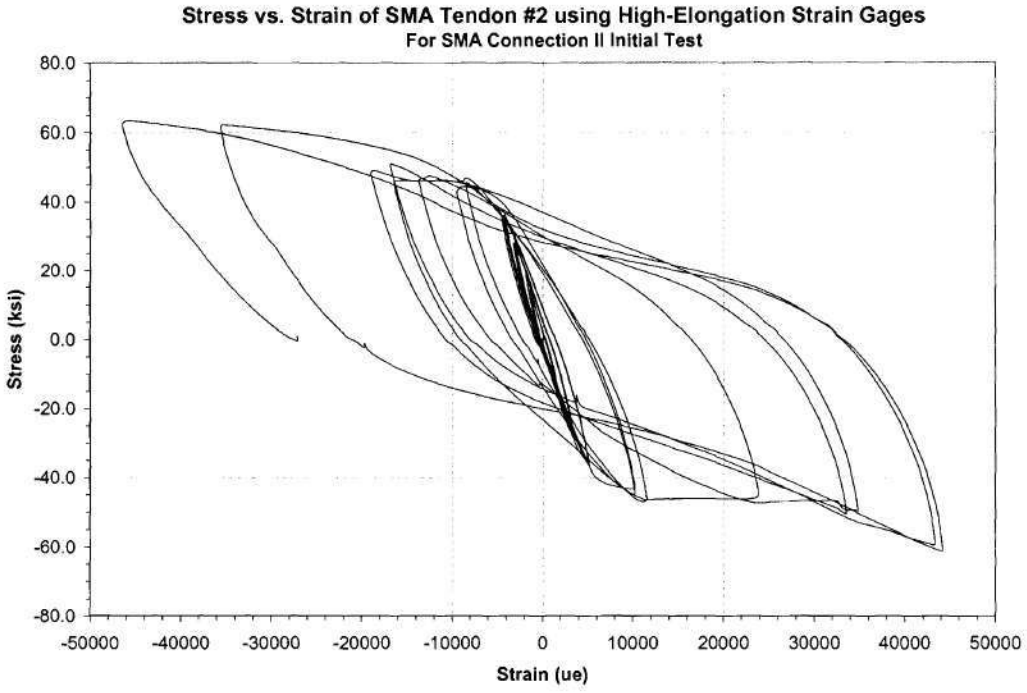

Figure 5-4 Stress/Strain History of SMA II Tendon 2

5.3 First Tendon Heat Straightening

In a real-world connection of this type, the tendons will always have load in them due to the dead load in the structure. This dead load influence was thought to affect the rebounding behavior of the SMA tendons, and thus the tendons were heated while a constant load was applied to the beam. The constant load was created by putting the actuator into load control, with -10 kips (44.5 kN) applied to the beam tip. This load corresponds to approximately 20 ksi (138 MPa) of stress in each tendon. It must be noted that the load was applied in a direction resisting the movement due to the tendons straightening out. Problems with the actuator controller caused an extra 0.5" (13 mm) of beam tip displacement to be added from where it was left after the initial SAC Protocol loading. This brought the residual tip displacement to -3.937" (-100 mm). Once the -10 kips (-44.5 kN) of load was applied to the beam tip, the beam displacement was brought to -4.963" (-126 mm). Each side of the connection, was heated simultaneously with one propane torch and one Mapp gas torch (see Figure 5-5). The first heating cycle lasted for 15 minutes and recovered 0.787" (20 mm) of tip displacement. Since these results were less than desirable, it was concluded to change the load in the actuator to +0.5 kips (2.2 kN) to help tendons; this brought the tip displacement to -2.999" (-76 mm). The tendons were heated for an additional 12 minutes, which recovered another 0.768" (19.5 mm). In total, 1.555" (39.5 mm) of tip displacement was recovered, which is only 41.9% of the total.

After the second heating cycle, a thermocouple was used to measure the surface temperature of one tendon. The surface temperature was measured to be 490 F, but it was also noted, this temperature was not uniform along the length of the tendon.

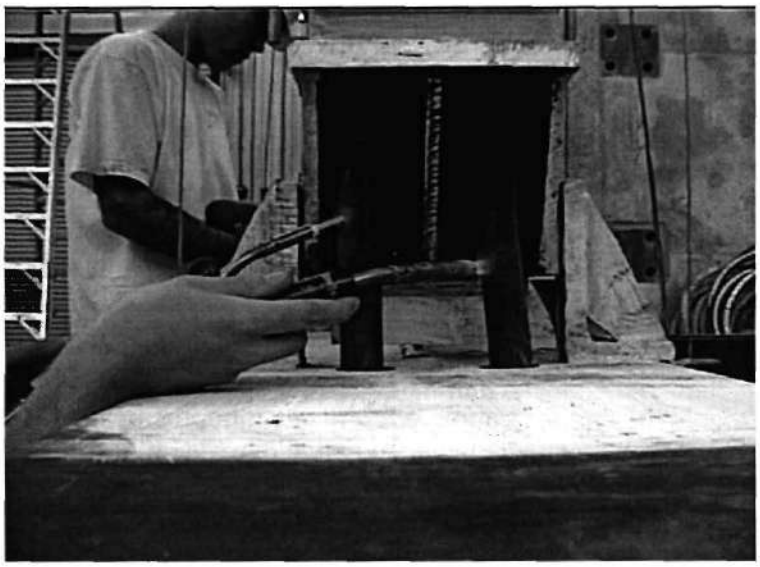

Figure 5-5 Tendon Heating with Propane/MAPP Gas Torches

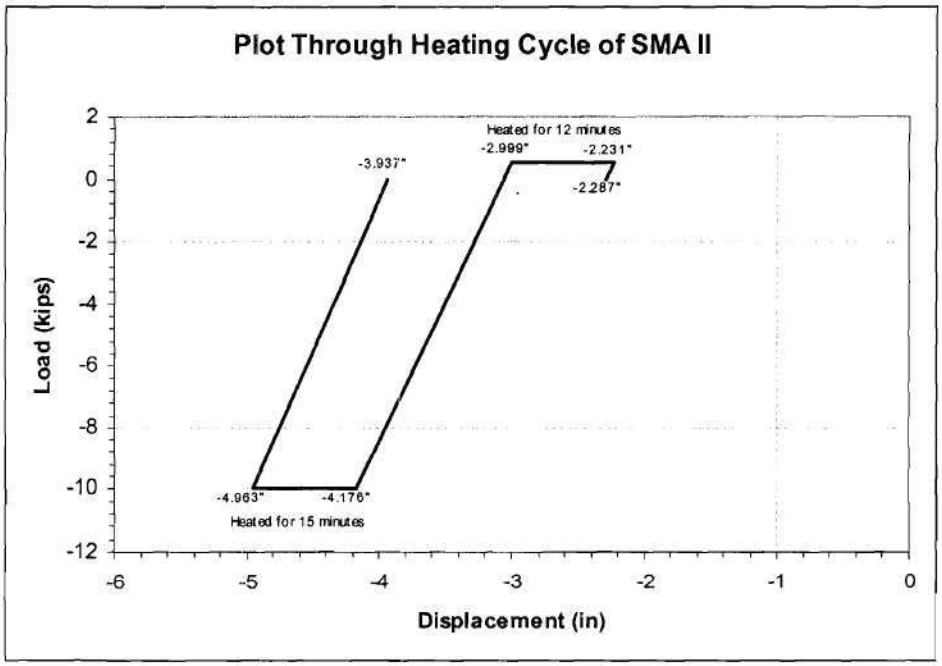

Figure 5-6 Load/Displacement History Through First Tendon Heating

5.4 Second Tendon Heating

In an attempt to apply more heat quickly, an oxy-acetylene torch with a #8 rosebud was used to reheat the tendons. The flame temperature of the rosebud was measured with a thermocouple to be around 2372 F (1300 C).

The actuator was kept in load control with +0.8 kips (3.6 kN) of load applied at the beam tip. One side of the connection was heated with the oxy-acetylene torch while the other side was kept "warm" with two Mapp gases used from the first heating, and the torches alternated sides every two minutes. After 12 minutes of heating, very little beam tip displacement was noticed and the tendon temperatures were measured to be about

392 F (200 C). After reading such a low temperature, the heating continued, this time moving the torches more slowly across the tendons. The tendons were heated for an additional 15 minutes but after 6 minutes it was noticed that most of the beam tip displacement happened with the acetylene torch heating the Bottom Side of the connection (the Bottom Side tendons were those which were left in the buckled condition after the initial testing). The remaining nine minutes of heating kept the acetylene torch on only the Bottom Side of the connection. After this, the tendon surface temperatures were measured to be 752 F (400 C). The temperature at the top, center of the tendon was measured to be 572 F (300 C) (see Figure 5-7). This was thought to give an indication of how hot the center got since this part of the tendon never saw flame from the torch being that it was inside the anchorage block

Through all 24 minutes of heating, only another 0.503" (13 mm) of beam tip displacement was recovered, this meant the beam tip displaced 2.058" (52 mm) through the two heating iterations which corresponds to 47.7% total recovery.

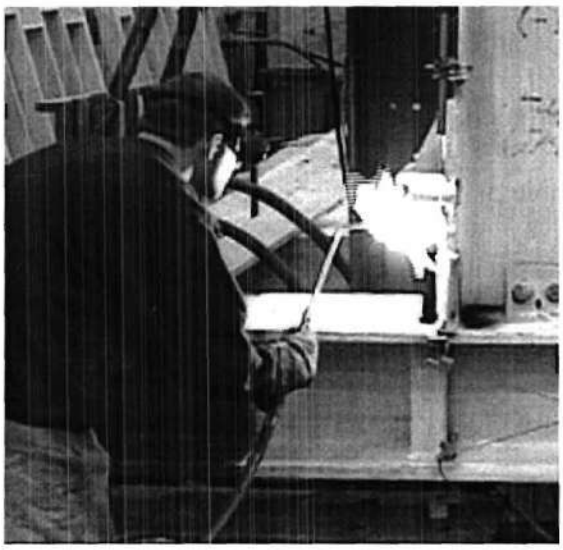

Figure 5-7 Oxy-Acetylene Torching

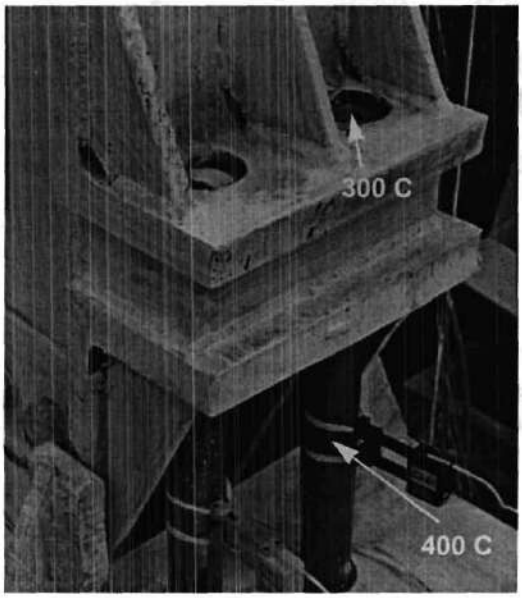

Figure 5-8 Tendon Temperature Gradient After Acetylene Torching

5.5 SMA Connection II Retest

The specimen was again cycled in displacement control according to the modified SAC protocol, outlined in Chapter 3.

No problems were encountered during the loading history for the retest, and no significant events occurred. The only event recorded was the noise made from the tendons rubbing against the beam as the tendons buckled. Also, the tendons were warm to the touch (~110 F) after all 8 - 4% drift cycles were complete.

Figure 5-9 Evidence of Tendon Rubbing

5.6 Experimental Results of Retest for SMA Connection II

This section outlines selected data from the testing of SMA Connection II, all other data can be found in the Appendix B

Figure 7-12 shows a plot of the actuator load versus beam tip displacement throughout the entire load history. The maximum displacement corresponded to the -4% drift cycle with a magnitude of -7.17" (182 mm), which created a load of -30.9 kips (137.5 kN) at the beam tip.

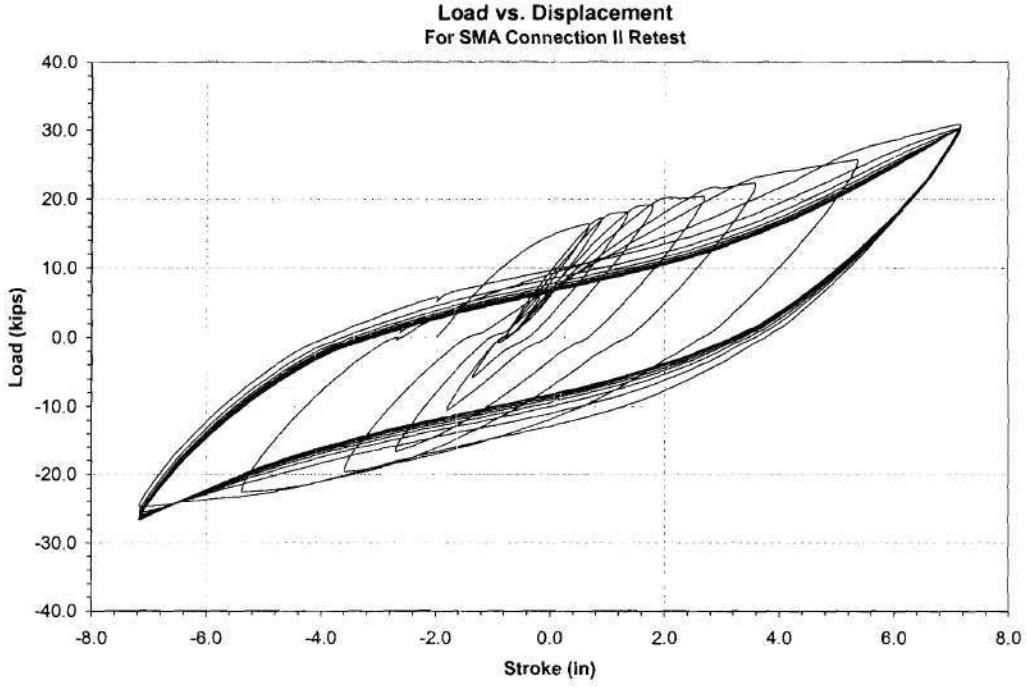

Figure 5-10 Load/Displacement History of SMA II Retest

Figure 5-11 shows the moment versus total rotation of SMA Connection II during the retest. The first thing to be noticed is the unsymmetric behavior of the connection in the early cycles. This was probably due to the fact that after both heating cycles, the buckled tendons never totally straightened out. Since the tendons were pre-buckled before the retest began, the small drift cycles did not induce enough beam tip displacement that could cause the pre-buckled tendons to straighten out. However, after the first 4% drift cycle, the connection seemed to work itself into symmetric behavior. At the end of the retest, the connection dissipated another 1906 k-in (215 kN-m).

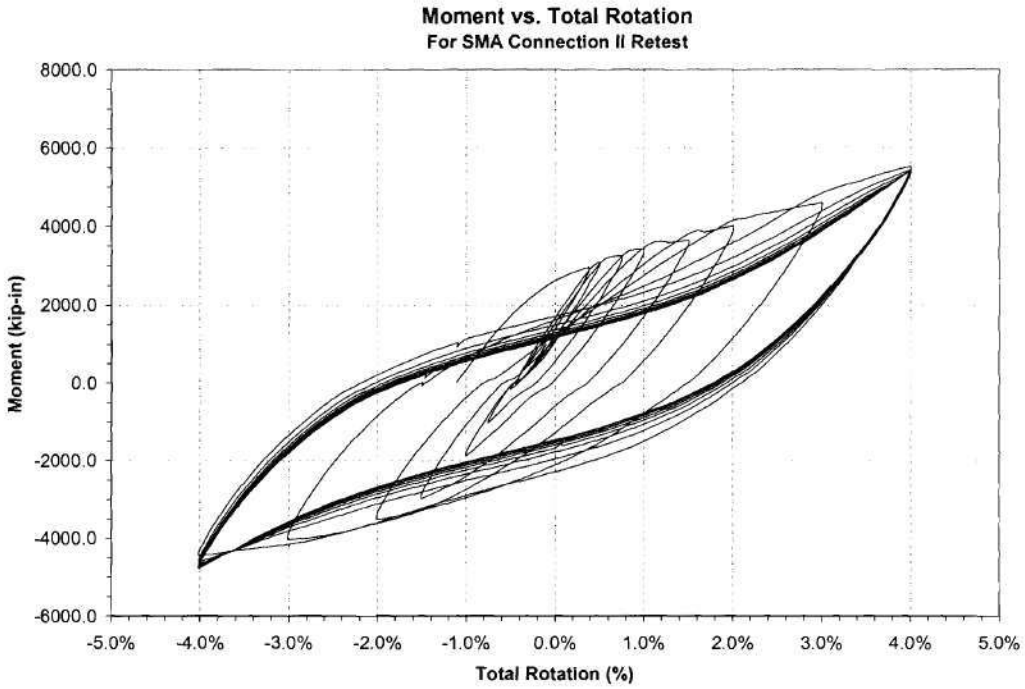

Figure 5-11 Moment/Total Rotation History of SMA II Retest

The strain gauge data also suggest an unsymmetric behavior of the connection. Figure 5-12 shows a shift of the stress/strain behavior of the tendons to the compression side. The most likely cause of this behavior was the tendons never totally straightened out after being heated, and were left with a residual buckle. Since the tendons were started in a buckled shape, it took awhile until the beam was subjected to high drift cycles before the tendons were straightened out, and then they exhibited symmetric behavior.

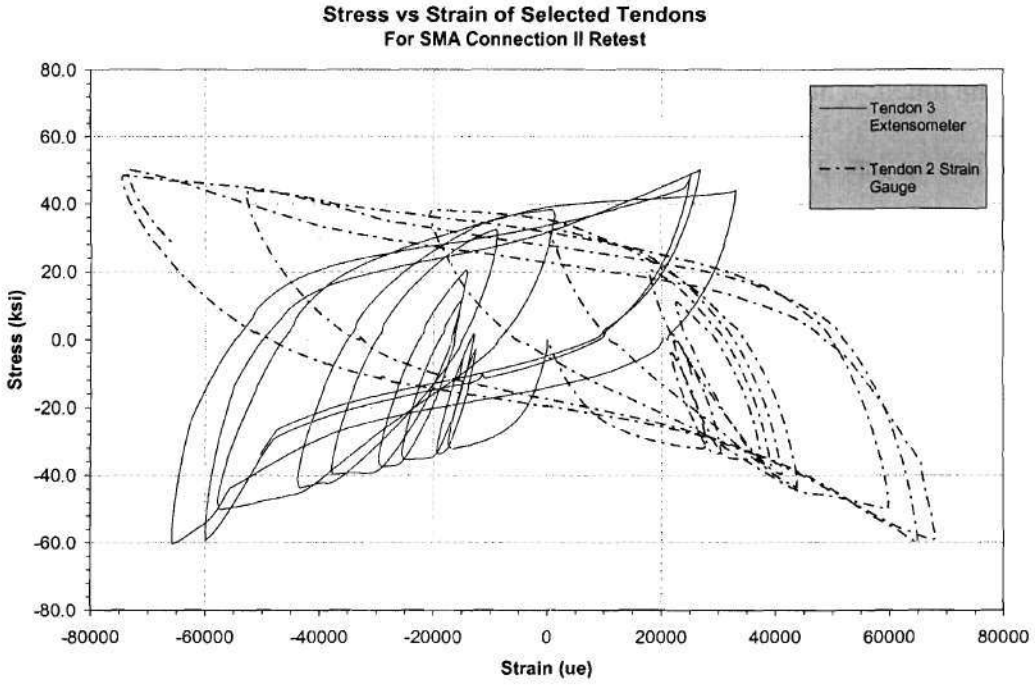

Figure 5-12 Stress/Strain History of Tendons for SMA II

5.7 Dynamic Testing of SMA Connection II

To see if the SMA tendons showed different properties under high loading rates, the connection was tested dynamically. Ideally, the connection was to be cycled at 3% drift at 0.5Hz. However, the dynamic response of the loading system was not known, the 3% drift cycles were first done at lower frequencies to make sure the actuator could perform at a dynamic rate. The first loading consisted of fifteen cycles at 3% drift, using a sine wave function with a frequency of 0.15Hz. At this point it was noticed the data collection system was not collecting fast enough, so its sampling rate was increased, and a faster loading frequency was tried. The tendons became very warm from these first fifteen cycles. The temperature was not recorded, but it was probably ~160 F (71 C) according to the touch. The next loading continued with 3% drift cycles but this time at 0.25 Hz. After five cycles, a load pop came from the load frame, signifying one of the tendons had fractured, and the loading was stopped. Inspection found Tendon #4 (Top-North) had broke near the Top Anchorage Block.

The fracture surface has two different colors in it, a light and dark grey. The light grey coloring was found to be the original fracture surface. The darker grey color occurred due to bearing deformations incurred from later drift cycles.

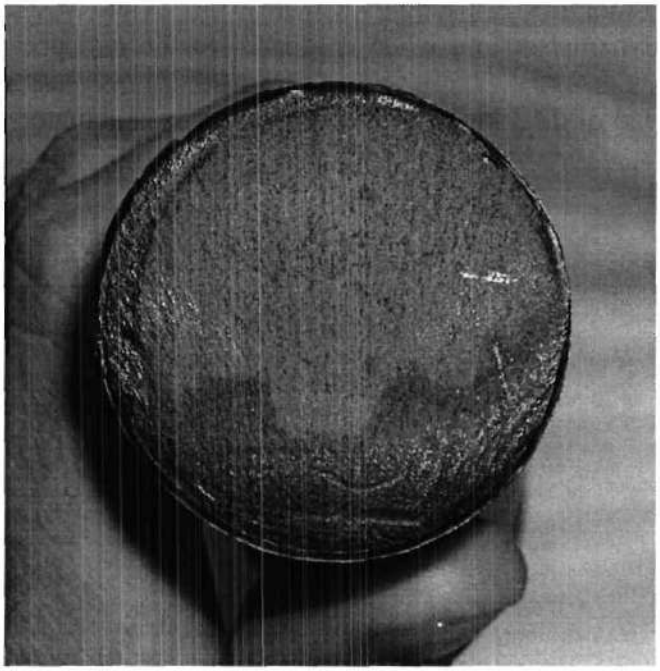

Figure 5-13 Fracture Surface of SMA II Tendon #4

The data for the dynamic 3% drift cycles at 0.15 Hz was lost due to operator error. However, paper plots of load/displacement were created during testing. The paper plots from the 0.15 Hz and 0.25 Hz were compared, by overlaying one on the other, after testing and the plots were nearly identical, therefore it was assumed that the data was the same for the two test.

The load/displacement history showed a much lower load level was reached during the dynamic testing when compared to the two previous quasi-static test. The maximum load of 22.3 kips (99.2 kN) occurred at a actuator displacement of 5.35" (136 mm).

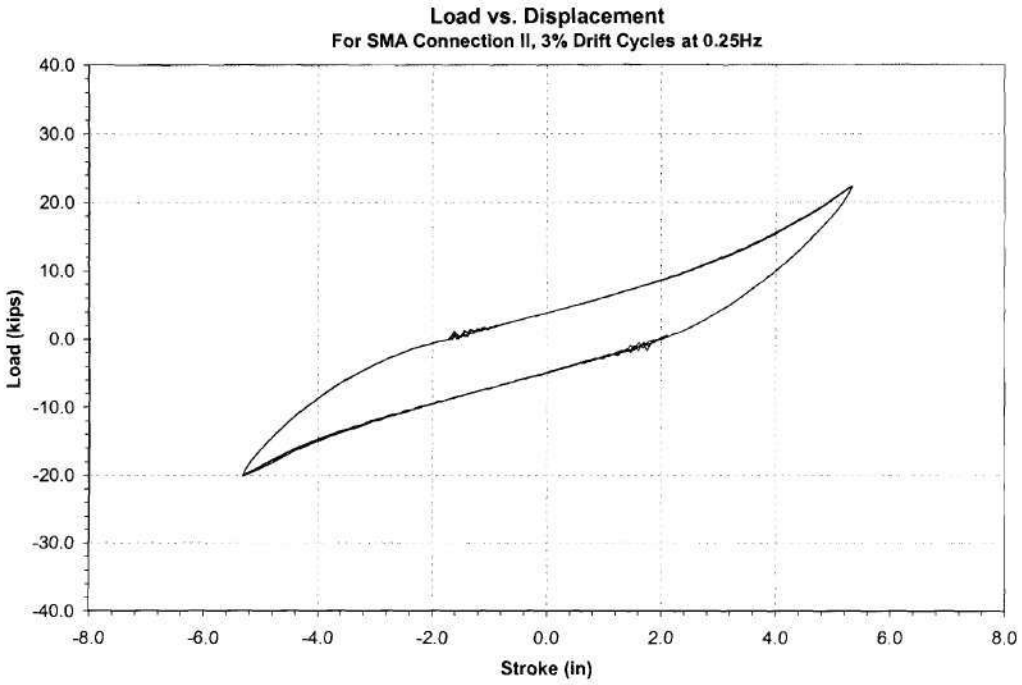

Figure 5-14 Load/Displacement History from Dynamic Test of SMA II

Through all the cycles put on during the two dynamic test, the connection dissipated another 1658 k-in (187 kN-m) of energy. The total energy dissipation up to tendon fracture was 4738 k-in (535kN-m).

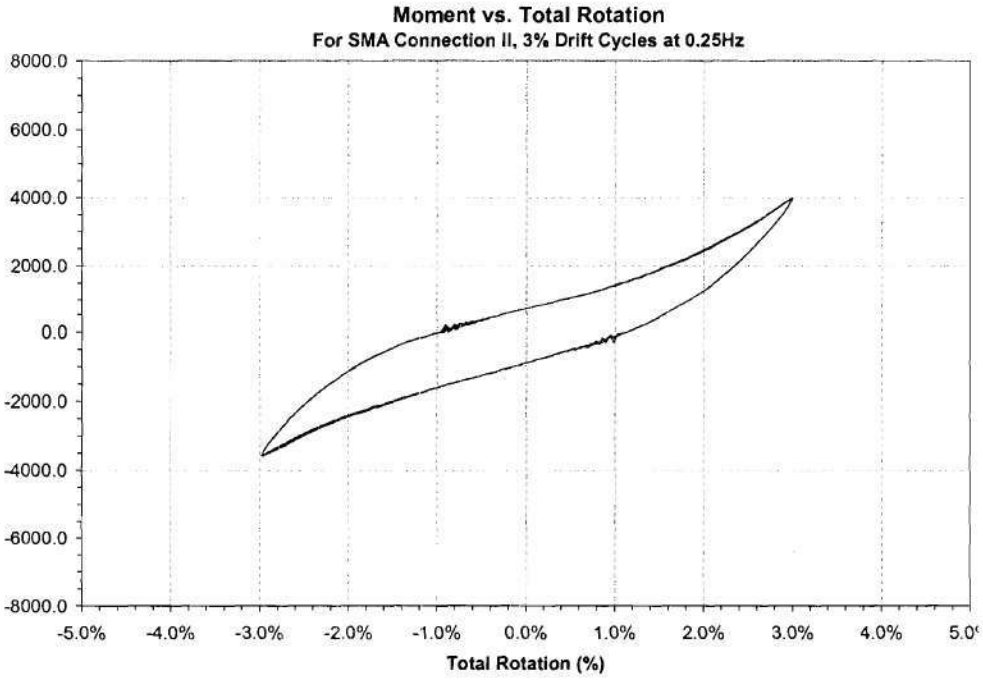

Figure 5-15 Moment/Total Rotation History from Dynamic Testing of SMA II

Three of the strain gauges on the tendons debonded during the dynamic testing, something which is inevitable when performing so many large strain cycles. Figure 5-18 shows the stress/strain curve of the one gauge that remained intact. The twisting of the hysteresis loop in the compression region arose from the strain gauge being placed on the tension side of the tendon when it buckled.

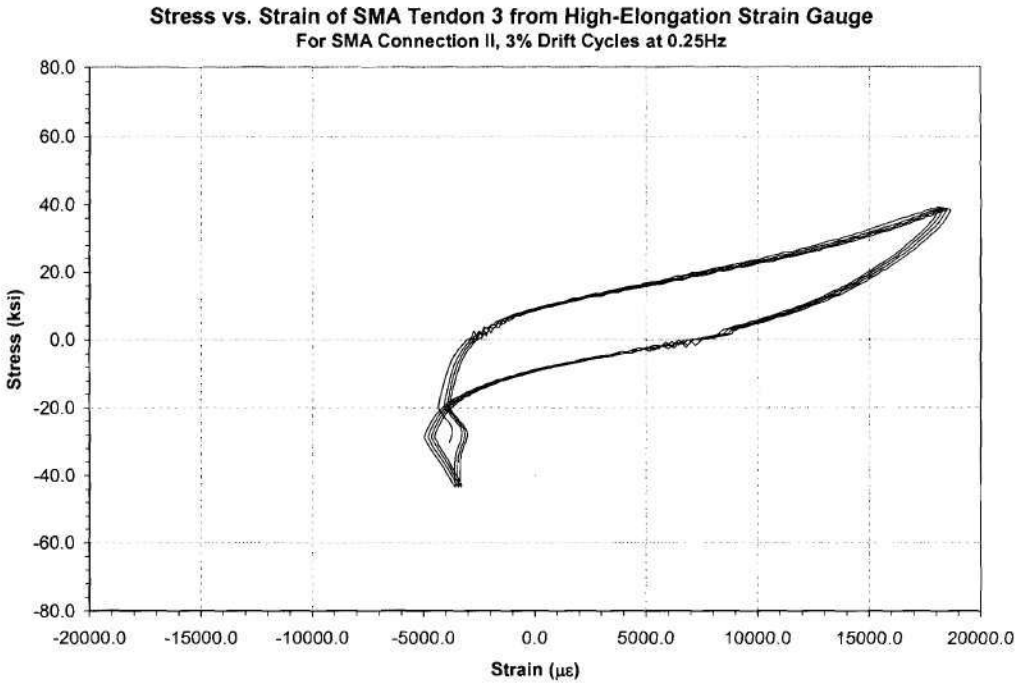

Figure 5-16 Stress/Strain History of Tendon 3 from Dynamic Testing of SMA II

Once Tendon #4 broke, it was decided to push the connection through a 5% drift cycle to see if Tendon #3 would break. The first half of the 5% cycle put Tendon #3 into tension by itself. The tendon carried the entire load and never broke, so the cycle was reversed and the Tendon #3 was put in compression. Though, no more tendons failed, the beam did sustain some damage on the Top Side, were only the single tendon remained. The beam flange directly above Tendon #3 developed yield lines during the 5% drift cycle since only half of the flange was being used to transfer the equivalent force of two tendons.

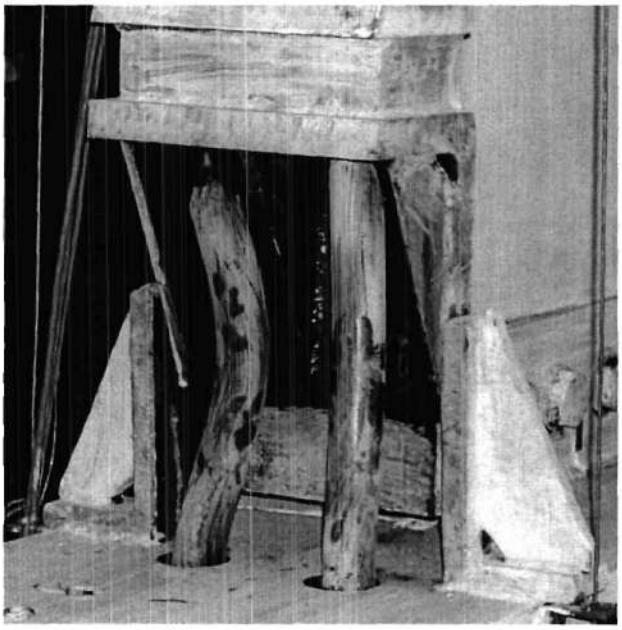

Figure 5-17 Tendon #3 in Tension at 5% Drift

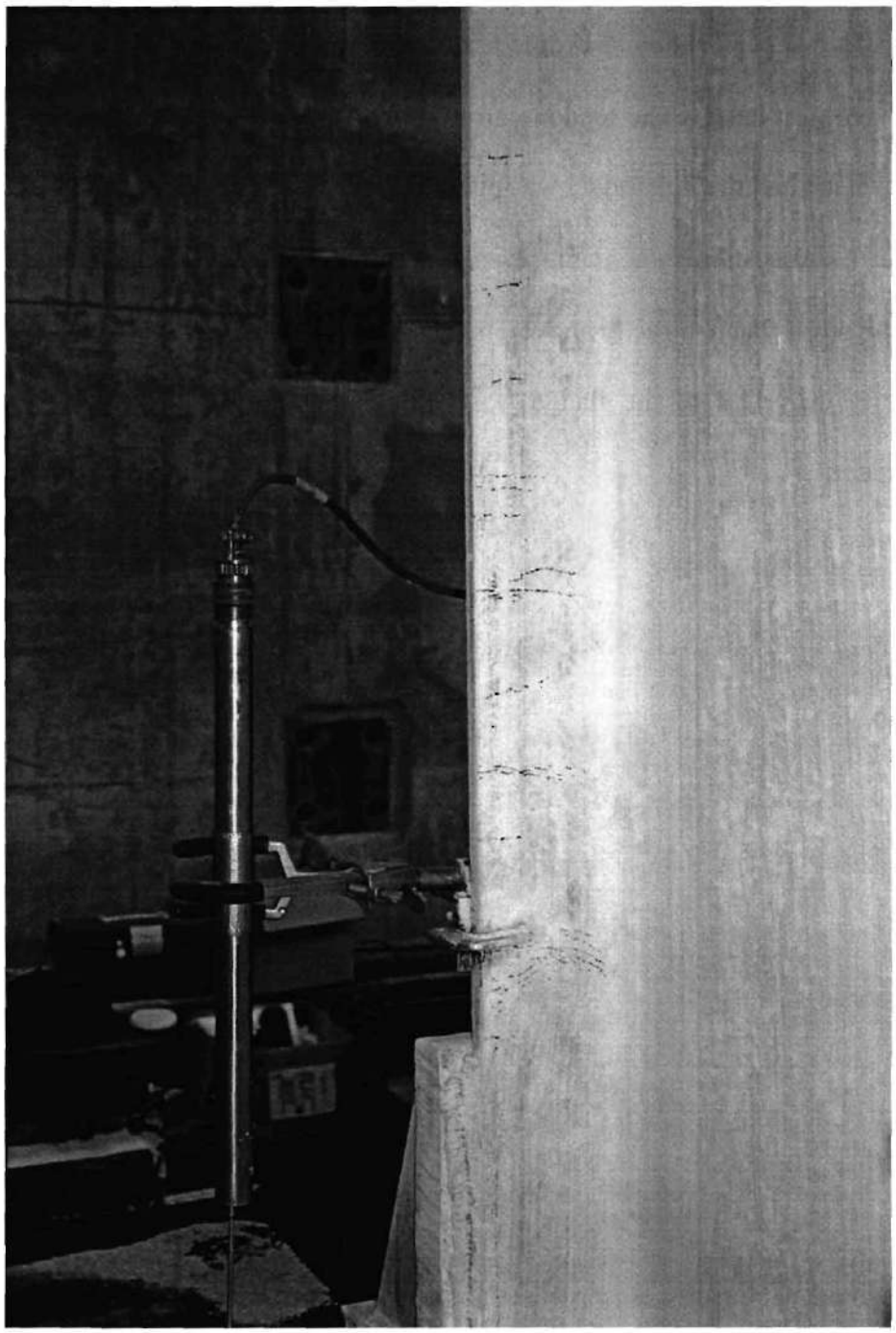

Figure 5-18 Beam Flange Yielding at 5% Drift

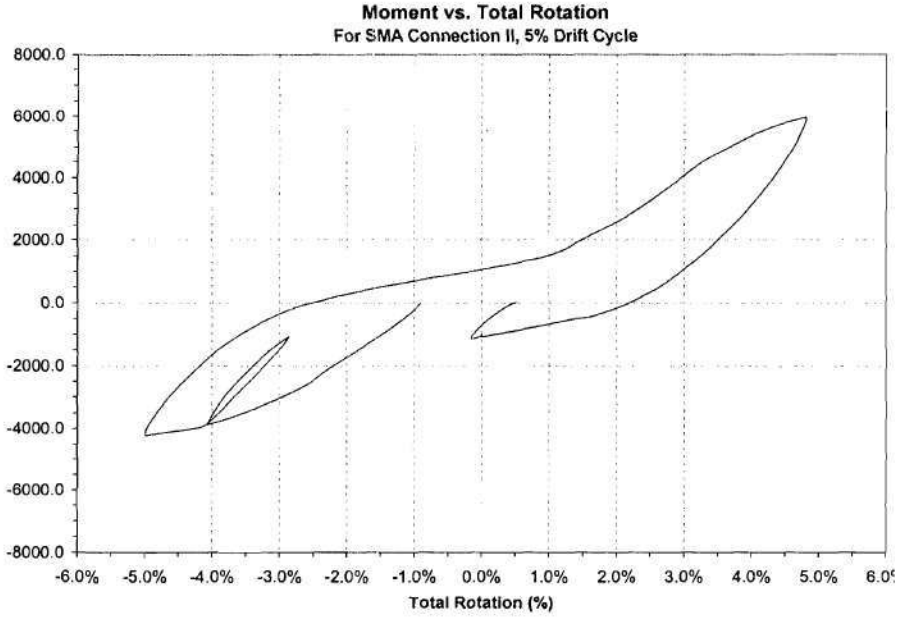

Figure 5-19 Moment/Total Rotation for 5% Drift Cycle for SMA II

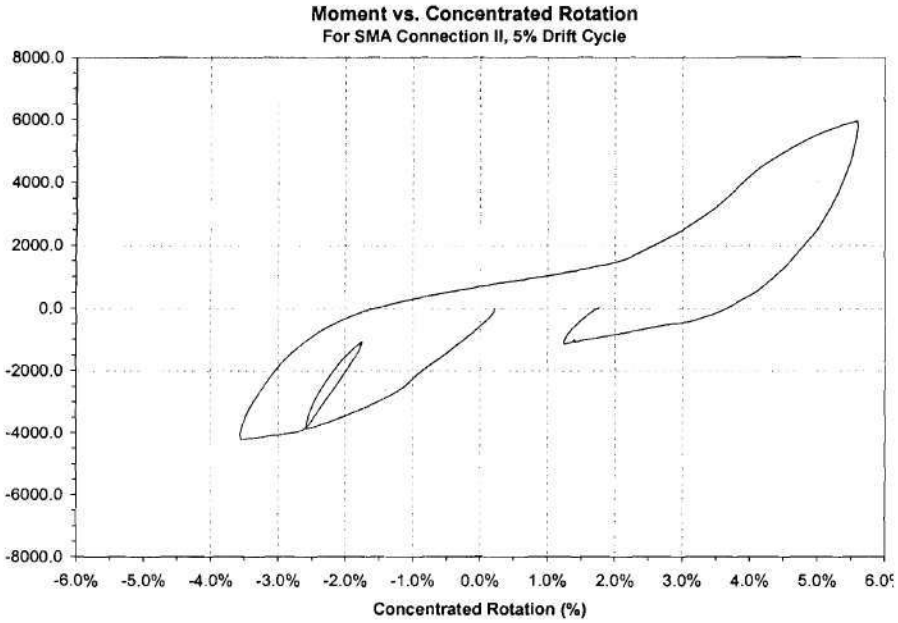

Figure 5-20 Moment/Concentrated Rotation at 5% Drift for SMA II

CHAPTER VI

CONNECTION COMPARISONS

This chapter is intended to provide comparisons of the of the test run for each connection, before and after the tendons were heated. In addition, a comparison shall be made between the two connections in an attempt to draw conclusions.

6.1 SMA Connection I Comparisons

For means of comparing the two tests for SMA Connection I, the first 4% drift cycles from both the initial and retests were plotted in Figure 6-1. This plot would show if there were degradation losses due to excessive cycling, or metallurgical changes in the SMA tendons after initiating the shape memory effect, which would alter the connection's performance.

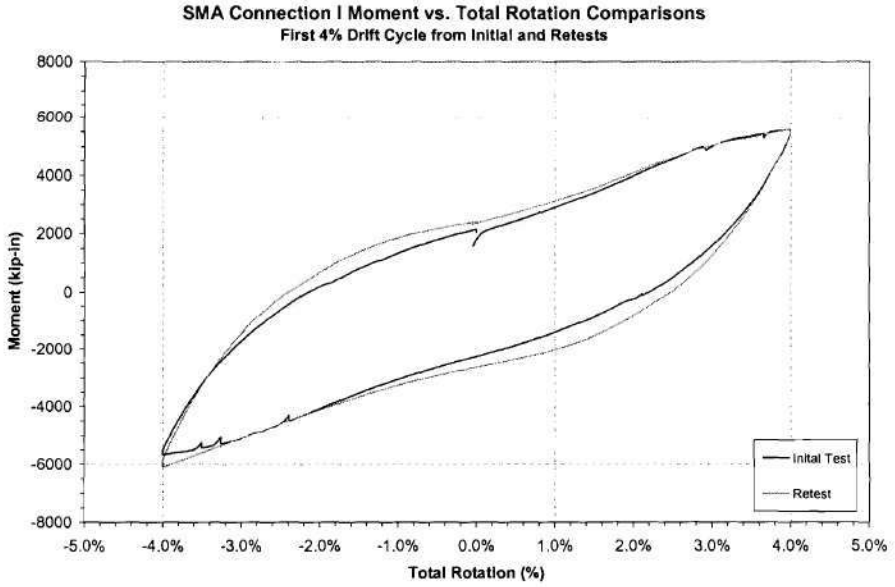

Figure 6-1 Moment/Total Rotation Comparison for SMA Connection I

Indeed, the two hysteresis loops plotted in Figure 6-1 are nearly identical. Even with the tendons' imperfect memory rebound and different boundary conditions[1], the SMA's hysteretic behavior was nearly identical. Thus, it can be assumed that lengthy heating of the material well above its A_f and less than ideal heating methods did not adversely damage the SMA tendons.

1.In the initial test, the Top Anchorage Block was unrestrained, and fully welded for the connection's retest.

6.2 SMA Connection II Comparisons

As with the first connection, SMA Connection II also showed the ability to produce repeatable hysteretic behavior from looking at the first 4% drift cycle. The only deviation was on the negative moment side of the hysteresis loop. This behavior was likely caused by the uneven tendon heat straightening process. During the oxy-acetylene tendon heating, much of the heat was concentrated on only the Bottom Side tendons, which may have affected the properties of only these two tendons. These tendons were put into compression under negative moment.

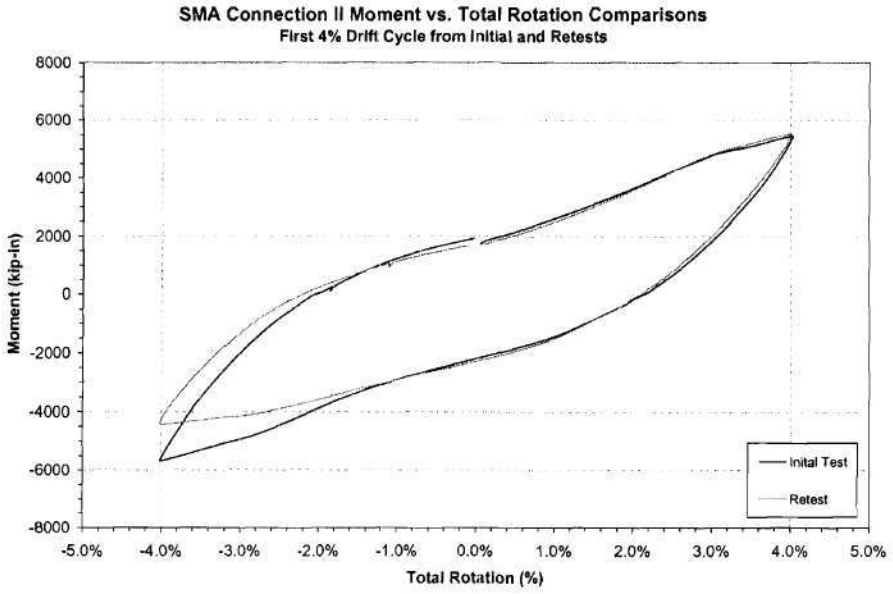

Figure 6-2 First 4% Drift cycles for SMA Connection II

In order to bring the dynamic test into the comparison, the 3% drift cycles had to be compared. As shown in Figure 6-3, the dynamic hysteresis area is much less than (~2 times) the initial and retests. The testing done on the extra SMA tendon at Illinois did not yield any dynamic stress/strain data and therefore the strain rate dependence of the tendons used was not known. Previous research has not found any conclusive evidence of strain rate dependence for martensitic SMA, but whether or not this was the cause for ~1/2 the energy dissipation during dynamic loading can not be justified. The reduced energy dissipation could also just be due to the temperature increase of the tendons from the extremely fast cycling.

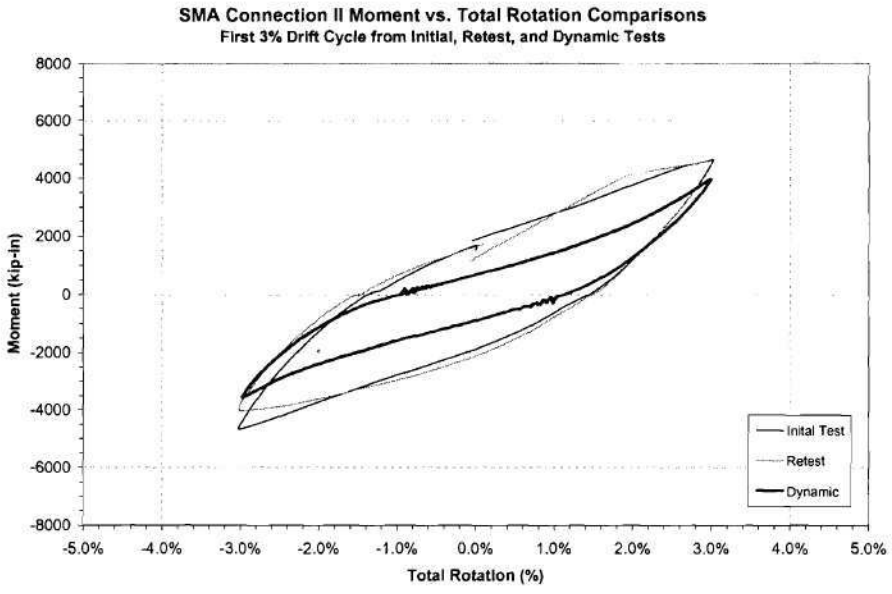

Figure 6-3 Moment/Total Rotation Comparisons for SMA Connection I

6.3 Comparisons of the Two Connections

6.3.1 Energy Dissipation

The tendon diameter for SMA Connection II was increased slightly but at the same time so was it's length. The actual stiffness of the tendons from the two test was similar, therefore the behavior of the two connections should also be similar. As seen in Figure 6-4, the Moment/Total Rotation hysteresis loops are quite similar indicating relatively little difference between the two connections despite different beam sections.

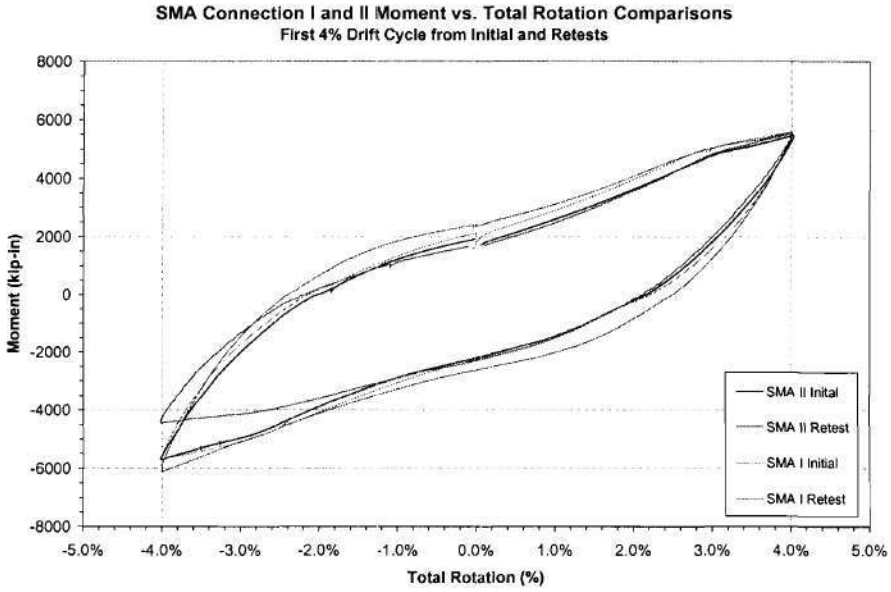

Figure 6-4 Connection I and II Moment/Total Rotation Comparison

Table 6-1 Connection Energy Dissipation Comparisons

	SMA Connection I		SMA Connection II	
	Energy Dissipation by Moment/Total Rotation (kip-in)	Energy Dissipation by Moment/Concentrated Rotation (kip-in)	Energy Dissipation by Moment/Total Rotation (kip-in)	Energy Dissipation by Moment/Concentrated Rotation (kip-in)
Initial Test	1141	1246	1174	1280
Retest	2825	3158	1906	2106
Dynamic Test	N/A	N/A	1658	1986
Total	3966	4404	4738	5372

The initial testing of the two connections produced relatively close energy dissipation results, but after the retest of the two connections, SMA Connection II started to lag from SMA Connection I. However, if energy dissipated up until first tendon fracture, the two connection exhibit extremely similar energy dissipations.

6.3.2 Fractures

One possible reason for the differences in the two connections is the metallurgy of the SMA tendons. The tendons were supposedly made from the same material, but they were definitely not from the same batch of Nitinol. The two tendons exhibited similar stress/strain characteristics, but the two fracture surfaces show a difference.

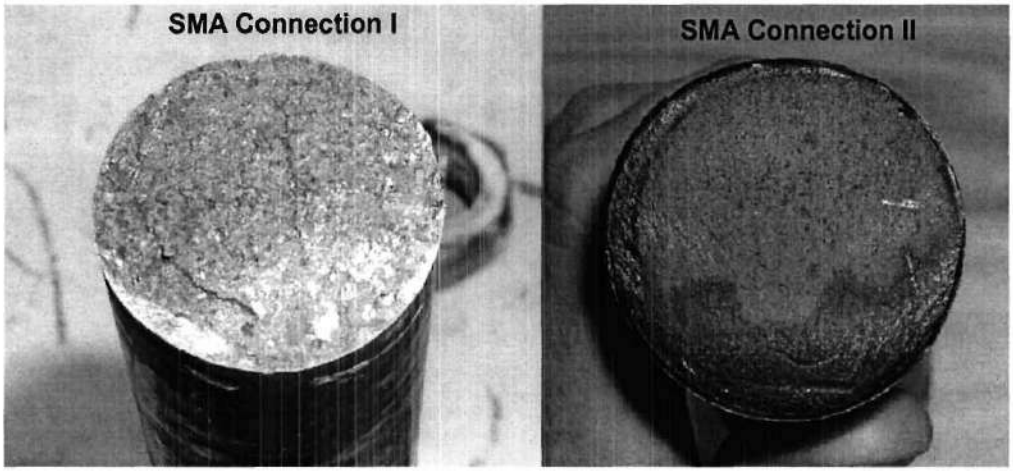

Figure 6-5 SMA Tendon Fracture Surfaces

The comparison to be made does not involve the coloration, but rather the texture of the fracture surface. The SMA Connection I fracture has a more grainy appearance than the SMA Connection II tendon. This may indicate a slightly different metallurgy, but more likely representative of a different heat treatment. It can not be determined if the different grain structures were built into the bars, or was due to the heat straightening process.

APPENDIX A

SMA CONNECTION I EXPERIMENTAL DATA

1.1 Initial Testing

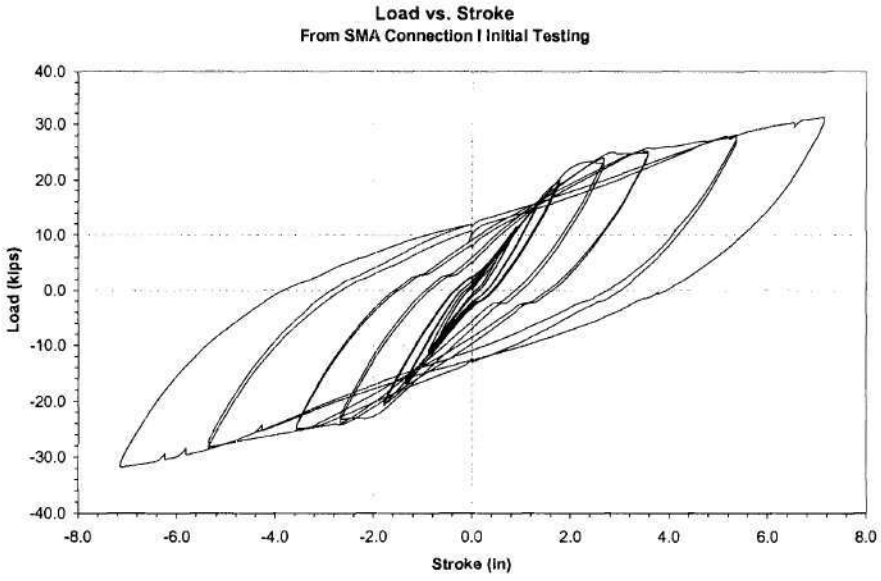

Figure A-1 Load/Displacement History from Initial Test

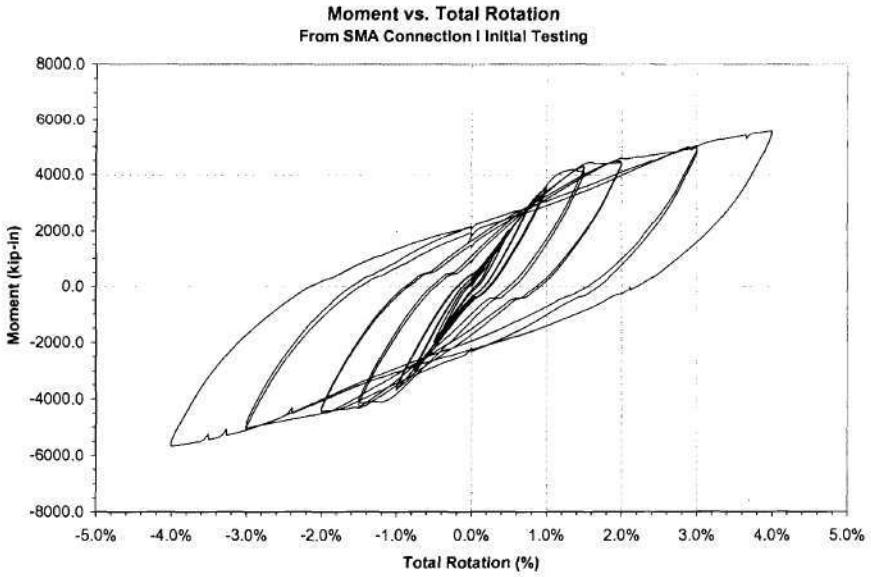

Figure A-2 Moment/Total Rotation History from Initial Test

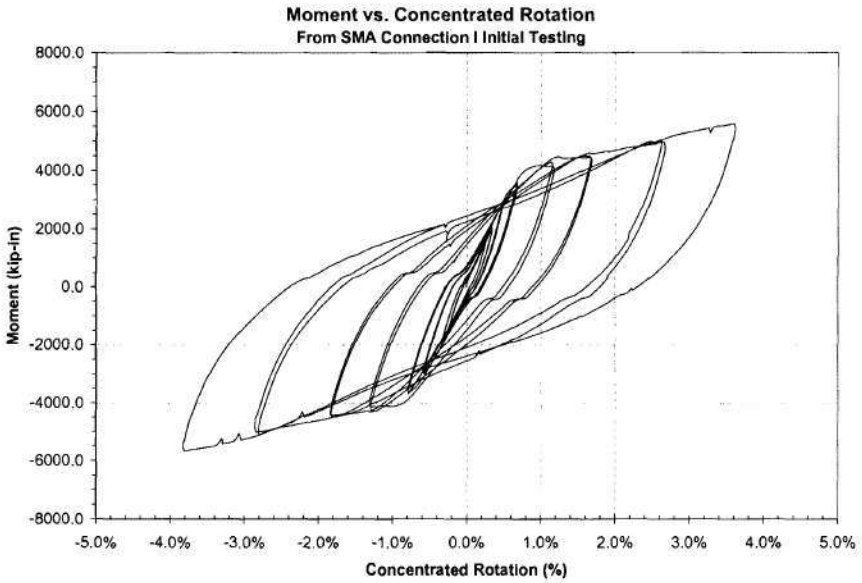

Figure A-3 Moment/Concentrated Rotation from Initial Test

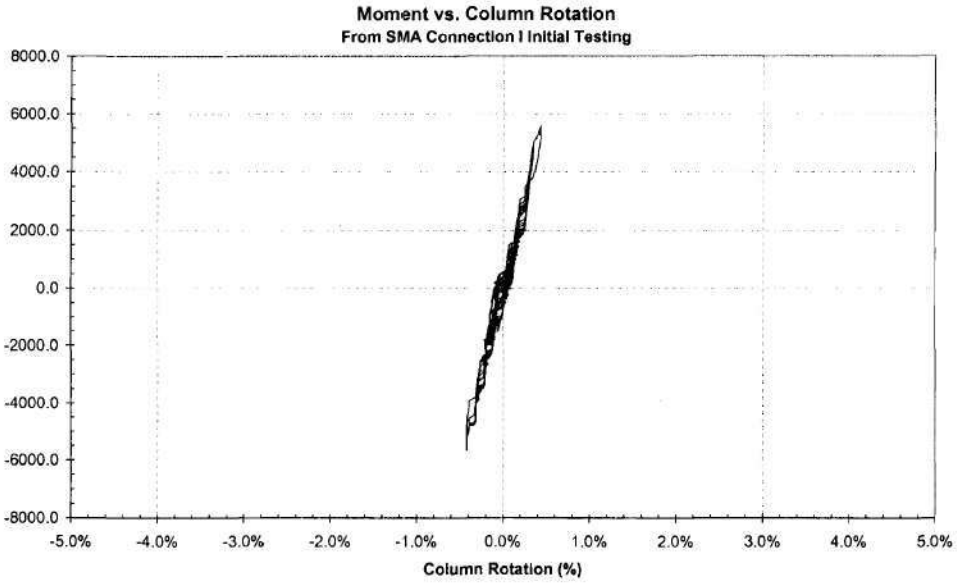

Figure A-4 Moment/Column Rotation History from Initial Test

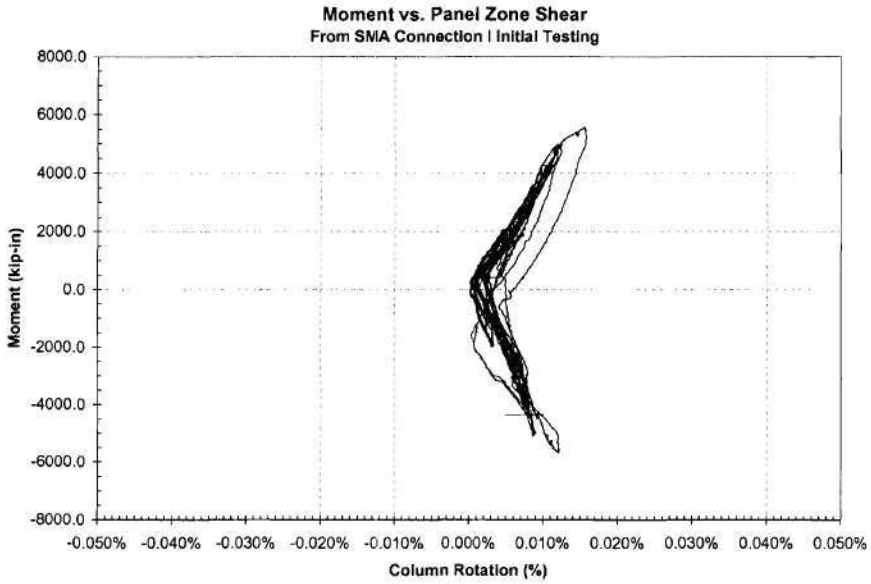

Figure A-5 Moment/Panel Zone Shear History from Initial Test

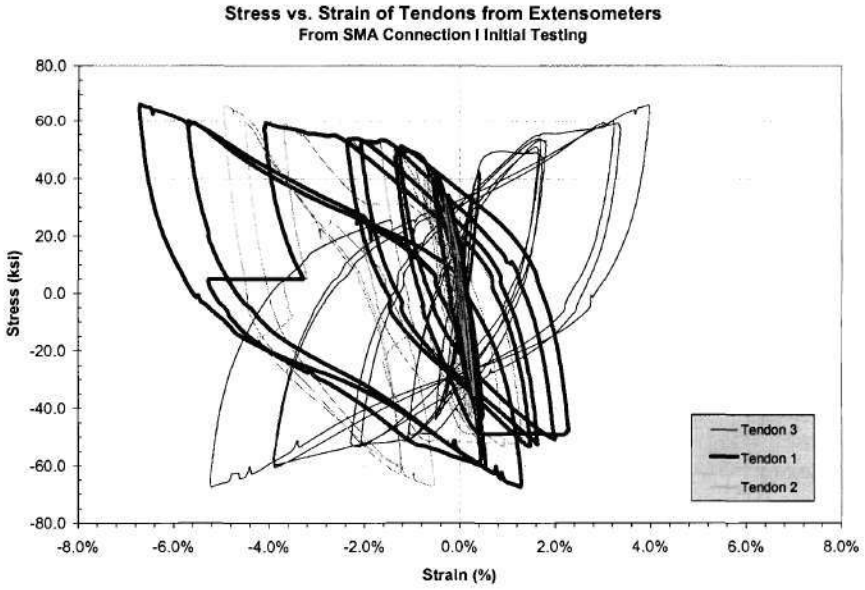

Figure A-6 Stress/Strain History of Tendons from Extensometers

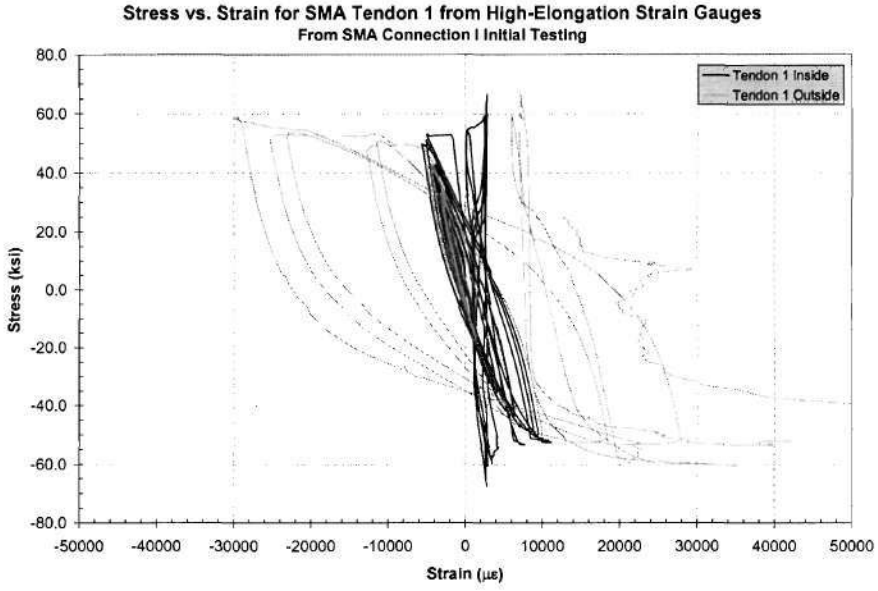

Figure A-7 Stress/Strain History of Tendon 1 using Strain Gauges

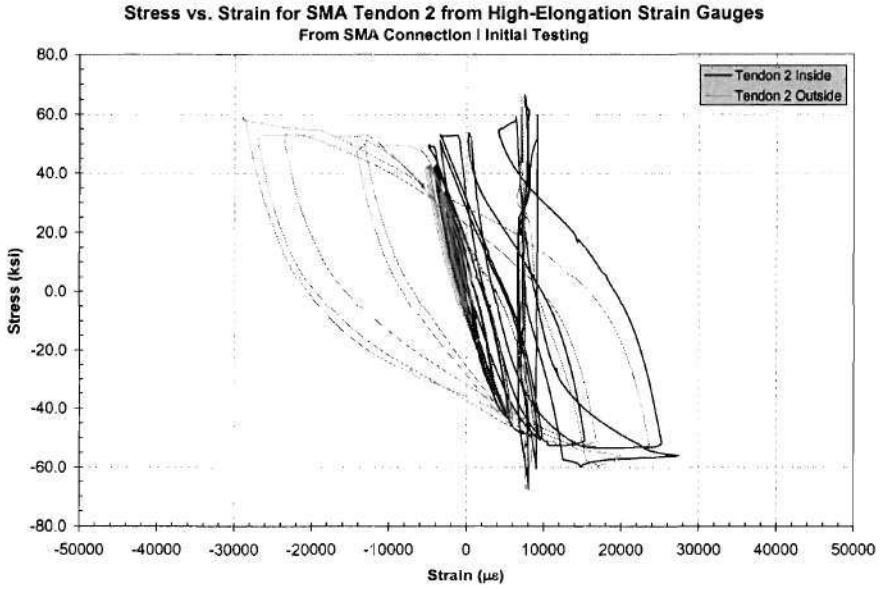

Figure A-8 Stress/Strain History of Tendon 2 using Strain Gauges

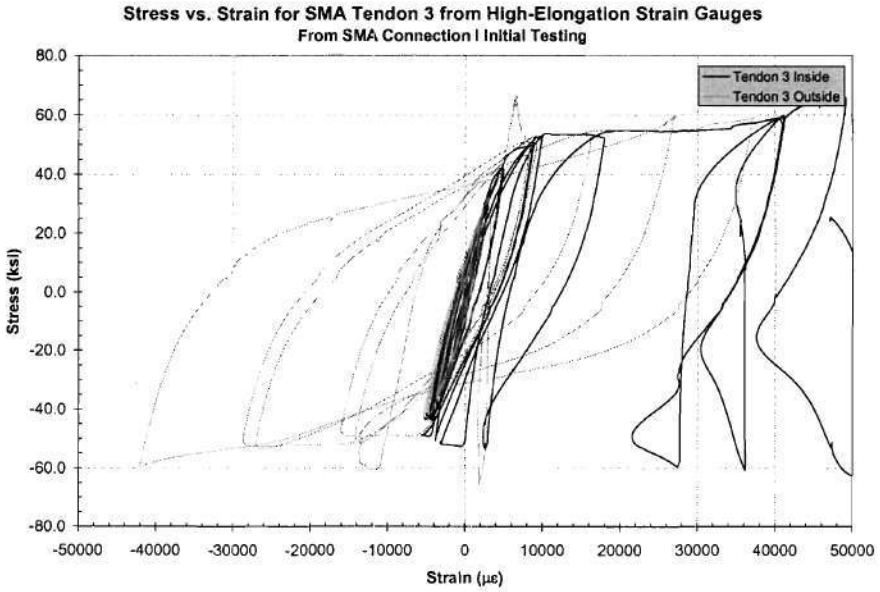

Figure A-9 Stress/Strain History of Tendon 3 using Strain Gauges

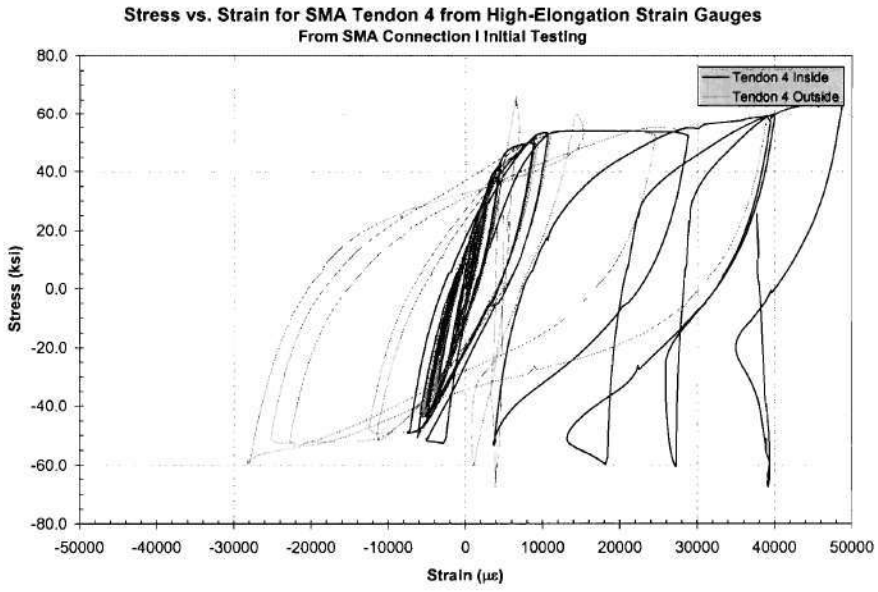

Figure A-10 Stress/Strain History of Tendon 4 using Strain Gauges

1.2 Retest

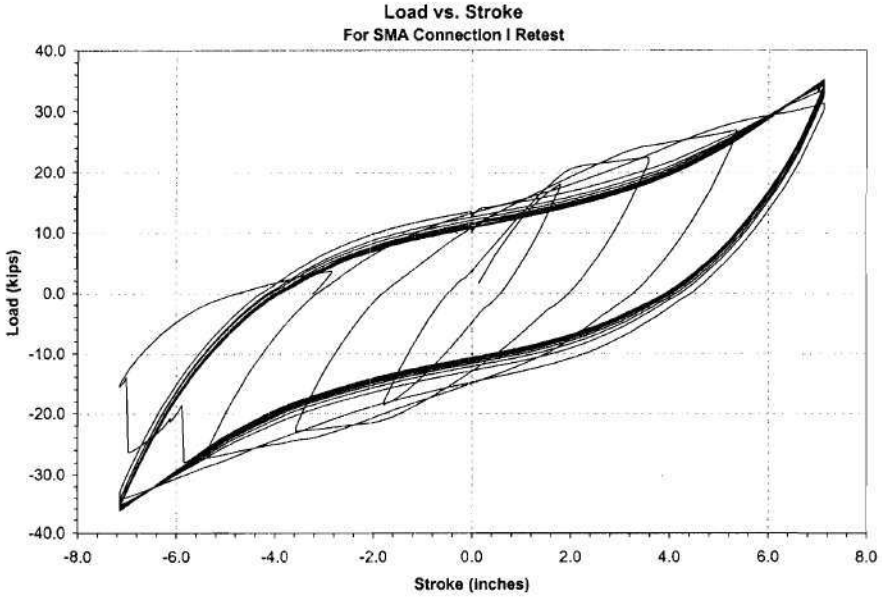

Figure A-11 Load/Stroke History for Retest

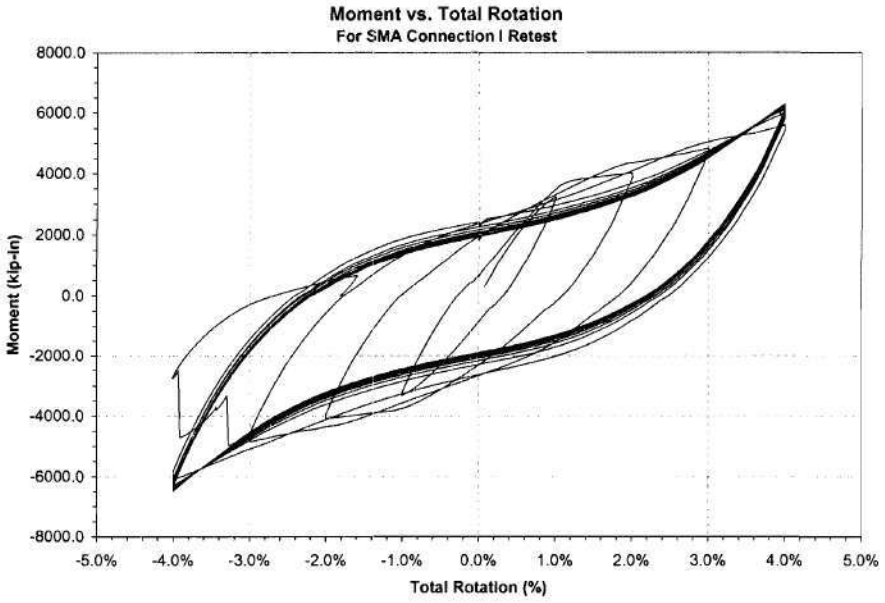

Figure A-12 Moment/Total Rotation for Retest

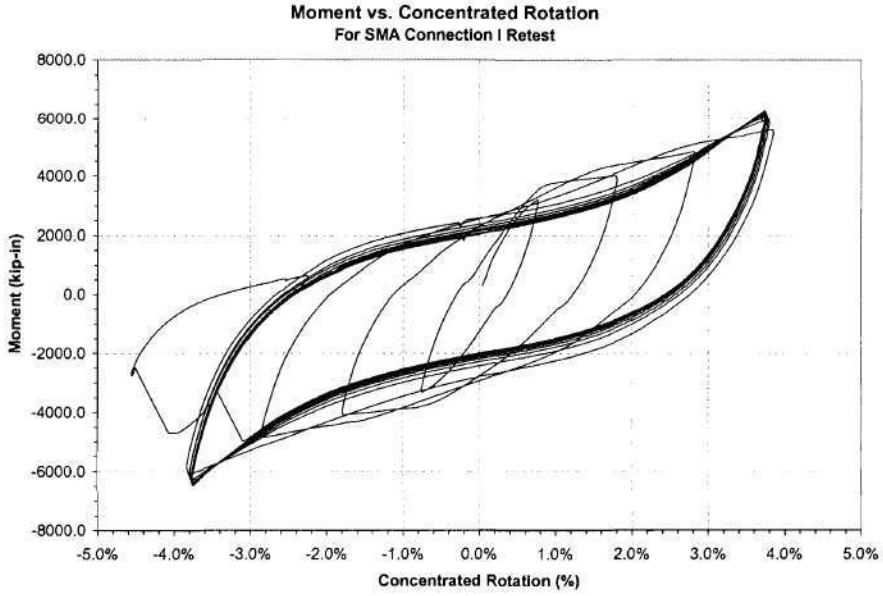

Figure A-13 Moment/Concentrated Rotation for Retest

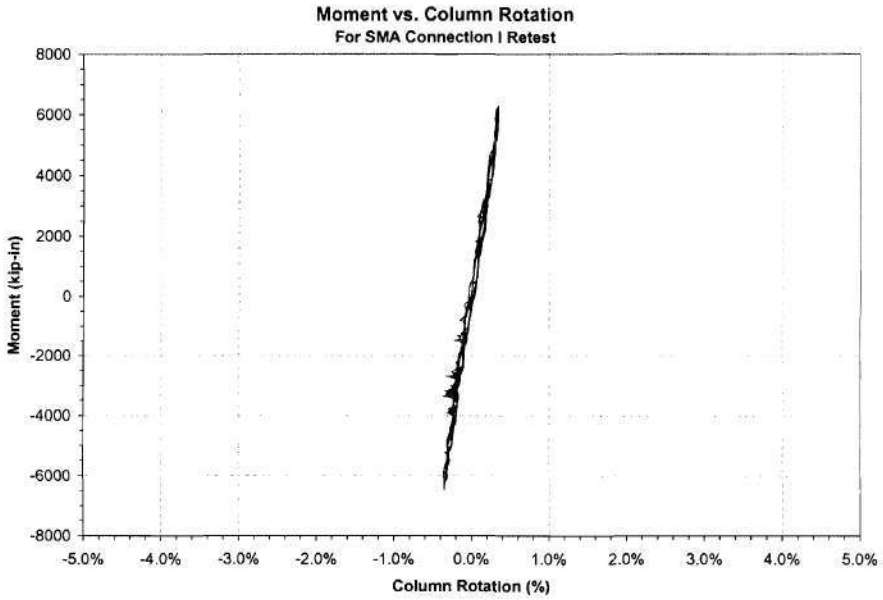

Figure A-14 Moment/Column Rotation History for Retest

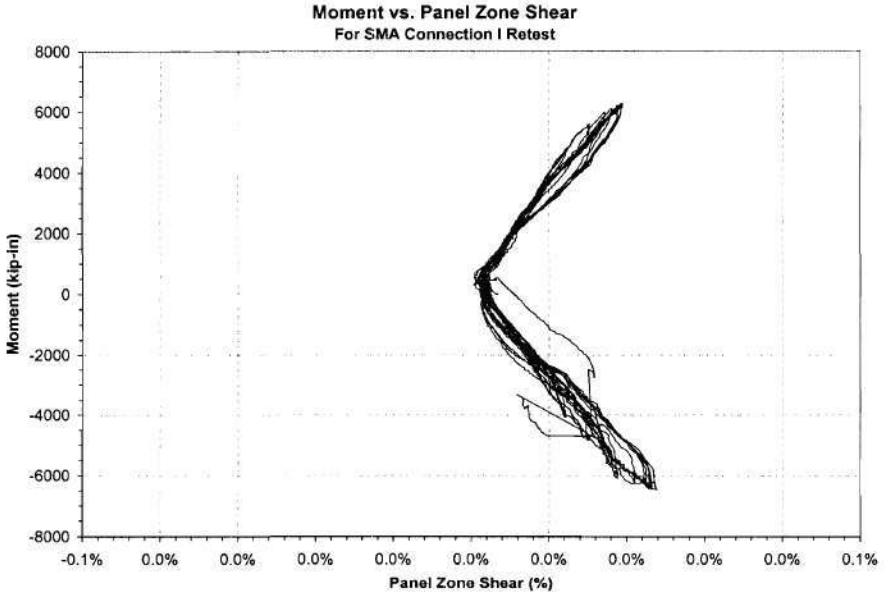

Figure A-15 Moment/Panel Zone Shear History for Retest

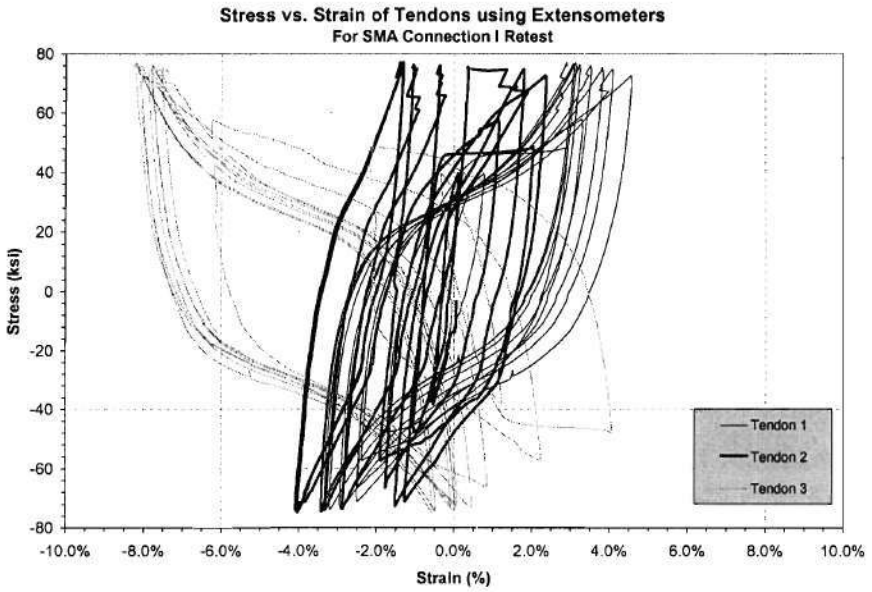

Figure A-16 Stress.Strain History of SMA Tendons for Retest

APPENDIX B

SMA CONNECTION II EXPERIMENTAL DATA

B.1 Initial Test

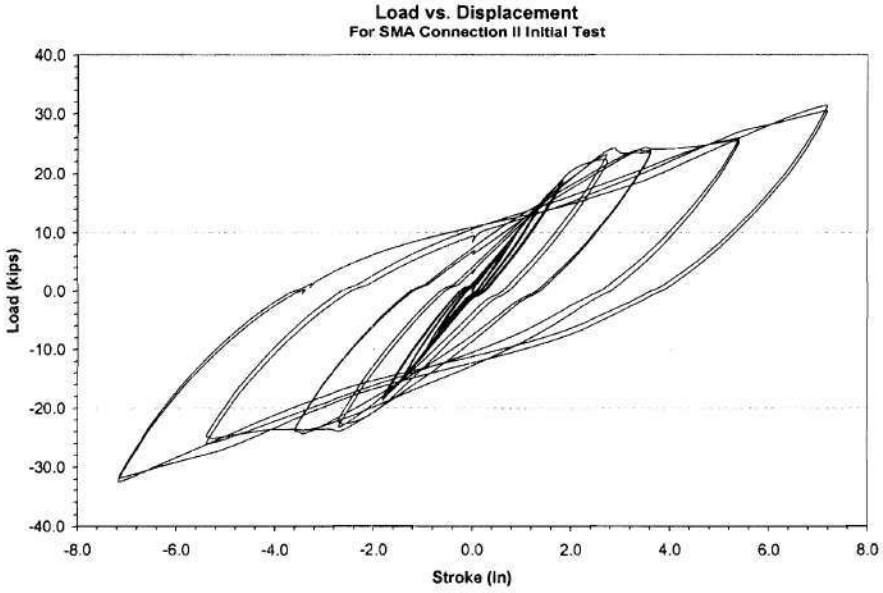

Figure B-1 Load/Displacement History for Initial Test

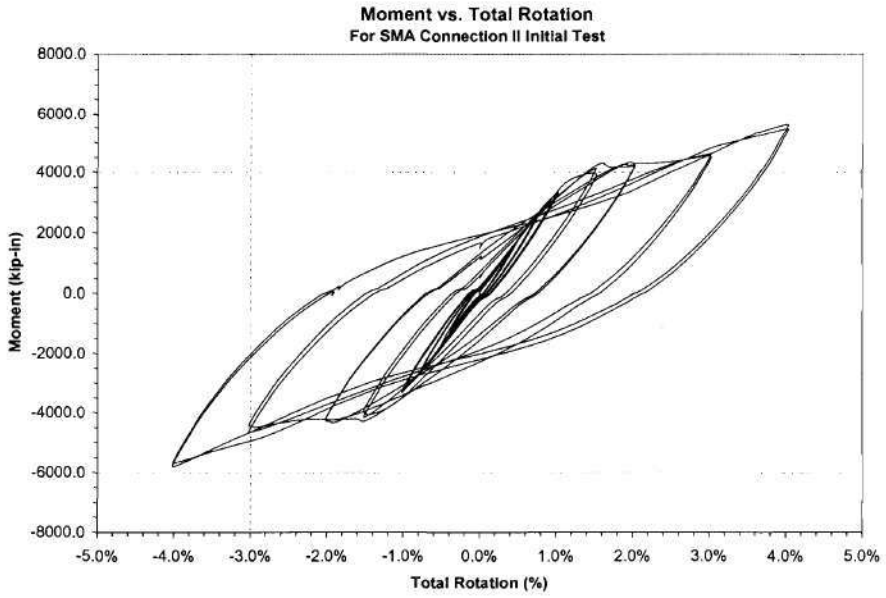

Figure B-2 Moment/Total Rotation History for Initial Test

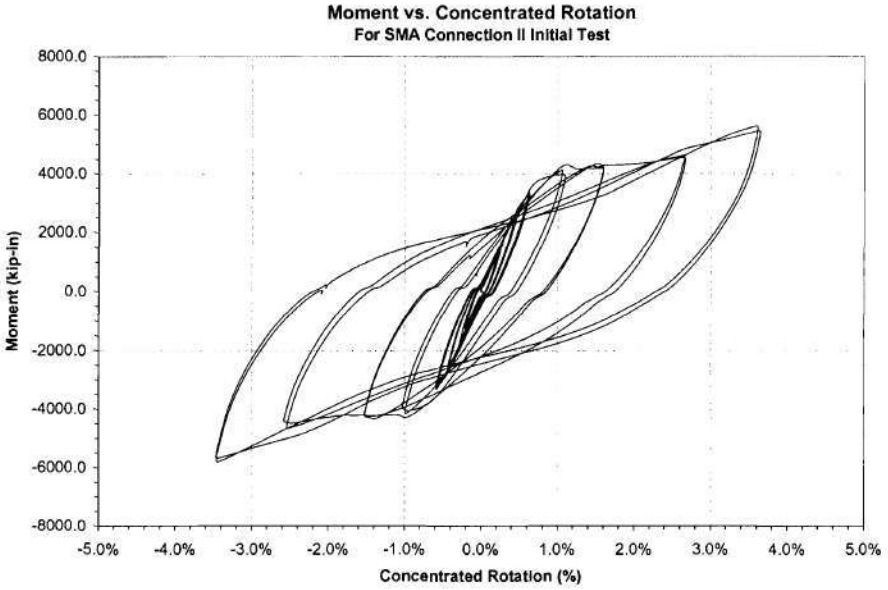

Figure B-3 Moment/Concentrated Rotation History for Initial Test

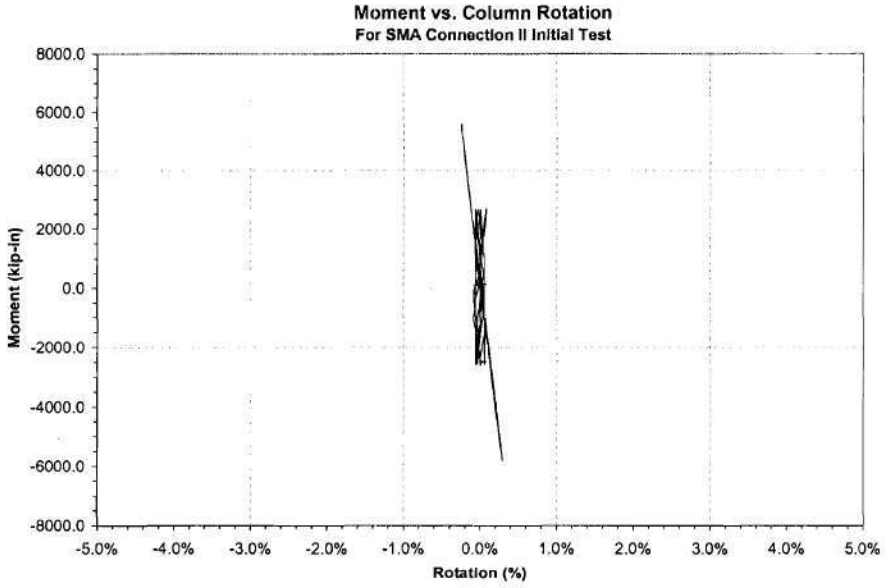

Figure B-4 Moment/Column Rotation History for Initial Test

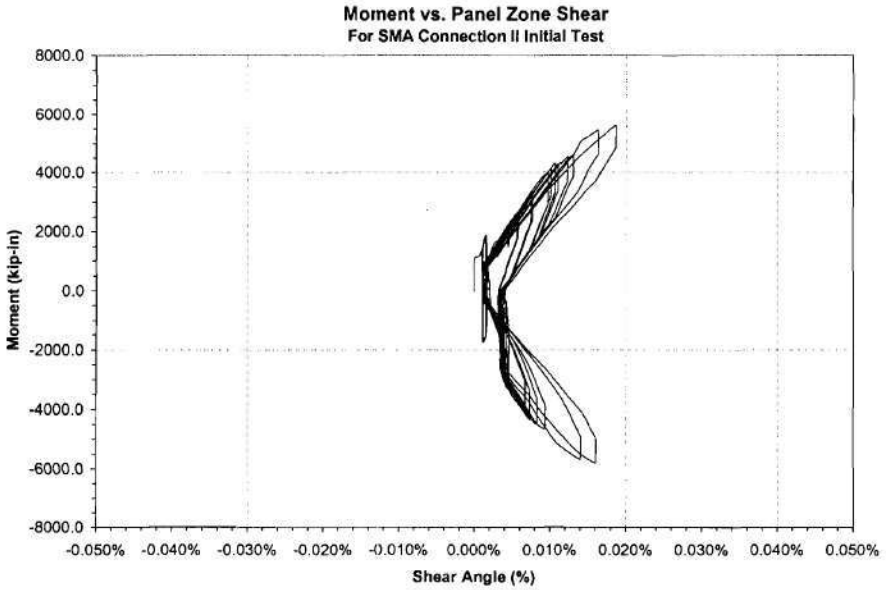

Figure B-5 Moment/Panel Zone Shear History for Initial Test

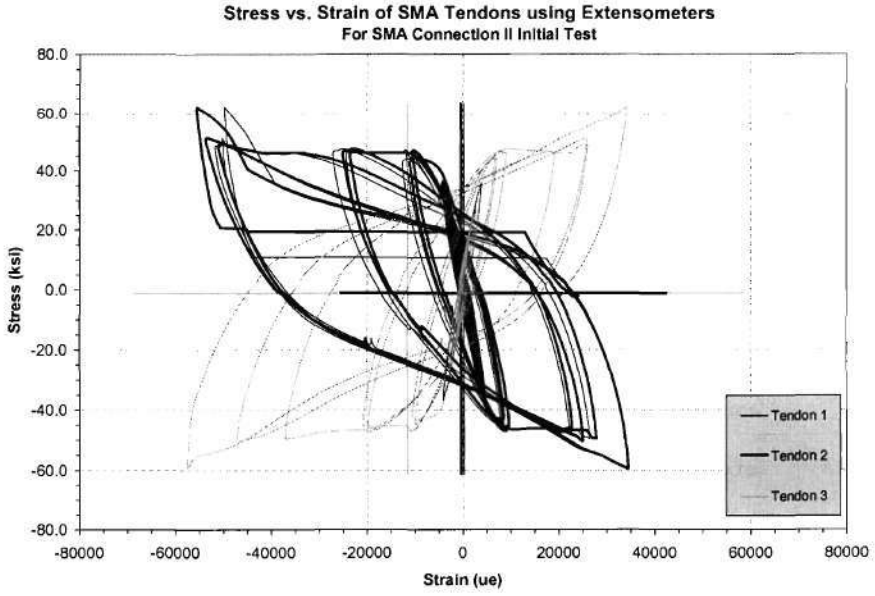

Figure B-6 Stress/Strain History for Tendons using Extensometers

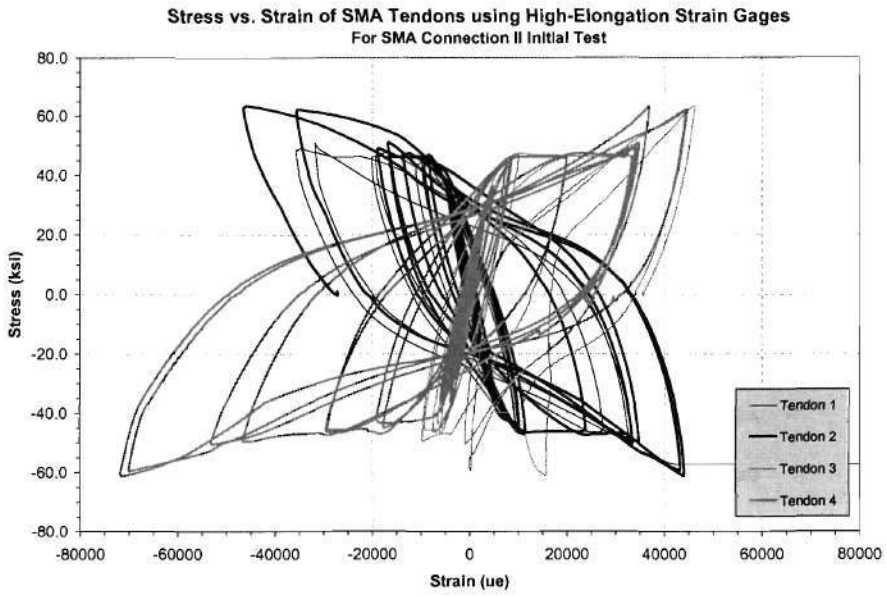

Figure B-7 Stress/Strain History for Tendons using Strain Gauges

B.2 Retest

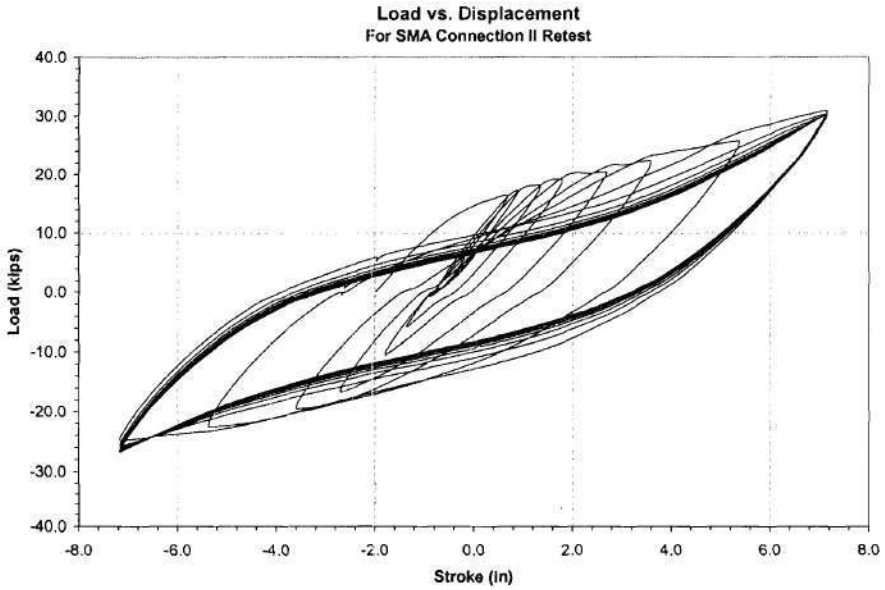

Figure B-8 Load/Displacement History for Retest

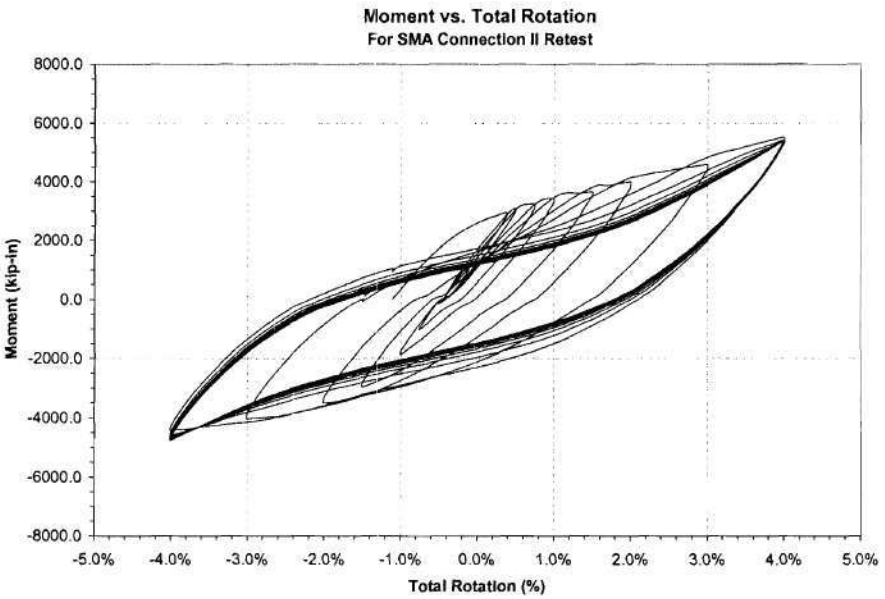

Figure B-9 Moment/Total Rotation History for Retest

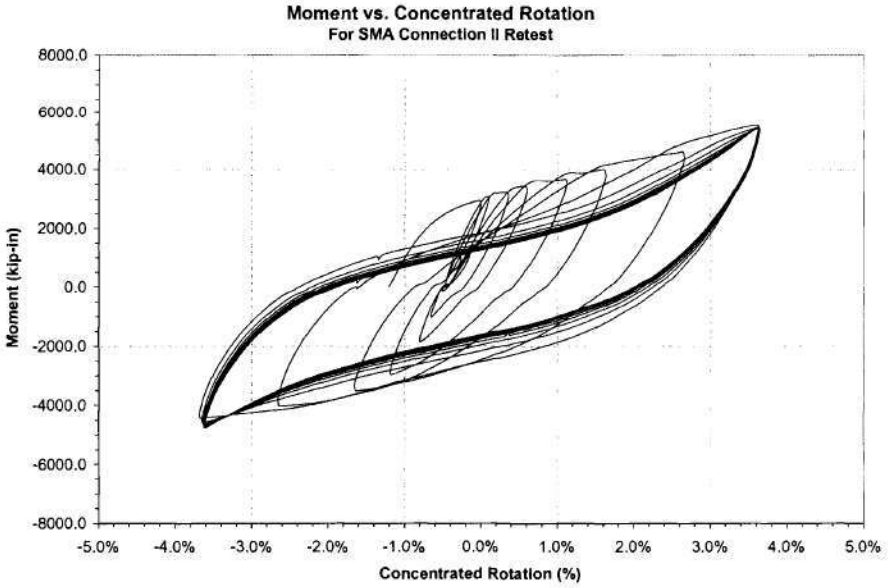

Figure B-10 Moment/Concentrated Rotation History for Retest

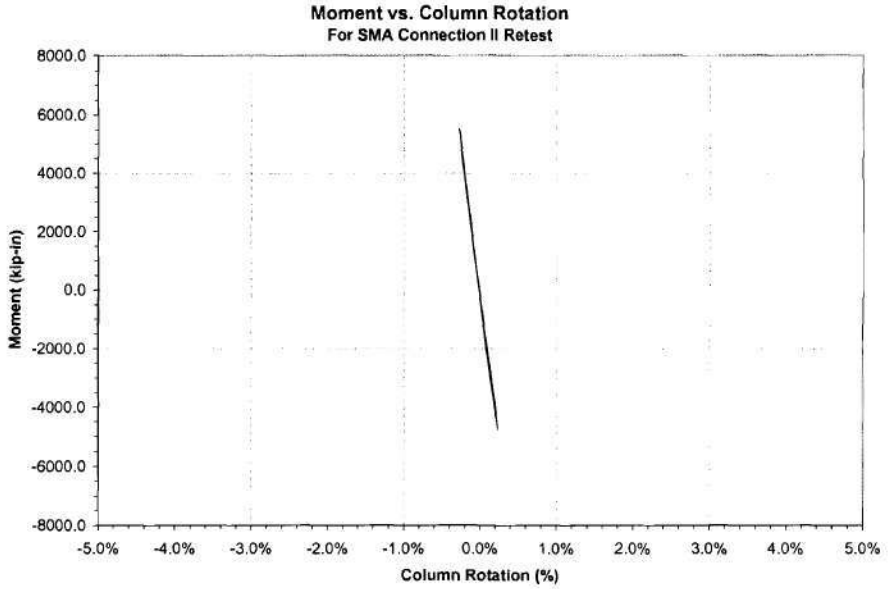

Figure B-11 Moment/Column Rotation History for Retest

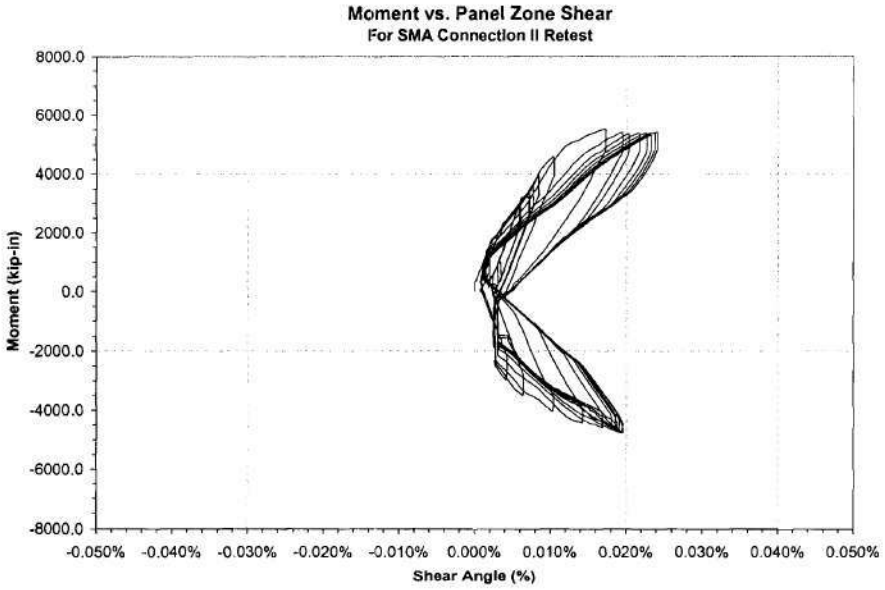

Figure B-12 Moment/Panel Zone Shear History for Retest

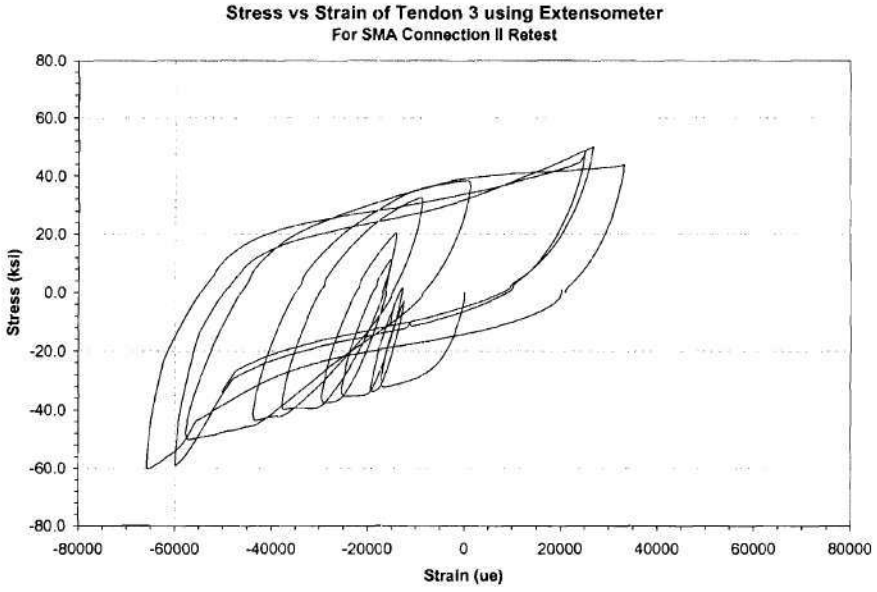

Figure B-13 Stress/Strain History of Tendon 3 for Retest

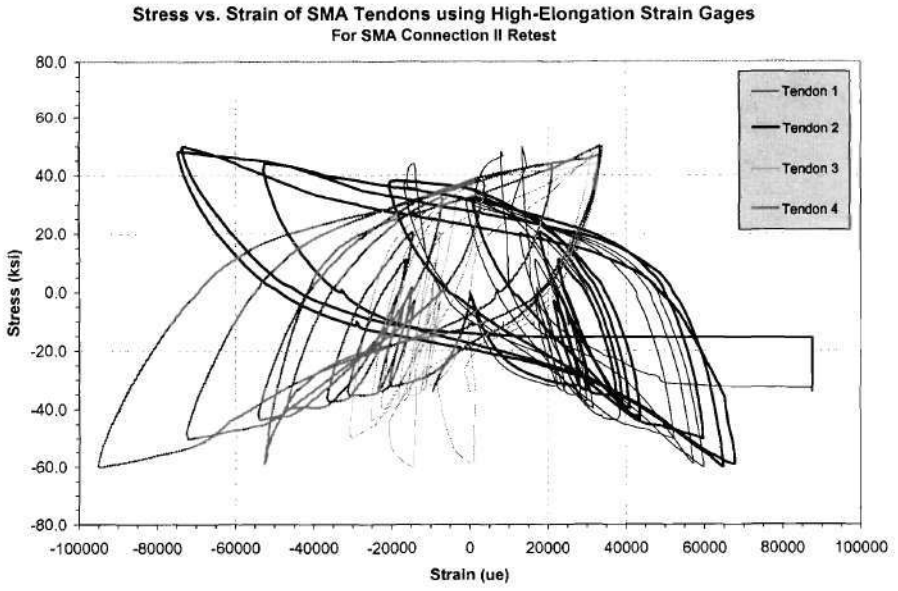

Figure B-14 Stress/Strain History of Tendons for Retest

B.3 Dynamic Testing

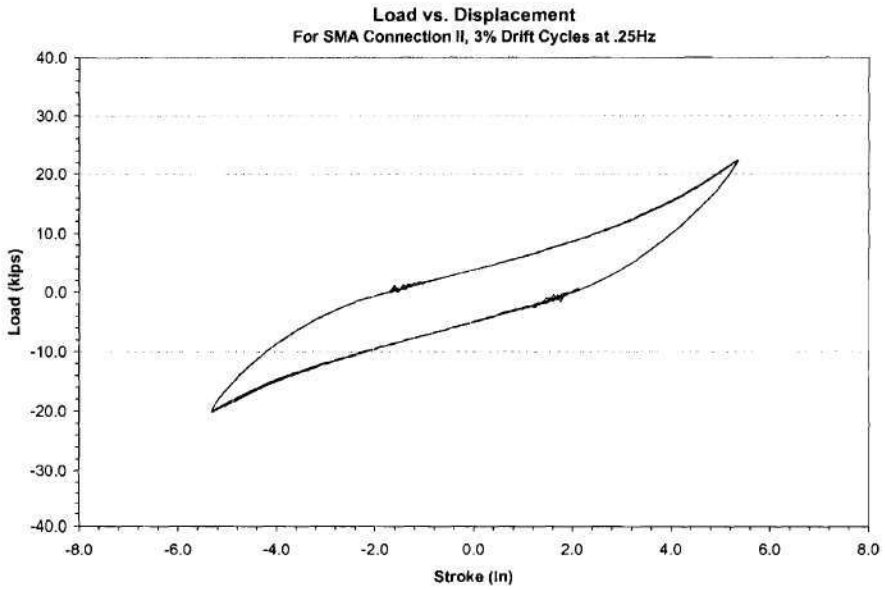

Figure B-15 Load/Displacement History for Dynamic Testing

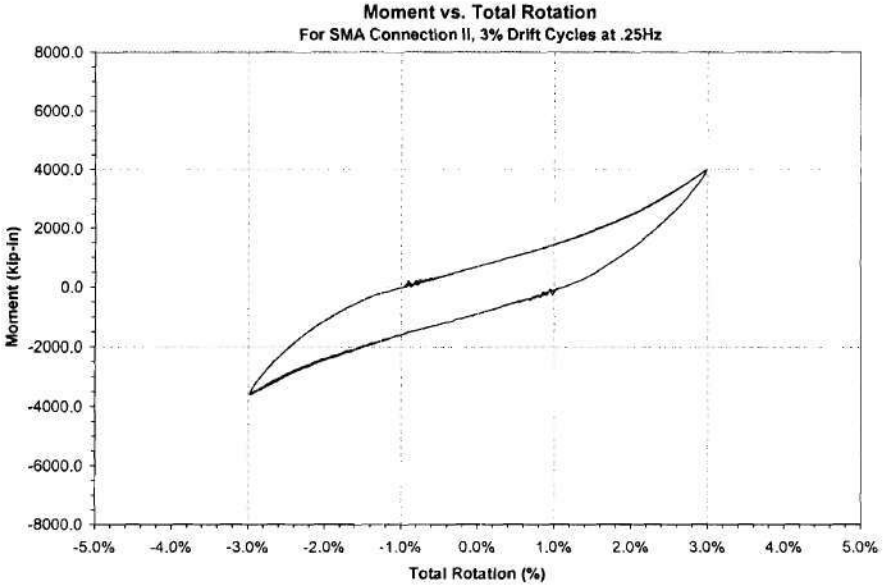

Figure B-16 Moment/Total Rotation History for Dynamic Testing

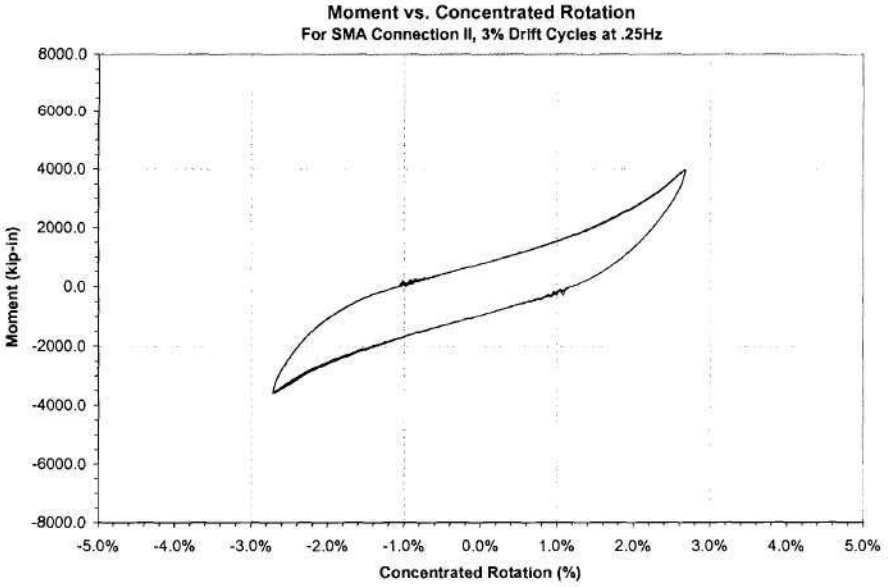

Figure B-17 Moment/Concentrated Rotation History for Dynamic Testing

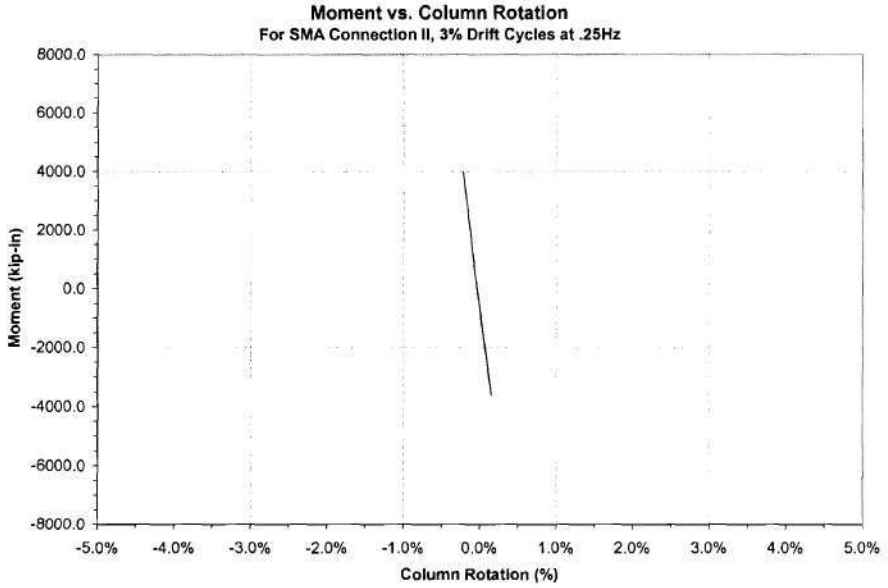

Figure B-18 Moment/Column Rotation History for Dynamic Testing

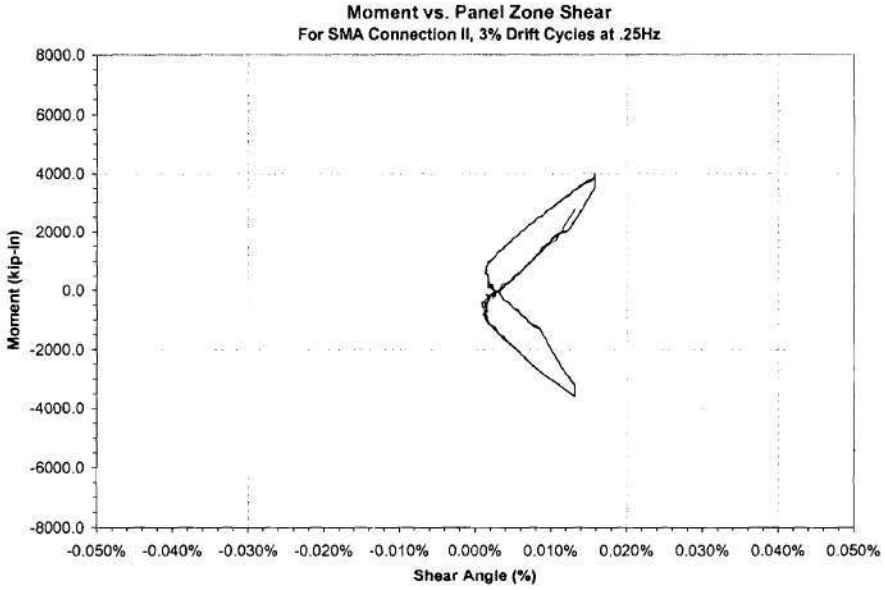

Figure B-19 Moment/Panel Zone Shear History for Dynamic Testing

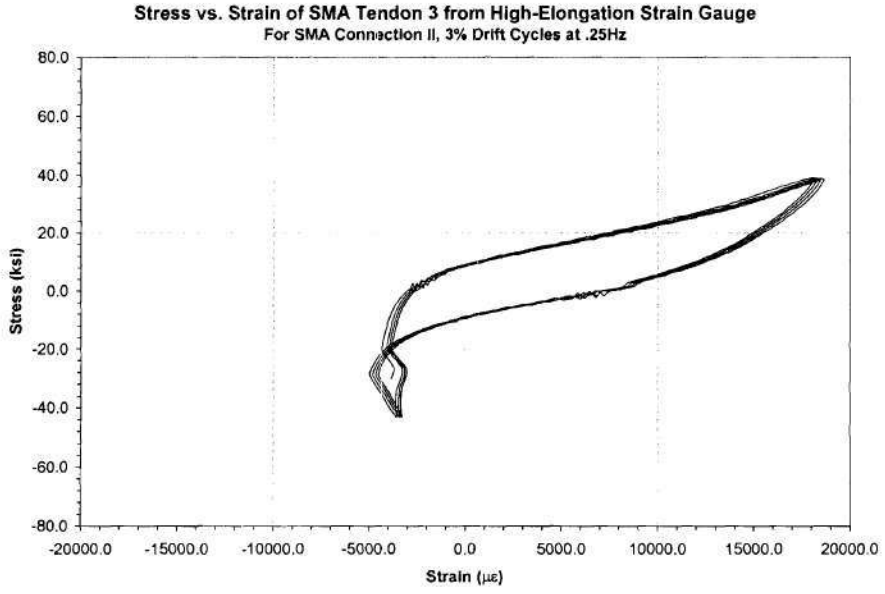

Figure B-20 Stress/Strain History for Tendon 3 using Strain Gauge

REFERENCES

1: Birman, Victor., "Review of mechanics of shape memory structures." *Applied Mech. Rev.*, vol. 50, no. 11, part 1, 1997.

2: Brady, Pamalee A., Sweeney, Steven C., and Hayes, John R., "Advancing Seismic Structural Resistance", *ASEE Annual Conference Proceedings*, 1995.

3: Casciati, F., Faravelli, L., and Petrini, L., "Energy Dissipation in Shape Memory Alloy Devices", *Computer-Aided Civil and Infrastructure Engineering 13*, 1998.

4: Dolce, M. and Marnetto, R., "Seismic Devices Based on Shape Memory Alloys", *MANSIDE Project - Final Workshop*,1999.

5: Duerig et al., "Engineering Aspects of Shape Memory Alloys", Butterworth-Heinemann Ltd., 1990.

6: "Effect of the Strain Rate and Sample Size on Features of Non-linear Deformation Behavior in Ti-Ni based Ribbons and Wires" *SMST-99 First European Conference on Shape Memory and Superelastic Technologies,* 5-9 September 1999. Antwerp Zoo, Belgium

7: Ford, D. S. and White, S. R., "Thermomechanical Behavior of 55Ni45Ti Nitinol", Acta Metallurgical Inc., 1996.

8: Hess, Gregory W., "*Cyclic Behavior of Shape Memory Alloy Tendons and Steel Bolted T-Stubs in Beam-Column Connections,"* Department of Civil and Environmental Engineering, Georgia Institute of Technology, November 2000.

9: Humbeeck, J. Van, "Damping Capacity of Shape Memory Alloys", *MANSIDE Project - Final Workshop*,1999.

10: Humbeeck, J. Van, "General Aspects of Shape Memory Alloys", *MANSIDE Project - Final Workshop*,1999.

11: Leon, Roberto T., "Partially Restrained Connections." *Handbook of Structural Steel Connection Design and Details.*

12: *Load & Resistance Factor Design*, Vol. I & II, Second Edition, American Institute of Steel Construction, 1995.

13: SAC, "Protocol for Fabrication, Inspection, Testing and Documentation of Beam-Column Connection Tests and Other Experimental Specimens", *SAC Report SAC/BD-97/02*, SAC Joint Venture, Sacramento, 1997.

14: Schrauben, Corey S., *Behavior of Full-Scale Bolted Beam-to-Column T-Stub and Clip Angle Connections Under Cyclic Loading"*, Department of Civil and Environmental Engineering, Georgia Institute of Technology, December 1999.

15: Smallidge, Jeffrey M., *Behavior of Bolted Beam-to-Column T-Stub Connections Under Cyclic Loading*, Department of Civil and Environmental Engineering, Georgia Institute of Technology, March 1999.

16: Swanson, James A., *Characterization of the Strength, Stiffness, and Ductility Behavior of T-Stub Connections*, Department of Civil and Environmental Engineering, Georgia Institute of Technology, August 1999.

17: Tobushi, H., Shimeno, Y., Hachisuka, T., Tanaka, K., "Influence of Strain Rate on Superelastic Properties of TiNi Shape Memory Alloy," *Mechanics of Materials,* Vol 30 1998, pp. 141-150

18: Whittaker, Andrew S., Krumme, R., Sweeney, Steven C., and Hayes, John R., *Structural Control of Buildings Response Using Shape Memory Alloys.* US Army Corp of Engineers Construction Engineering Research Laboratories, 1995.

19: Wolons, D., Gandhi, F., and Malovrh, B., "Experimental Investigation of the Pseudoelastic Hysteresis Dampening Characteristics of Shape Memory Alloy Wires." *Journal of Intelligent Material Systems and Structures*, Vol. 9 - February 1998, pp 116-129.

20: Yang, Dazhi, "Shape Memory Alloy and Smart Hybrid Composites - Advanced Materials for the 21st Century", *Materials & Design 21*, 2000.